2-2018

Comparison of Processed and Non-Processed Biomass Digestion

Richard Bruce Clark III

Comparison of Processed and Non-Processed Biomass Digestion

A Thesis

Submitted to the Faculty

of

Rose-Hulman Institute of Technology

by

Richard Bruce Clark III

In Partial Fulfillment of the Requirements for the Degree

of

Master of Science in Chemistry

February 2018

ROSE-HULMAN INSTITUTE OF TECHNOLOGY

Final Examination Report

Richard Clark — Name

Chemistry — Graduate Major

Thesis Title **Comparison of Processed and Non-Processed Biomass Digestion**

DATE OF EXAM: 1/19/2018

EXAMINATION COMMITTEE:

	Thesis Advisory Committee	Department
Thesis Advisor:	Rebecca DeVasher	CHEM
	Daniel Morris	CHEM
	Sharon Sauer	CHE
	Lorraine Olson	ME

PASSED X **FAILED** _____

Clark, Richard Bruce, III

M.S. Chemistry

Rose-Hulman Institute of Technology

February 2018

Comparison of Processed and Non-Processed Biomass Digestion

Thesis Advisor: Dr. Rebecca DeVasher

Lignocellulosic ethanol is the main focus of second-generation biofuels [1]. Because cellulose is the most abundant organic material on earth, second-generation biofuels are a more sustainable option than the classical first-generation biofuels that use foodstuffs as the main feedstock in ethanol production [1]. Furthermore, biofuel can be produced not only from unprocessed biomass such as corn husks but also from processed material like paper [1].

Ionic liquids have shown to be quite effective in dissolving naturally occurring, and traditionally insoluble, polymers such as cellulose into solution, and cellulase enzymes have been shown to effectively digest cellulose into simple sugars [2]. This paper covers the results of a series of experiments which attempt to analyze the thermodynamics and yields of microwave-assisted digestion of biomass, as well as the performance of the protic ionic liquids, triethylammonium bisulfate (TEA-BS) and triethylammonium triflate (TEA-OTF), and the cellulase enzyme from *Trichoderma reesei* in assisting in these digestions. This paper discusses the metrics of ethanol content obtained using processed and unprocessed biomass, ionic liquids, and cellulase enzymes.

Keywords: chemistry, protic ionic liquids, biofuel, ethanol, biomass digestion

DEDICATION

To my family, my friends, my mentors, and everybody else who supported me along the way.

ACKNOWLEDGEMENTS

First and foremost, I would like to thank my thesis advisor, Dr. Rebecca DeVasher, for her guidance, support, kindness, knowledge, and patience throughout my time at Rose-Hulman Institute of Technology. I would also like to thank Lou Johnson, Instrumentation Manager, and Cyndi Erwin, Chemical Stockroom Manager, for all that they have done over the years to maintain and improve upon the chemistry laboratories at Rose-Hulman. I would like to thank all of the members of my committee: First, to Dr. Lorraine Olson, for her patience and support as a committee member, Second, to Dr. Sharon Sauer, for her wisdom, guidance, and encouragement as my instructor, my academic advisor, and finally, as one of my committee members, Third, to Dr. Daniel Morris, for his wisdom, kindness, and dedication to chemistry. There are several other professors I would also like to thank, including Dr. Allen White for his kindness and support as a fellow of the chemical sciences, Dr. Stephanie Poland for her support during the early days of my research, Dr. Mark Brandt for teaching me how to use several pieces of equipment and for allowing me to participate in the Interdisciplinary Research Collaborative in order to improve upon my research and presentation skills, and Dr. Kim Henthorn for her guidance and instruction. I would like to acknowledge a few students from Rose-Hulman, whom I feel deserve special thanks. First to Seth Clark and Jeff Tribble, for their collective efforts in the synthesis of ionic liquids, and the development of the gas chromatography calibration curve. Second to Rachel Shubella for her support as part of my research team. Finally, I would like to thank Dr. Michael Mueller, for helping me decide to get a Master's degree, and for his patience, guidance, and support in determining the right path for me along the way.

TABLE OF CONTENTS

LIST OF FIGURES

LIST OF TABLES

LIST OF ABBREVIATIONS

BTL	biomass-to-liquids
F-T	Fischer-Tropsch
FID	Flame ionization detector
GC	gas chromatography
HF	Hartee-Fock
HPLC	high-pressure liquid chromatography
IL	ionic liquid
MARS	Microwave Accelerated Reaction System
MS	mass spectrometry
NMR	nuclear magnetic resonance
PIL	protic ionic liquid
pH	Potential of hydrogen
RFS	renewable fuel standard
RTIL	room temperature ionic liquid
T. reesei	*Trichoderma reesei*
TEA-BS	triethylammonium bisulfate
TEA-OTF	triethylammonium triflate
TMS	Tetramethylsilane

LIST OF EQUATIONS

LIST OF SYMBOLS

A_{EtOH}	Area of ethanol in GC curves
A_{PrOH}	Area of propanol in GC curves
b_0	Intercept
$C_{EtOH,CC}$	Concentration of ethanol used in calibration curve
$C_{EtOH,solution}$	Concentration of ethanol in solution
G	Gibbs free energy
Gr	Grubbs G-value
$Gr_{critical}$	Critical Grubbs G-value
H	Enthalpy
k_B	Boltzmann constant
$m_{EtOH,true}$	True mass of ethanol
m_{EtOH}	Mass of ethanol
m_0	Slope
N	Number of moles
n	Number of data points
P	Pressure
R_{area}	Propanol-ethanol area ratio
$R_{area,adjusted}$	Area ratio which has been scaled up
S	Entropy
$\underline{S^{Excess}}$	Excess entropy due to mixing
s_x	Standard deviation
T	Temperature
U	Internal energy
V	Volume
$V_{injected,cal.curve}$	Volume injected from the original calibration curve
V_{total}	Total volume injected into the chromatogram
V_{EtOH}	Volume of ethanol in solution
x	Independent variable of linear equation
$\bar{x}$	Average of a set of data
x_i	Data point in a set of data
x_P	Molar fraction of polymer
x_S	Molar fraction of solvent
y	Dependent variable of linear equation
α	Statistical significance
ΔG	Change in Gibbs free energy
$\underline{\Delta G}$	Molar change in Gibbs free energy
$\underline{\Delta G_{mix}}$	Molar change in Gibbs free energy of mixing
ΔH	Change in enthalpy

ΔP	Change in pressure
ΔS	Change in entropy
ΔS_{mix}	Change in entropy of mixing
$\Delta \underline{S}_{mix}$	Molar change in entropy
ΔT	Change in temperature
$\Delta \underline{U}$	Molar change in internal energy
$\Delta \underline{U}$	Molar change in internal energy
$\Delta \underline{U_{mix}}$	Molar change in internal energy of mixing
$\Delta \underline{U_{rxn}}$	Molar change in internal energy of reaction
ΔV	Change in volume
ρ_{EtOH}	Density of ethanol
χ_{PS}	Flory-Huggins polymer-solvent mixing parameter

1. INTRODUCTION

Lignocellulosic ethanol is a promising area of research for bioethanol production due to its potential to increase the current global output of biofuel by preventing the rationing of crops for use as ethanol feedstocks [1,3–22]. Lignocellulosic ethanol has the potential to eliminate the food-vs-fuel debates of this century [1,3–8,10,12–14,16,17,20–24]. These types of biofuels are also referred to as second-generation biofuels. Second-generation biofuels have been a topic of discussion since the early days of ethanol fuel production in the 1900's, but its implementations were not in place until decades later [1,17,21,25]. One of the boundaries to the use of lignocellulosic biomass as a means of producing ethanol is the structure of the lignocellulosic material. Plant refuse typically consists of a polymer matrix of cellulose and hemicellulose, surrounded by a tough lignin barrier, which protects the cellulose from being hydrolyzed into simple sugars such as glucose [1,2,4,6,12,26,27].

Ionic liquids, and protic ionic liquids, in particular have promising potential as cellulose solvents [22,27,28]. Room-temperature ionic liquids (RTIL's) have shown promising results as solvents, and protic ionic liquids (PIL's) have added pH benefit to aid in the acid-catalyzed hydrolysis of the acetal linkages in cellulose. Two PIL's of interest are triethylammonium bisulfate (TEA-BS) and triethylammonium triflate (TEA-OTF). Both of these PIL's have been able to yield ethanol from lignocellulosic biomass [6].

Cellulase enzymes are another point of interest in the production of lignocellulosic ethanol since they are particularly efficient at breaking down cellulose into simpler sugars [1–

3,5,9,11,12,15,17,18,22,25–27,29–33]. One of the most widely used cellulase enzymes comes from *Trichoderma reesei*, a fungus which breaks down plant matter [1,9,15,17,22,25,26,29–33].

A key point of interest in lignocellulosic ethanol research is combined IL and cellulase treatments. When used together, they have the potential to increase the output of ethanol by dissolving cellulose present in biomass and subsequently hydrolyzing it with the enzyme [2,11,15,27,29]. One drawback, however, to combined treatments is the potential for cellulase to be inhibited, deactivated, or even denatured by some of these ionic liquids [2,11,15,29]. This paper will attempt to address some of the metrics of ethanol production from lignocellulosic biomass, using both processed paper, and unprocessed corn stover. Treatment methods, including cellulase digestion from *T. reesei* and microwave-assisted digestion in PIL's, namely TEA-BS and TEA-OTF, will also be discussed. Finally, thermodynamic analyses from computer-aided simulations will attempt to help justify results from the hydrolysis and fermentation of processed and unprocessed lignocellulosic biomass.

2. BACKGROUND

2.1. Applications and Demand for Biologically Derived Chemicals

2.1.1. Applications and Demand for Bio-chemicals

From solvents to polymers, from food additives to fuel, biologically-derived chemicals are an important part of our everyday lives. Naturally derived chemicals including furfural, ethanol, and lactic acid are used for solvents, fuel, food additives, and other important auxiliaries and precursors to widely used molecules [18]. Furfural is an example of a compound produced from agricultural waste that can be utilized in a number of different applications, mainly for fuel additives [18,34]. Current world production of furfural is approximately 300-700 thousand tons per year [18,34].

Ethanol is another biologically-derived chemical which has a significant advantage over furfural in terms of production; its total global output is over 71 million tons per year [18]. Since the early days of fuel production, efforts have been focused on finding a naturally occurring and renewable source for fuel, and ethanol was one that was highly sought after. Thus, ethanol became the most produced biochemical in the market, with 93% of production coming from biologically derived sources [17,18]. Ethanol has been used both as a substitute for gasoline, and, by dehydrating to ethylene, as a precursor to several of the most widely used polymers, including polyethylene, polyethylene terephthalate, polyethylene glycol, polyvinyl acetate, polyvinyl chloride, and polystyrene, as well as ethylene glycol [18]. **Table 2.1-1** illustrates the total global production and sales of ethanol and ethanol-based products.

Table 2.1-1: Total global production of ethylene, ethylene glycol, and ethanol

Compound	**Production (kt/year)**	**Annual sales**
Ethylene	127,000	$ 241,500 MM
Ethylene glycol	28,000	$ 28,000 MM
Ethanol	76,677	$ 63,141 MM
Total	231,677	$ 332,641 MM

Reproduced, from [18].

According to a report from the European Commission, only 0.2% of ethylene and 1.5% of ethylene glycol is produced from biologically-derived sources and the remainder is produced from petroleum [18]. From the above table, bioethanol is already a large portion of the chemical market, with the potential to be used in a market that is five times as large. If newer technology can be developed to produce higher yields of bioethanol, the price of ethanol may decrease, making it a more sought after feedstock for ethylene production.

2.2. Generations of Biologically Derived Ethanol

2.2.1. First-Generation Technology

First-generation biofuels have helped pave the road towards naturally occurring renewable feedstocks. These types of biofuels are made directly from food sources and consist mainly of biodiesel and bioethanol [1,3–5,7,10,12–14,17–19,21–25,35–38]. Biodiesel can be synthesized from naturally-occurring triglycerides, such as soybean oil, palm oil, and other vegetable oils, as well as grease and animal fats via the transesterification reaction [1,4,5,16–18,21,23,25,35,36,38]:

$$R_3C_6O_6H_6 + 3\ MeOH \rightarrow C_3H_8O_3 + Biodiesel$$

Biodiesel is typically blended with petroleum-based diesel at 5 and 20% biodiesel, although B100 (100% biodiesel) has been used by some vehicles, such as Indy racecars [21,35].

Bioethanol is the other main type of first-generation biofuel, and it can be synthesized from sugarcane, sugar beets, wheat, corn, sorghum, and other crops with large amounts of sucrose or starch [1,4–6,10,12–14,16–19,21–25,35,37–39]. The technology behind first-generation bioethanol comes from the well-established hydrolysis reaction of sucrose and subsequent fermentation reaction of glucose [1,4–6,13,17–19,23,25,35,38,40], represented by the following chemical equations, respectively:

$$C_{12}H_{22}O_{11} + H_2O \rightarrow 2\ C_6H_{12}O_6$$

$$C_6H_{12}O_6 \rightarrow 2\ CO_2 + 2\ C_2H_5OH$$

The fermentation reaction has been utilized since the early days of civilization when it was first used as a component in drinks [1,9,41].

With crops that contain starch instead of sucrose, an additional step is needed; the available starch must first be hydrolyzed to glucose via the saccharification reaction sequence [1,4,5,17,18,25,30,38,42]. This reaction series requires the use of enzymes and acid to break down the complex polysaccharides, amylopectin and amylose found in starch, into simpler sugars which can then be more easily fermented [1,4,5,13,17,18,25,42]:

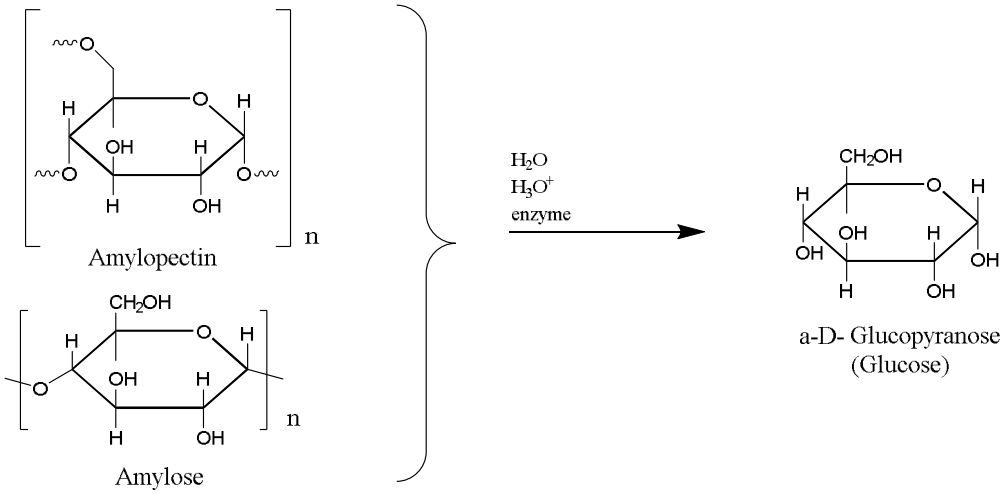

Figure 2.2-1: Hydrolysis reaction of starch.

The first instance of ethanol being used as an alternative fuel source was in the 1800s, as a cheaper alternative for whale oil in lamps when it was blended with turpentine derived from pine trees [1,5,17,19,21,25,37]. In 1826, Samuel Morey received a patent for the invention of an internal combustion engine, which was powered by this same mixture, and could power a boat for speeds of up to 8 mph [1,17,21,25,37,43]. In 1860, Nicolaus August Otto developed another early version of the internal combustion engine which was also powered by ethanol [1,17,21,25,37,44]. Later in the 1860s, the use of ethanol as a fuel was halted because of a liquor tax which was enacted to help fund the Civil War [1,19,21,37]. It was not until the early 20th century that ethanol's use as an engine fuel was brought back. In 1906, the liquor tax was lifted, and in 1908, Henry Ford invented the Model T, an automobile that could run on a mixture of gasoline and ethanol [1,17,19,21,25,37,44]. These two events helped bring back ethanol as a fuel.

In the following years, scientists were promoting the widespread use of ethanol, even going so far as to advocate for the production of lignocellulosic ethanol [1,17,21,25]. In 1919, the Prohibition banned pure ethanol as a fuel; however, it could still be sold if it was mixed with

petroleum [19,21]. In the 1930s, over 2000 gas stations in the Midwest used gasoline mixed with ethanol [17,21,25]. The oil companies were favoring tetraethyl lead over ethanol as an octane booster and anti-knock additive, which contributed to the competition between ethanol and petroleum in the 1920s and as a response the oil companies were pushing to stop the production of ethanol as it was a growing threat to their business [17,21,25]. During WWI and WWII, demand for ethanol-based fuel had increased dramatically, reaching consumption levels of 600 million gallons per year, as oil was being rationed during that time [17,19,21,25,37,44]. After WWII, petroleum became cheaper once more, and ethanol was phased out until the 1970s [1,17,19,21,25,37,44]. During the 1973 oil crisis, ethanol was once again sought as an alternative fuel to curb the rising costs of gasoline [1,17,21,25,37,44]. In 1978, the United States Energy Tax Act was passed, which provided subsidies on renewable fuels [5,16,16,19,21,37]. Around the same time, the EPA ended the use of tetraethyl lead as a fuel additive by passing the Clean Air Act of 1970 [21,35].

Between the 1970's and 2000's, ethanol production plants were being established, and advocacy groups had continued to push for the production of bioethanol [1,4,5,7–9,18,21,23,27,40,45]. In 2005, in his State Of The Union address, former US President George Bush proposed a preliminary renewable fuels standard (RFS) to produce 35 billion gallons per year of bioethanol by 2017 [6,14,21,23,24,37]. In 2007, Congress passed the Energy Independence and Security Act, which set an RFS of 36 billion gallons of biofuel, with one billion gallons being biodiesel, by 2022 [5,13,14,16,19,24,37]. In 2015, 14 billion gallons of ethanol had been added to gasoline, and to this day ethanol research and full-scale production continues to make progress as efforts are being made to reach the target of 36 billion gallons by 2022 [13,19,22]

Current production of bioethanol primarily consists of two types of milling: wet and dry [1,4,5,13,17,25,27,35]. Dry mills make up between 70-90% of bioethanol plants in the United States [13,17,25,35]. Dry mills are typically smaller and require fewer resources; however, they do not produce as diverse products as wet mills [4,17,25]. Along with bioethanol, wet mills can produce a wider variety of products, such as high fructose corn syrup, but wet mills typically have a lower ethanol conversion, at 2.5 gallons per bushel of corn, versus 2.8 gallons per bushel for dry mills [4,13,17,25]. Typical wet-mill and dry-mill processes are summarized in **Figure 2.2-2**.

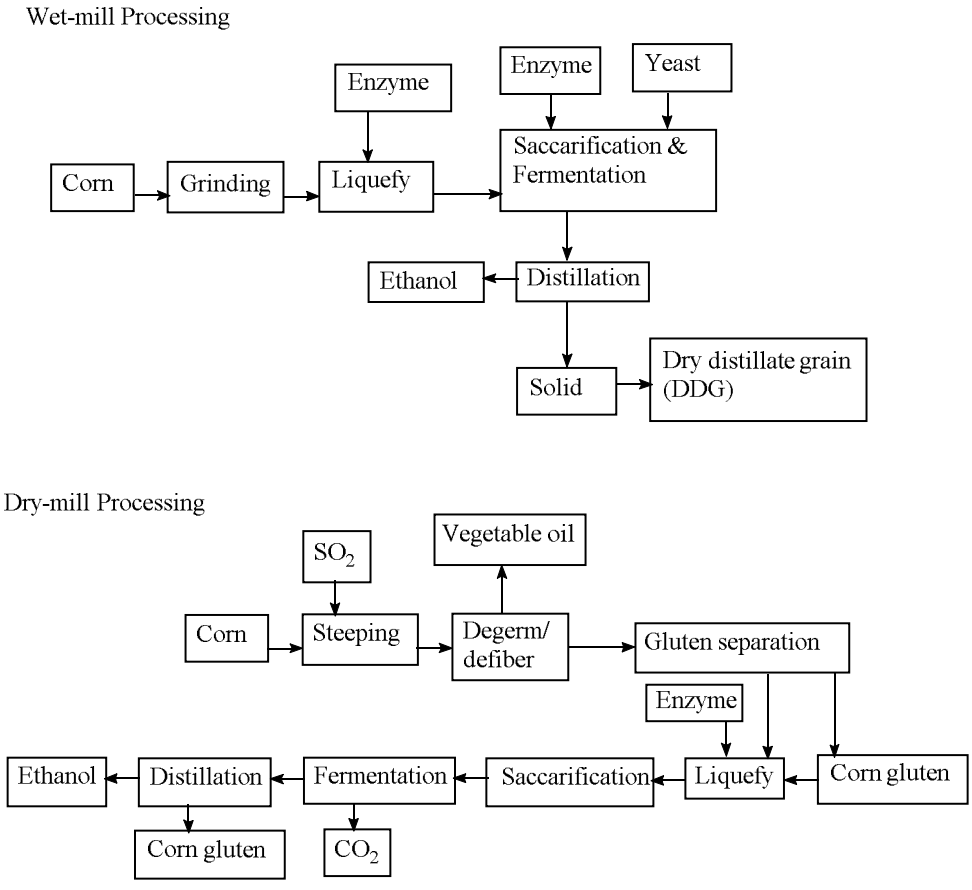

Figure 2.2-2: Block flow diagrams of typical wet-mill and dry-mill processes. Reproduced from [4]

2.2.2. Second-Generation Technology

Second-generation biofuels are a relatively new type of biofuel technology that derives its feedstock from non-food sources [1,3–8,10,12–14,16,17,20–24]. It can be inferred that the majority of the feedstock used in second-generation biofuel comes from lignocellulosic biomass [1,3–22]. There are two main routes for the production of second-generation biofuels: bio- and thermochemical [1,3–5,17,18,20,23,35,46]. The biochemical pathway refers to an enzymatic treatment of cellulose, hemicellulose, and other polysaccharides present in the lignocellulosic biomass [1–5,9,11,12,15,17,18,20,23,27,30,40,46]. Similar to the saccharification route as discussed in the previous section, an enzymatic treatment of lignocellulosic material is required, which results in the formation of simple sugars that can then be fermented to produce ethanol [1–5,11,12,14,15,17,18,27,29,46]. In this route, the feedstock is introduced to a class of enzymes known as cellulase, produced by bacterial and fungal species [1,3,5,7,9,11,12,15,17,18,22,26,29,31–33]. The enzymatic hydrolysis reaction series is illustrated in **Figure 2.2-3** as follows [5,9,26,29–32,40]:

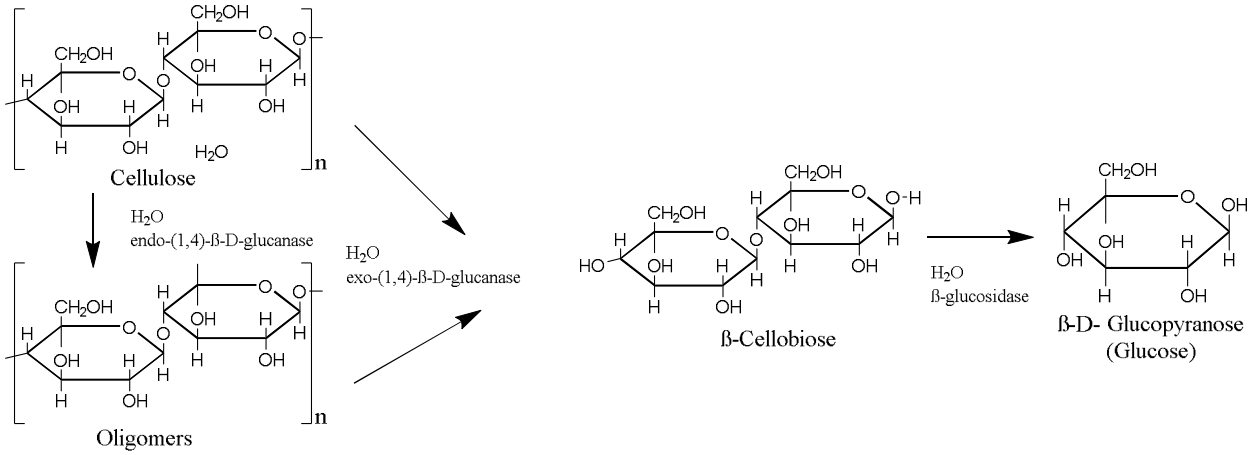

Figure 2.2-3: The enzymatic hydrolysis reaction sequence for the conversion of cellulose to glucose

In the biochemical process, the water-soluble enzyme group acts as a heterogeneous catalyst for the hydrolysis of cellulose [3,5,7,9,18,26,27,30–32,47]. This process is relatively immature; however, it is currently being developed and implemented by some companies such as DuPont, Abengoa, and POET [1,17,18,24,35].

In the thermochemical route, also known as the biomass-to-liquids (BTL) route, biomass undergoes pyrolysis, gasification, liquefaction, or direct combustion to form a synthesis gas, or syngas, composed of CO and H_2, and can then be processed to form a variety of biofuels, including synthetic diesel, aviation fuel, ethanol, and other hydrocarbons, via the Fischer-Tropsch (F-T) process: [1,3–5,17,20,23,48]

$$(2n + 1)\ H_2 + n\ CO \rightarrow C_nH_{(2n+2)} + n\ H_2O$$

Biofuel produced by this process, which is illustrated in **Figure 2.2-4**, substitutes renewable biomass for coal as the primary feedstock [4,17,48].

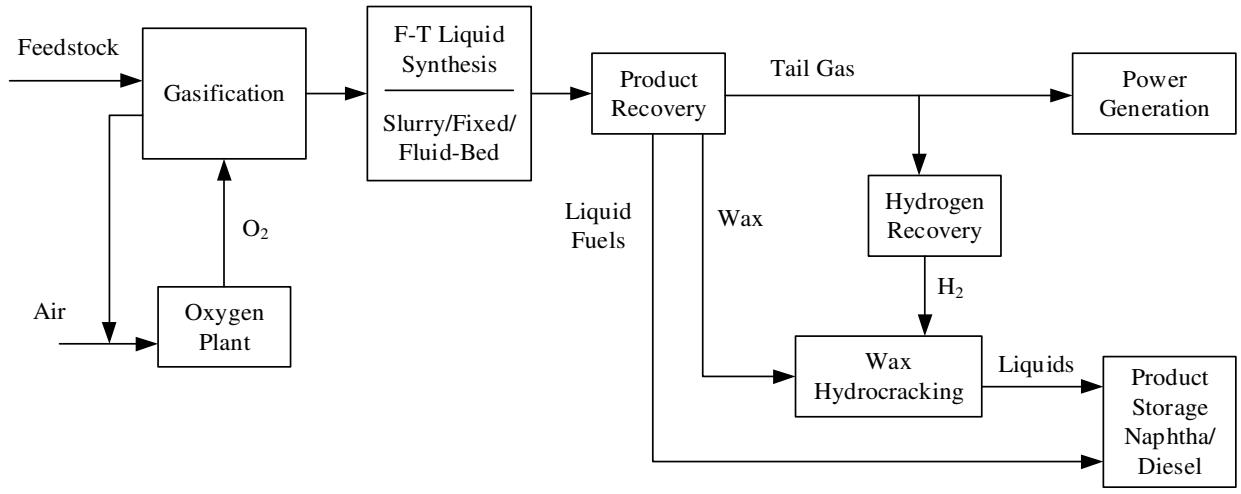

Figure 2.2-4: A simplified flow diagram of a typical F-T process, where coal or biomass can be used as the feedstock.
Reproduced from [6,48]

The F-T process has been widely implemented in India, China, Denmark, Germany, and other EU nations, since the 1920's, and has become technologically mature [1,3–5,23,48]. Thus,

there is little room for economic improvement of thermochemical second-generation biofuel technology [1,3–5,23]. Biochemical technology, on the other hand, is relatively immature; it is a newer technology with limited industrial implementations and therefore has a greater potential to become more economically feasible at a production scale than thermochemical technology [3,5,23].

2.2.3. First- vs. Second-Generation

First-generation biofuel technologies have certain advantages over second-generation technologies. First-generation technology has been well-established, and knowledge of the chemistry behind first-generation has been known since the early days of civilization [1,4–6,9,13,17–19,23,25,35,38,40,41]. In addition, the processes have reached maturity, and are becoming increasingly efficient, and widely available [1,4,5,7–9,13,18,19,21–23,27,40,45]. On the other hand, there are certain problems that arise from relying on first-generation biofuel alone to meet the renewable fuel standard of 36 billion gallons of biofuel by 2022 [3,4,7,13,17,35,36,38]. In recent years, grain-based biofuels have been a subject of food-vs-fuel debates, because of the material source involved [1,3,4,6–8,12–14,16,17,35,36,38,39]. Based on current productions, in order to meet the RFS from grain-based ethanol alone, there would need to be over twice as many dedicated crops reserved for biofuel. Allocating more land for farms typically requires unsustainable practices such as deforestation, and can lead to increased soil erosion and increased greenhouse gas emissions [3,5,10,13,17].

Second-generation biofuel technologies, as immature as they are, have the potential to work with currently present first-generation technology to reach the RFS by 2022. During the era of the Model T, when scientists were advocating the use of ethanol as fuel, scientists and inventors, including Alexander Graham Bell, anticipated the rise of second-generation biofuel,

long before its time [1,17,21,25]. As much as 90 percent of the material found in crop residues can be utilized to produce biofuel, or other chemicals [1,6,26]. In many cases, a fraction of total crop residue can be harvested without adverse effects, such as soil erosion or significant nutrient depletion [14,24,49]. According to a report by the US Department of Energy, it is estimated that over 500 million dry tons of crop residue will be produced by 2030 [49]. Second-generation technology uses cellulose, the most abundant organic material on Earth, which comes from nearly all plants; therefore, this newer generation of biofuel technology does not require a food source unlike first-generation technology [1,3–8,10,12–14,16,17,20–24]. In order to make use of the potential for this newer biofuel technology, however, the technology must be developed further at full production scale [1,17,18,24,35]. Additionally, the process for extracting and converting the material from lignocellulosic biomass into bioethanol requires additional steps that first-generation technologies do not [1,2,6,26].

2.3. Extraction of Material from Lignocellulosic Biomass

2.3.1. Issues with Extraction of Cellulose

Second-generation bioethanol technology requires the extraction of cellulose from biomass, as discussed in the previous sections [1–5,9,11,12,15,17,18,20,23,27,30,40,46]. This process, however, requires additional steps to collect and hydrolyze the glucose polymer [1,2,6,26]. In most lignocellulosic biomass, the cellulose exists within a matrix of lignin and hemicellulose [1,2,4,6,12,26,27]. **Figure 2.3-1** portrays a typical lignocellulosic matrix in which the cellulose is located within protective lignin barriers.

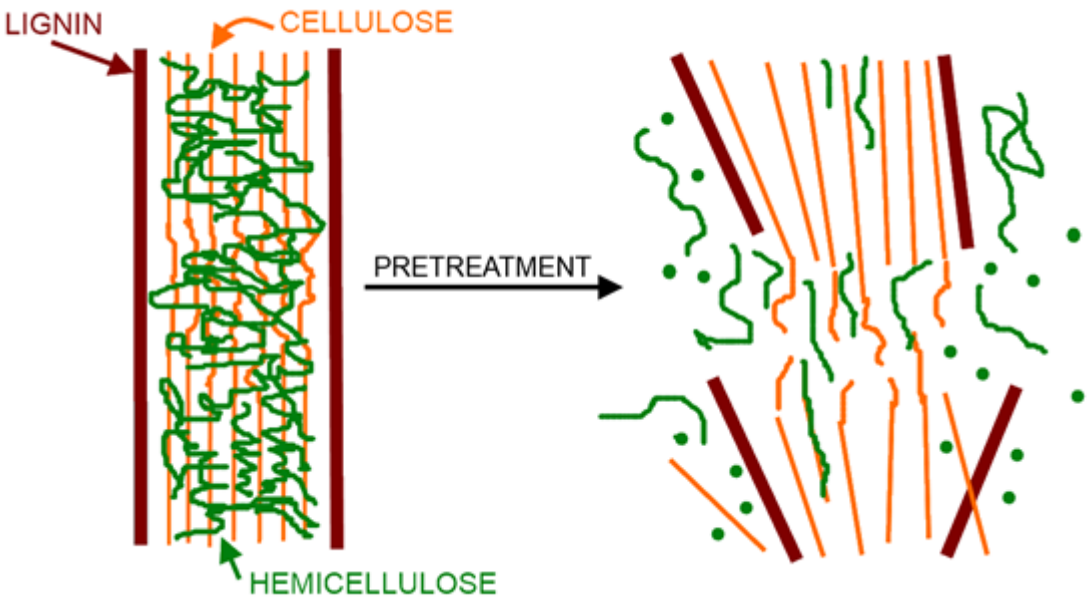

Figure 2.3-1: A simplified macromolecular view of lignocellulosic biomass. Reproduced, with modifications from [12].

Lignin is a naturally-occurring polymer that is water-resistant, which helps to prevent the hydrolysis and breakdown of cellulose against weather and rain, as lignocellulose is important in maintaining the structural integrity of the plant during its life [12,26]. Some animals derive most of their energy from lignocellulosic material [26]. These animals have evolved adaptations to these lignin barriers, including specialized bacteria and development of their own enzymes so that they can obtain the necessary nutrients from these plants [26].

2.3.2. Current Implementations and their Environmental Issues

Cellulose extraction from lignin as a means of producing bioethanol is not currently a major source of biofuel; however, it is under development by universities as well as some chemical companies [1,17,18,24,35]. Production-scale processes utilize thermomechanical and thermochemical techniques, usually consisting of harsh chemicals, highly corrosive acids and bases, and high pressures and temperatures [1,4,6,12,26,27]. While these processes are not

environmentally-friendly, nor are they efficient, they produce the highest yield in the shortest amount of time [4,12,26,27]. This may allow the production of ethanol from lignocellulosic biomass to be more profitable and sought after in the future. If there can be a way to increase the yield without using harsh production methods, more environmentally friendly options could be considered.

2.4. Ionic Liquid and Enzymatic Treatment of Biomass

2.4.1. Ionic Liquids as a Treatment Method

Room temperature ionic liquids (RTIL's), or simply ionic liquids (IL's) are a class of ionic salts that exist as a liquid either at room temperature or temperatures less than 100 °C [22,27,28]. Protic ionic liquids (PIL's) are a type of ionic liquid formed when a proton is transferred from a Brønsted acid to a Brønsted base [45]. Such examples of protic ionic liquids are triethylammonium triflate and triethylammonium bisulfate, as illustrated in **Figure 2.4-1** [6].

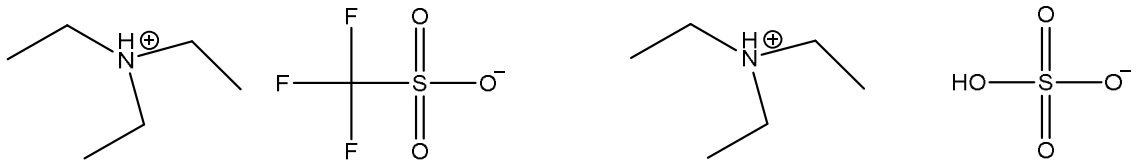

Triethylammonium Triflate (TEA-OTF)

Triethylammonium Bisulfate (TEA-BS)

Figure 2.4-1: The structures for triethylammonium triflate and triethylammonium bisulfate [6]

Ionic liquids, especially quaternary ammonium IL's, have been shown to be viable solvents for dissolving naturally occurring polymers, including cellulose, because of their ability to disrupt the bonds in the lignocellulose, and thus have promise in assisting the digestion of lignocellulosic biomass [2,6,11,22,27,28]. In addition, ionic liquids have been found to have low vapor pressures, allowing them to easily be distilled from solution and recycled for use in later batches [6,28].

2.4.2. Enzymatic Digestion as a Treatment Method

Cellulase is a naturally occurring enzyme which comes from some species of bacteria and fungi and has the innate ability to hydrolyze cellulose effectively [1–3,5,9,11,12,15,17,18,22,25–27,29–33]. One of the most widely used and researched cellulase-producing organism is *Trichoderma reesei*, named after its discoverer, Elwyn T. Reese [1,9,15,17,22,25,26,29–33]. A diagram of the cellulase enzyme can be seen in **Figure 2.4-2.**

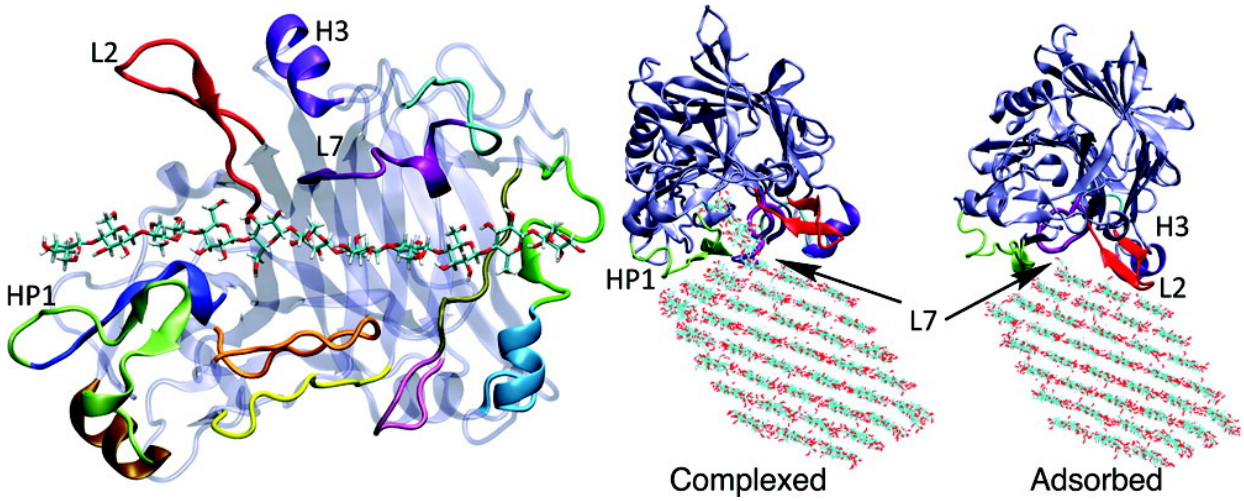

Figure 2.4-2: An illustration of the cellulase enzyme from *Trichoderma reesei* Reproduced from [22].

2.4.3. Combined Treatment Methods

One growing area of research in lignocellulosic ethanol is using ionic liquids and enzymes in combination [2,11,15,27,29]. Using the ionic liquids first to break apart the lignin barriers in the biomass, followed by enzymatic treatment of the now-dissolved cellulose is predicted to increase the yield of simple, fermentable sugars, and as a result, the yield of ethanol produced [2,11,15,27,29]. The caveat to this, however, is the stability of the cellulase enzyme in the presence of ionic liquids. Cellulase and other enzymes have been shown to be inhibited in

some types of ionic liquids [2,11,15,29]. One of the objectives of this paper is to study the ability of cellulase from *T. reesei* to hydrolyze cellulose in the presence of triethylammonium triflate.

3. EXPERIMENTAL METHODS

3.1. Preparation of Ionic Liquids

Each of the ionic liquids used in these experiments was prepared in the Chemistry laboratories of Rose-Hulman Institute of Technology. The triethylamine and triflic acid were obtained from Sigma Aldrich. All other ionic liquids used in these experiments were previously synthesized in accordance with the procedures, as described below [6]. The ^{1}H and ^{13}C NMR spectra were acquired on a Bruker Ultrashield 300 MHz NMR spectrometer.

Triethylammonium Triflate (TEA-OTF)

25 mL of triethylamine was placed in a 100 mL round bottom flask, along with a magnetic stir bar. The flask was then placed in a -78 °C dry ice and acetone bath. Next, 16 mL of trifluoromethanesulfonic (triflic) acid was added to the round bottom flask slowly in a dropwise manner. The round bottom flask was then removed from the dry ice and acetone bath and was allowed to stir overnight at room temperature. The mixture was then washed in a separatory funnel with diethyl ether, and was then rotary evaporated under vacuum. The product was characterized by ^{1}H NMR and ^{13}C NMR in $CDCl_3$ with TMS as the standard. The ionic liquid is shelf-stable and was used in later experiments.

Triethylammonium Bisulfate (TEA-BS)

25 mL of triethylamine was placed in a 100 round bottom flask, along with a magnetic stir bar. The flask was then placed in a -78 °C dry ice and acetone bath. Next, 3.1 ml of concentrated sulfuric acid was added to the round bottom flask slowly in a dropwise manner. The round bottom flask was then removed from the dry ice and acetone bath and was allowed to stir

overnight at room temperature. The mixture was then rinsed in a separatory funnel with diethyl ether and was then rotary evaporated under vacuum. The product was characterized by ^{1}H NMR in $CDCl_3$ with TMS as the standard. The TEA-BS is shelf-stable, and it was synthesized from previous experiments and used for this experiment [6]. Therefore, it was not necessary to synthesize additional TEA-BS.

3.2. Thermodynamic Analysis

Interaction between Ionic Liquid and Carbohydrates

When assessing the thermodynamics of the hydrolysis reaction, it is important to consider the intermolecular interactions. This can provide some insight as to how difficult it would be to allow reactions, such as cellulose hydrolysis, to occur. In order to determine whether the interactions between the ionic liquids and the cellulose polymer would be thermodynamically favored, a series of quantum mechanical calculations were performed for each ionic liquid, as well as for oligomers of cellulose. All quantum calculations for this experiment were performed using the Spartan '16 by Wavefunction, Inc. [50].

Each ionic liquid was built piecewise, by performing quantum calculations of each ion separately, and then bringing them together in a configuration that seemed to be the most stable based on the charges of the molecules and the locations of their respective charge densities. All quantum mechanical calculations, unless otherwise stated, utilized the Hartree-Fock *ab initio* method, with a 6-31G* basis set, in aqueous solution. The equilibrium geometry was first calculated for each ion separately, and afterwards was calculated for the ionic pair. **Figure 3.2-1** illustrates an example of two individual ionic liquid components in their most stable form as determined by quantum mechanical calculations, before being introduced to each other in the same system.

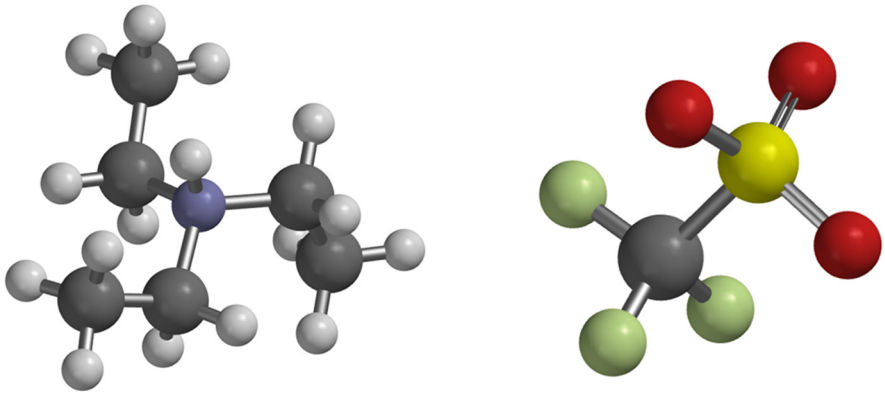

Figure 3.2-1: Triethylammonium and triflate in their most stable forms as determined by Spartan

After obtaining the equilibrium geometries of each ion, and each ion pair, the geometry-optimized molecules were added to the same simulation as the geometry-optimized ionic pair. This allowed Spartan to calculate the energy difference between the geometries of the separate ions, and the resulting ionic pair, which is expressed as the change in energy for the reaction of the formation of the ionic liquid.

Once the IL formation reaction energies were obtained, the next step in the experiment was to perform equilibrium geometry calculations for the monomer of cellulose. Using β-D-glucose, each of the equilibrium geometries was calculated, using the same method and basis set as previously described. In order to determine the most probable site for interaction with the ionic liquid, a quantum calculation was performed for the interactions with the individual hydroxy groups associated with the 6-membered glucose ring. Beginning with the anomeric carbon and going clockwise through the ring, reaction energy was obtained for each complex formation. After determining the most probable site of complexation, distances between hydrogen bonds were obtained.

Derivation of Thermodynamic Solvation Parameters

In order to assess the favorability of cellulose dissolution into ionic liquids and water, it is necessary to determine the thermodynamic parameters of the mixing of the polymer and solvent. The Flory-Huggins theory utilizes lattice models to derive an equation for the internal energy of mixing. This theory makes use of the mean field approximation, as well as the simplifying assumption that mixing is ideal. The second assumption is especially important, as it enables one to derive the free energy of mixing by stating that the enthalpy and internal energy are equal. If one so desires, this theory can be used to derive an expression for the free energy of mixing as a function of temperature, mole fraction, and a parameter known as the Flory-Huggins interaction parameter, or the chi parameter [51]. The equations can be seen below:

Equation 1: Flory-Huggins energy of mixing

$$\Delta U_{mix} = N\, x_P\, x_S\, k_B\, T\, \chi_{PS}$$

Equation 2: Gibbs free energy of mixing in fully expanded form

$$\Delta G_{mix} = N\, x_A\, x_S\, k_B\, T\, \chi_{PS} - N\, k_B\, T\, (x_P ln\, x_P + x_S ln\, x_S)$$

In order to obtain the Flory-Huggins parameter, the free energy of mixing must first be calculated. In order to do this, the enthalpy must be obtained. Fortunately, the underlying assumptions from the Flory-Huggins theory can also be applied to a process that breaks the entire dissolution and hydrolysis reaction up into two processes. These processes are shown below:

$$\text{cellulose}_{(s)} \rightarrow \text{cellulose}_{(aq)} + H_2O \rightarrow \text{glucose}$$

Unfortunately, it is currently difficult to obtain real-world parameters for the dissolution of cellulose in the water, as facilitated by the ionic liquid with a multicomponent model, due to the lack of existing thermodynamic data on ionic liquids. It is possible, however, to obtain an

approximation of these parameters by using quantum mechanical calculations. By using the cellulose dimer, cellobiose, energy of depolymerization and mixing can be approximated by quantum mechanical calculations. Since enthalpy and internal energy are both state functions, the reaction parameters for the overall reaction can be calculated. The change in internal energy of reaction for the overall system and the calculated energy from computer models can then be used to obtain the necessary thermodynamic parameters for the mixing of polymer and solvent.

To determine these thermodynamic parameters, three quantum calculations were set up using Spartan. Similar to the process as described in the previous section, a quantum mechanical calculation was performed on cellobiose, the triethylammonium cation, the triflate anion, and water, using the same method and basis set. Next, a quantum mechanical calculation was performed with cellobiose in the presence of the ionic liquid components. Another quantum mechanical calculation was then performed for two molecules of glucose in the presence of the ionic liquid. A third quantum mechanical calculation was performed on cellobiose in gas.

Finally, the reaction energy was calculated by comparing the changes in energy between the starting materials and the resulting products. **Figure 3.2-2** illustrates the most stable configuration for cellobiose and TEA-OTF as determined by Spartan.

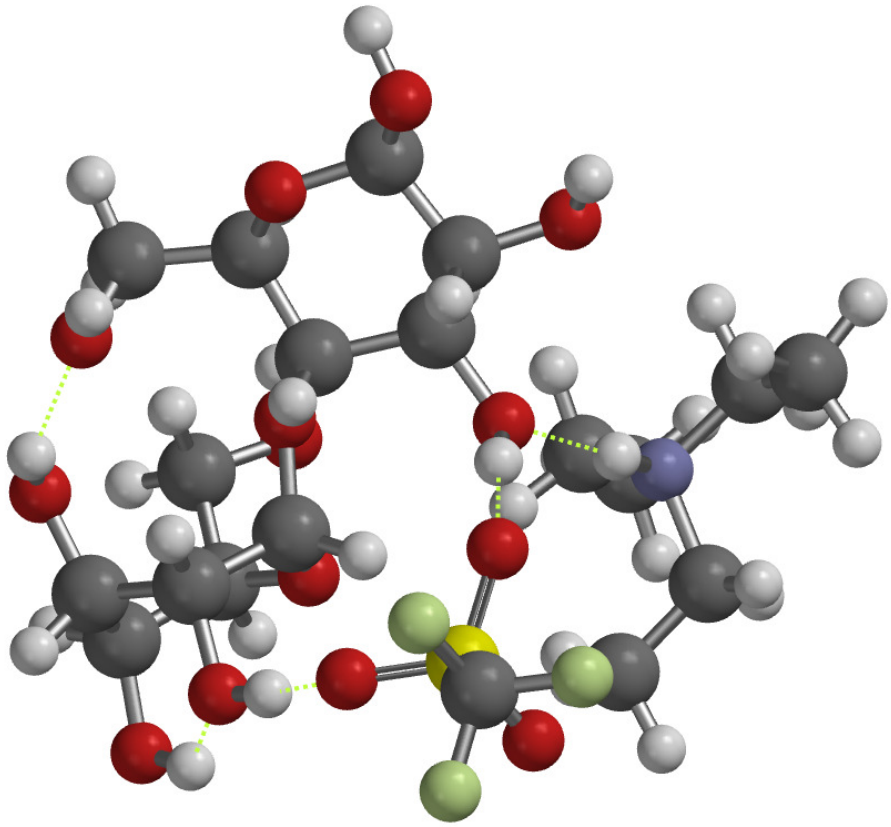

Figure 3.2-2: The system of cellobiose and TEA-OTF in its most stable configuration as determined by Spartan. Green dotted lines indicate hydrogen bonds.

3.3. Feedstock Hydrolysis and Fermentation

The lignocellulosic feedstocks used in this experiment were corn husks obtained from Indiana farmland. The control feedstock material used was standard printer paper. The cellulase enzyme was from *Trichoderma reesei* obtained from Sigma-Aldrich. The yeast used was Lallemand Biofuels Eagle C6 biofuel grade dry yeast. Finally, the microwave used in this experiment was a CEM MARS model. Microwave reactor vessels were GlassChem vessels. Microwave digestion was selected for ease of use, and shorter times for complete digestion. To begin the hydrolysis and fermentation, 0.05 grams of feedstock, which consisted of either dry corn husks or dry paper, were collected by manually tearing away small pieces which assisted in

obtaining more precise measurements, and had the added benefit of increasing the available surface area for reaction within the substrate. The substrate was then placed into the GlassChem microwave reactor vessel, which was followed by the addition of the treatment materials. For each type of treatment performed, three trials were run together, in separate vials, which would be used to obtain standard deviations, as well as to determine if outliers were present.

IL Treatment

0.05 g of dry substrate was combined with 1 g of ionic liquid and 10 mL of deionized water in a microwave reactor vessel. The microwave was set to operate using the GlassChem Method at 400W, with a ramp-up time of 5 minutes, 50 seconds to a temperature of 170 °C and a hold time of 10 minutes. These times and settings were selected because they were found to be the most optimal in previous experiments.

Microwave Treatment (Control)

0.05 g of dry substrate was combined with 10 mL of deionized water in a microwave reactor vessel. The microwave was set to operate using the GlassChem Method at 400W, with a ramp-up time of 5:50 minutes to a temperature of 170 °C and a hold time of 10 minutes.

Enzymatic Treatment

0.05 g of dry substrate was combined with 1 mL of cellulase enzyme in a beaker. The pH was adjusted to 4.5 using dilute HCl and NaOH. After the pH was adjusted, the contents were transferred to a sealable container and were placed in an oil bath over a hot plate with a thermocouple which assisted in maintaining the temperature of the oil bath at 37 °C for 24 hours.

IL + Enzymatic Treatment

0.05 g of dry substrate was combined with 1 g of ionic liquid and 10 mL of deionized water in a microwave reactor vessel. The microwave was set to operate using the GlassChem Method at 400W, with a ramp-up time of 5:50 minutes to a temperature of 170 °C and a hold time of 10 minutes. The mixture was combined with 1 mL of cellulase enzyme into a beaker. The pH was balanced to 4.5 using dilute HCl and NaOH. After the pH was balanced, the contents were transferred to a sealable container and were placed in an oil bath over a hot plate with a thermocouple which assisted in maintaining the temperature of the oil bath at 37 °C for 24 hours.

Procedure for Fermentation

After treating the substrate under the specified conditions, a fermentation apparatus was set up according to **Figure 3.3-1**. The Erlenmeyer flask was covered by a stopper which was connected to a bubbler tube that feeds into a test tube covered with a similar stopper and filled with water. The intent of this apparatus was to create an anaerobic environment which favors the production of ethanol.

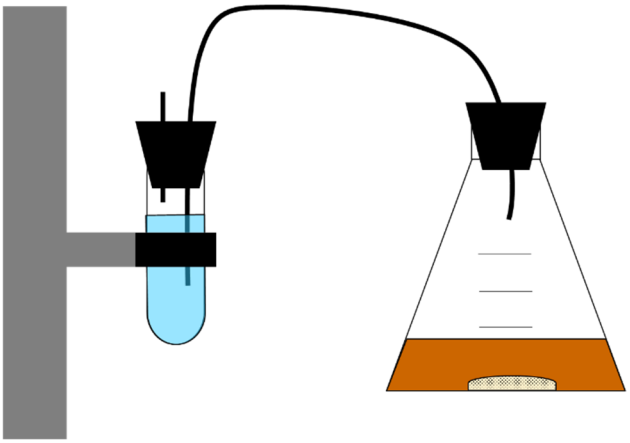

Figure 3.3-1: An illustration of the fermentation apparatus

The substrates which had not previously been pH balanced were pH balanced to 4.5 after treatment, using dilute HCl and NaOH, and then transferred to the Erlenmeyer flasks for fermentation. The substrates which were previously balanced were transferred over without balancing the pH a second time. 0.10 g of dry biofuel grade yeast were added to each Erlenmeyer flask to initiate the fermentation reaction. The Erlenmeyer flasks were then sealed and allowed to ferment over 3-5 days at room temperature. After fermentation, the reactions were filtered three times, first by gravity filtration, second by syringe through a 45 µm filter, and third by syringe through a 22 µm filter. After filtering, n-propanol was added to the fermented solution to create a solution of 10 % n-propanol by volume in the fermented solution as an internal standard for the GC analysis.

3.4. Determination of Material Present

Determination of Sugars Present In Post-Treatment Solution Using HPLC-MS

The liquid chromatograph used in this experiment was a Shimadzu LCMS-2020, which was had an atmospheric-pressure chemical ionization mass spectrometer. The column had a length of 50 mm and a diameter of 4.6 mm, with Shimadzu C18 as the packing material. A mixture of acetic acid and methanol were used as the mobile phase. Flow rates of 0.16 mL/min of 0.1% acetic acid and 0.04 mL/min of methanol were maintained by the chromatograph. The pressure was also maintained to stay below 3000 psi. Liquid nitrogen was used as the drying agent for the mass spectrometer. An autosampler was used to collect data on each solution, using 1.5 mL 105 rack vials, with a volume of 5 µL for each sample. The end time was set to 10 minutes.

In order to characterize the material present in digested biomass, an HPLC-MS protocol was developed. A set of standards were made, using glucose in 100 mL water. Five

concentrations of glucose in water were selected, and these solutions were made. The following concentrations used for this experiment are listed in the table below. Chromatograms were generated for each solution, and mass spectra were also generated. Positive and negative ion mode mass spectra were collected for each sample.

Table 3.4-1: Masses and concentrations of glucose in each standard solution of 100 mL water

Standard	**Glucose added (mg)**	**Concentration (M)**
1	0	0
2	15	8.33E-04
3	40	2.22E-03
4	58	3.22E-03
5	78	4.33E-03

Determination of Ethanol Using Gas Chromatography

The gas chromatograph used in this experiment was a Shimadzu GC-2014 chromatograph which used flame ionization detection. Hydrogen and compressed air were used as the fuel for the FID, and helium was used as the mobile phase. The column temperature was set at 185 °C, and the injector was set at 200 °C. A DC200 column was used, which had a length of 4 feet, and an outer diameter of 0.125 inches. The flow rate was set at 20 mL/min.

In order to determine the amount of ethanol obtained from fermentation, it was first necessary to create a calibration curve using solutions of 10% n-propanol in ethanol and water. Five concentrations of 95% ethanol in water were selected, and solutions of 10% n-propanol were made for each solution. Chromatograms were generated for each solution, and from the resulting peak areas, a series of points were used to create a calibration curve. This calibration

curve was previously generated from past experiments, with the graph shown in **Figure 3.4-1** below. The data for the calibration curve are also tabulated in **Appendix B.2**.

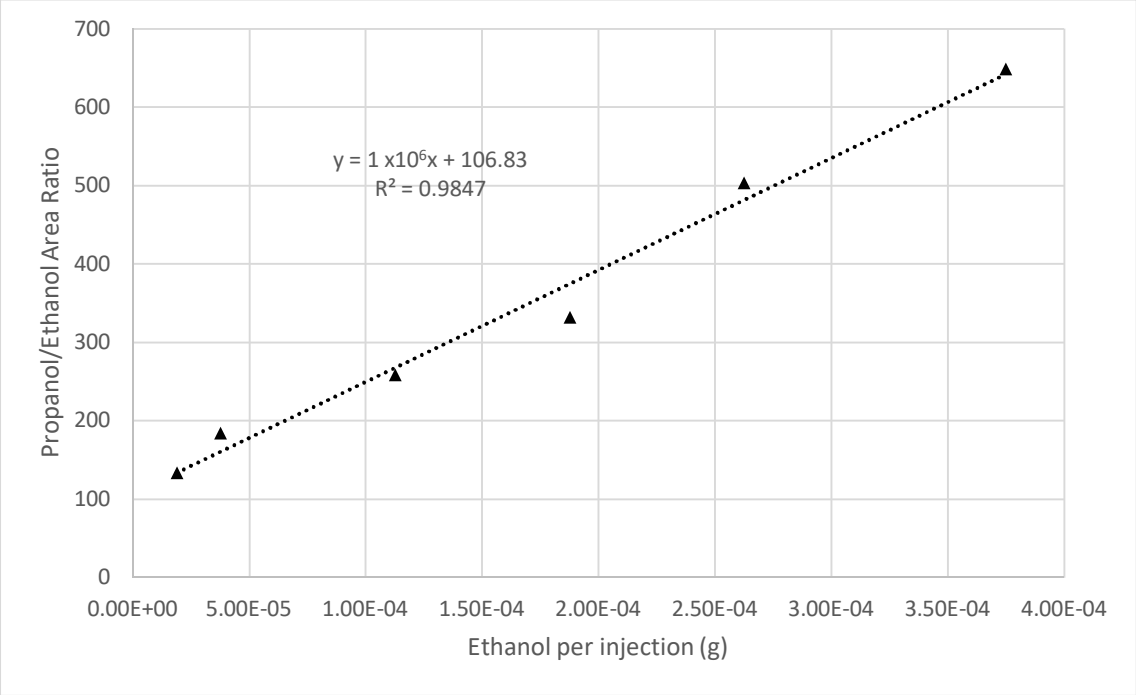

Figure 3.4-1: The GC calibration curve

For the gas chromatography analysis of the fermented product, a mixture of hydrogen and air was made by varying the pressures of the gas cylinders. A chromatogram was obtained for each sample, by injecting 2 μL of solution into the chromatograph and allowing it to collect the necessary data to use in the back-calculation to obtain the amount of ethanol in solution. It is important to note that the calibration curve was originally developed by injecting 5 μL, while the fermentation analysis used only 2 μL. Since area ratio of propanol to ethanol is a function of the mass of the two components, the resulting value which is back-calculated from the calibration curve will reflect the mass of the ethanol if it were in a 5 μL solution. From this, the concentration of the solution and true mass can then be obtained.

4. RESULTS

4.1. Synthesis of TEA-OTF

The ^{1}H and ^{13}C NMR spectra can be seen in **Appendix B.1 (Figures B-1 – B-6)**. The ^{1}H NMR spectrum gave peaks indicative of triethylammonium [6]. The peaks are summarized in **Table 4.1-1** below.

Table 4.1-1: ^{1}HNMR peaks corresponding to triethylammonium

δ (ppm)	**Peak splitting**	**# of hydrogens**
6-12	singlet	1
3.1-3.2	quartet	2
1.2-1.4	triplet	3

Produced from [**6**].

Expanded views of the ^{1}H NMR spectrum can be seen in **Figures B-2** and **B-3**. The peak at 8 ppm is indicative of the hydrogen bonded to the nitrogen in the triethylammonium ion. Peaks at 1.3 ppm and 3.25 ppm are indicative of the hydrogens connected to the terminal and internal carbons of triethylammonium, respectively. The small peak at 4.8 ppm is indicative of water still present in the ionic liquid, the peak at 7.45 ppm is attributed to impurities in the $CDCl_3$, and the peaks at 2 and 2.5 ppm may be attributed to other impurities or starting materials still present [6]. In the ^{13}C NMR there are two main peaks of focus which can be seen in full view in **Figure B-4**, or in expanded view in **Figures B-5** and **B-6**. The peak at 46 ppm is indicative of the carbons connected to the nitrogen of triethylammonium, and the peak at 8 ppm is indicative of the terminal carbons. The remaining peaks may likely be attributed to small amounts of impurities in the ionic liquid. Based on the experimental procedure, the impurities in

question are likely water and diethyl ether that have not been fully removed from the ionic liquid after separation.

4.2. Thermodynamic Analysis

Interaction between Ionic Liquid and Carbohydrates

Renderings of the most stable configurations of TEA-BS and TEA-OTF with hydrogen bonds can be seen in **Figures A-1** and **A-2**, respectively. **Table 4.2-1** below gives the change in energy of mixing of the ions, along with the interatomic distances of the relevant hydrogen bonds.

Table 4.2-1: Change in energy associated with the coupling of the IL's, and the hydrogen bonding distance.

IL	**ΔU (kJ/mol)**	**Distance (Å)**
TEA-BS	-24.20	1.916
TEA-OTF	-17.63	1.957

The change in energy is one way of determining the favorability of the two ions mixing together, and the stability of the configuration determined by Spartan. The quantum mechanical calculations indicate that the TEA-BS is more stable in the configuration illustrated in **Figure A-1**, than that of TEA-OTF, illustrated in **Figure A-2**. Furthermore, the hydrogen bond length is shorter for TEA-BS than TEA-OTF. One factor that may affect this result is the electron-withdrawing fluorine groups present on the adjacent carbon in the triflate, and as a result, the oxygen exhibits less of a negative charge. The interactions of the triethylammonium with the hydroxy groups associated with the ring of the glucose monomer are illustrated in **Appendix A.2**. **Table 4.2-2** summarizes the results.

Table 4.2-2: Change in energy associated with the coupling of the triethylammonium ion with the hydroxy groups of glucose, and the hydrogen bonding distances associated with them.

-OH group	**$\Delta\underline{U}$ (kJ/mol)**	**Distance (Å)**
1 (anomeric)	-15.32	2.031
2	-14.34	2.045
3	-14.18	2.022
4	-24.55	1.955

Illustrations of the glucose ring interacting with the triethylammonium ion are depicted in **Figures A-3 – A-6**, with each of the carbons labeled as shown in the **Table 4.2-2**. The data show that the most favorable location for the triethylammonium ion is near the fourth carbon of the glucose ring, with mixing energy of -24.55 kJ/mol. This can prove to be an important result, as the oxygen associated with the fourth carbon is responsible for the linkage between glucose monomer units in the cellulose polymer. Furthermore, it was shown that the association of the triethylammonium with the glucose at this site had a greater negative energy than the association of both the TEA-BS (with a net energy of -0.35 kJ/mol) and TEA-OTF (with a net energy of -6.92 kJ/mol). These findings could help explain why ionic liquids are able to assist in disrupting the bonds in the cellulose polymer, and can ultimately lead to the development of ionic liquids that are even more effective in dissolving the polymer. The high stability of the coordination of triethylammonium with bisulfate as opposed to the coordination with glucose is also consistent with some of the findings that the bisulfate ionic liquid was the least effective in yielding ethanol as discussed in later sections. Likewise, this could also explain why TEA-OTF was the most effective in yielding ethanol.

Flory-Huggins Mixing Parameters

In order to obtain numerical results for the thermodynamic analysis, it was necessary to assume the number of moles of polymer were equal to that of the solvent. The purpose of

assuming an equimolar solution was to simplify the computationally intensive quantum mechanical calculation as much as possible by only building one of each necessary molecule. The second important assumption was that changes in volume and pressure upon mixing were considered to be negligible which allowed changes in enthalpy and internal energy to be the same, thus simplifying the derivation of free energy of mixing. The mixing process is considered to be dilute in aqueous solution, so changes in volume upon mixing may be considered as negligible. After obtaining the change in energy from Spartan, it was then possible to obtain a chi parameter for the system of TEA-OTF and cellulose in aqueous solution using the Flory-Huggins equation. **Table 4.2-3** below indicates these results.

Table 4.2-3: Flory-Huggins solvent mixing parameter for an equimolar solution, as determined by its listed parameters, including energy of mixing which was obtained from quantum mechanical calculations

ΔU_{mix} (kJ/mol)	-160.91
x_P	0.5
x_S	0.5
T (K)	298.15
χ	-259.64761

Quantum mechanical calculations indicate that the change in internal energy is negative, which shows that solvation is potentially favorable. The chi parameter being negative, also indicates that the solution of polymer and solvent is stable [52]. This could prove to be an important first step in future work, which may involve simulations with different polymer lengths, varying temperatures, varying compositions, and different solvents. The heat of reaction of the hydrolysis reaction in the presence of TEA-OTF was also determined, by building each system individually and bringing them together in Spartan, similar to every other quantum mechanical calculation performed in this series of experiments. Quantum mechanical

calculations yielded a value of -51.3 kJ/mol for the change in energy of the hydrolysis reaction. The combined solvation and hydrolysis energy of cellobiose in the presence of the TEA-OTF IL was found to be -212.21 kJ/mol, indicating a favorable solvation and hydrolysis. Calculations are shown in **Appendix C.1**. From the chi parameter, it was then possible to generate a series of data using **Equation 2** to create a curve which indicated the most favorable composition of polymer and solvent. The data are tabulated in **Table A-1** and illustrated graphically in **Figure 4.2-1**.

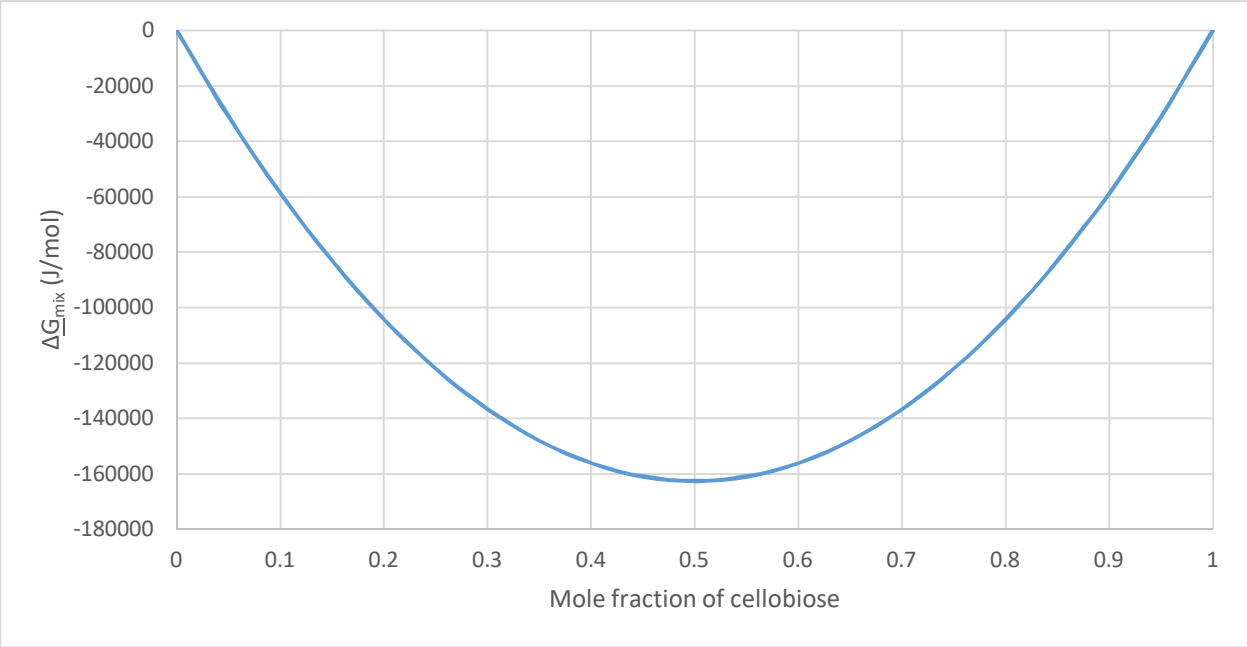

Figure 4.2-1: Change in Gibbs free energy of mixing of cellulose and TEA-OTF as a function of composition at 298.15 K.

Based purely on the quantum mechanical calculations and the Flory-Huggins chi parameter, the magnitude of free energy of mixing associated with cellulose and TEA-OTF is maximized at the 50/50 molar ratio, with a value of -162.628 kJ/mol, and a chi value of -259.64761. All calculations for the free energy can also be found in **Appendix C.1**.

4.3. Feedstock Hydrolysis and Fermentation

It was observed that during the fermentation process, mold had grown in some of the solutions, and some solutions had also attracted fruit flies as evidenced by the large number of dead fruit flies found in close proximity to the fermentation apparatuses, which can be seen in the preliminary fermentation trials as shown in **Figures 4.3-1 and 4.3-2**. Unfortunately, this implies that the seals on some of the flasks were not perfectly tight, which allowed bacteria to enter through the air, as well as allowing volatile chemicals to escape which likely attracted the fruit flies. On a more positive note, however, the presence of microorganisms in the form of mold, as well as the presence of fruit flies also implies that the cellulose was able to break down into fermentable sugars [53]. In addition, the fermented solutions gave off an odor that was similar to that of fermented sugars and ethanol. In future trials, special measures were taken to ensure the seals on the flasks were tight as to avoid this incident again. After taking careful measures to seal the flasks, fruit flies were no longer attracted, however occasional mold growth still occurred, especially in trials that contained corn husks, which may be attributed partially to lack of perfect sterility in the laboratories.

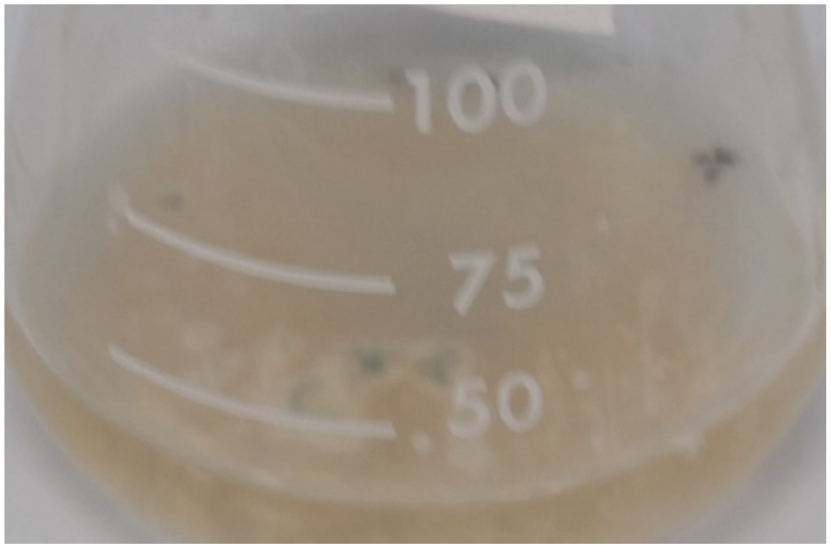

Figure 4.3-1: Image of mold growing in one of the fermentation flasks after fermenting for three days

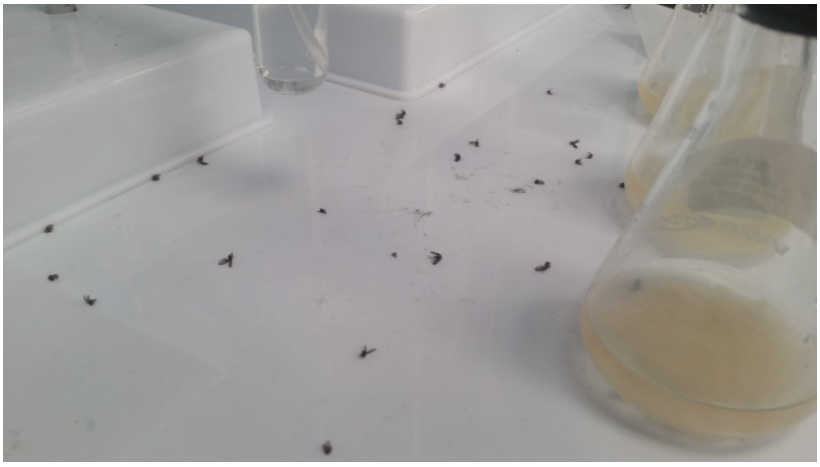

Figure 4.3-2: Image of the fruit flies found near the fermentation apparatuses after fermenting for three days.

4.4. Determination of Material Present

Determination of Sugars Present In Post-Treatment Solution Using HPLC-MS

The chromatograms from the HPLC experiments can be found in **Appendix B.5 (Figures B-26 – B-35)**. It was not until the concentration of 40 mg glucose that the peaks began to exhibit Gaussian behavior, which was shown further as the concentration increased. A peak which is likely indicative of glucose is consistently present at approximately 3 min. The mass spectra show several peaks which could not be identified in the spectral databank, and which likely do not correspond to glucose. A mass spectrum of glucose from literature is shown below in **Figure 4.4-1**, along with the spectra for the 15 mg solution in **Figure 4.4-2** for comparison.

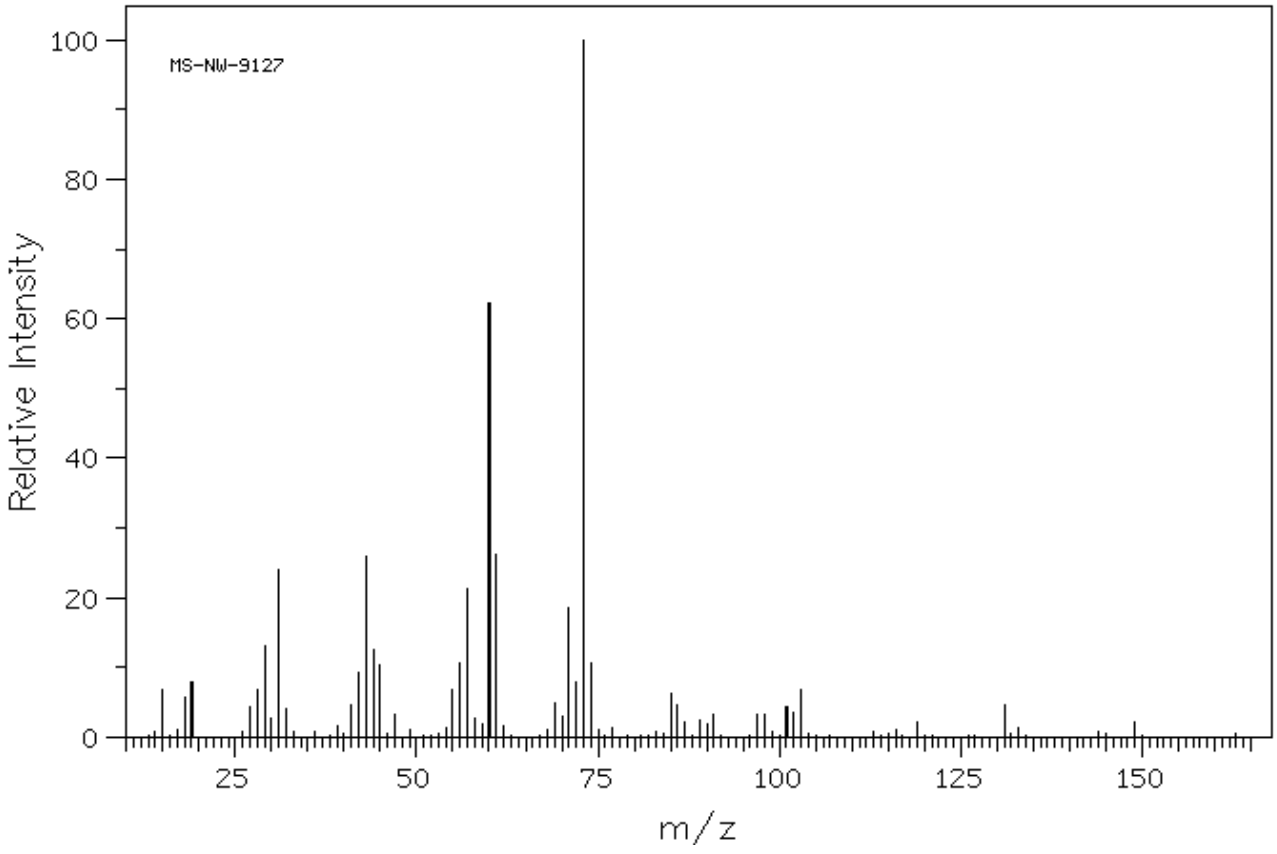

Figure 4.4-1: Mass spectrum of glucose
Obtained from [**54**].

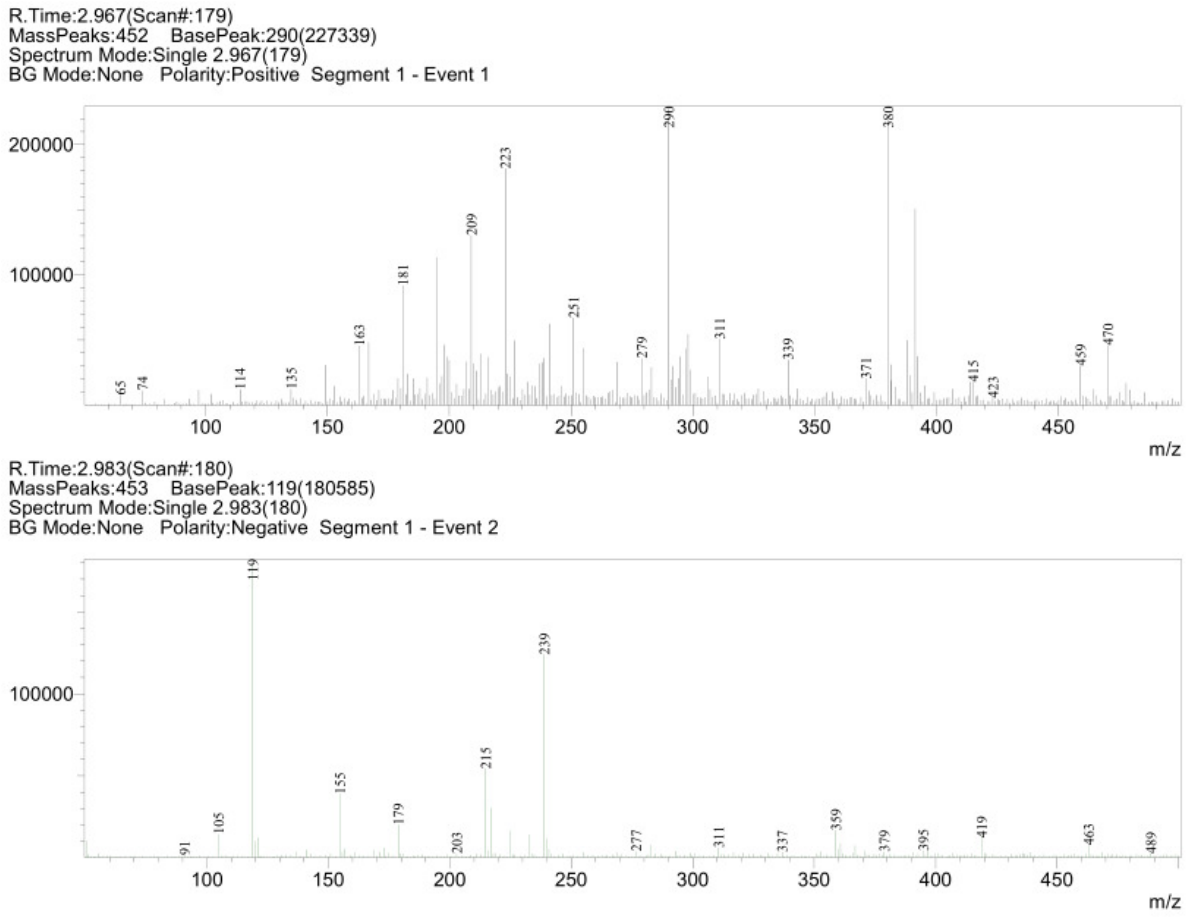

Figure 4.4-2: Positive and negative ion mass spectra for the solution containing 15 mg glucose in 100 mL water

An investigation later found that an experiment from a previous research group had necessitated the use of the liquid chromatograph and that some of the analyte from that experiment was still present in the columns. This means that the results for the HPLC-MS experiment are inconclusive, and future work will need to be done to obtain a calibration curve which can characterize the content and amount of the carbohydrates present in hydrolyzed biomass.

Determination of Ethanol Using Gas Chromatography

The gas chromatograms along with all peaks, heights, and areas, can be found in **Appendix B.3**. A table which summarizes the peak area data, calculated area ratios, and ratios that have been scaled up in order to utilize the calibration curve can be found in **Table B.4**. Using the

calibration curve as previously described in the experimental section, the ethanol concentrations were able to be back-calculated using the ratios of the areas of the peaks present in the chromatograms. The calculated masses are shown in **Table B-5** along with their scaled-down values based on the actual volume injected. A table summarizing the initial results can be found in **Table B-6**. It was later found that possible outliers were present. A Grubbs analysis determined the third trial of the combined TEA-OTF and enzyme treatment of corn husks was outside the standard significance level of 5%. Therefore, it was rejected and new values for ethanol mass and concentrations were obtained. These results are summarized in **Table 4.4-1**.

Table 4.4-1: Average data for each of the fermentation trials, along with the scaled down mass based on the actual volume in the chromatograph

Treatment Method(s)	**Substrate**	**Mass EtOH (g) (Calibration curve)**	**Concentration of EtOH**	**Mass EtOH (g) (scaled down)**
Control	Husk	$3.39 \pm 0.76 \times 10^{-4}$	9.03 ± 2.04 %	$1.36 \pm 0.30 \times 10^{-4}$
Control	Paper	$1.25 \pm 2.57 \times 10^{-4}$	3.34 ± 6.85 %	$5.00 \pm 10.3 \times 10^{-5}$
Cellulase	Paper	$1.61 \pm 0.65 \times 10^{-4}$	4.29 ± 1.74 %	$6.44 \pm 2.60 \times 10^{-5}$
TEABS	Husk	$1.35 \pm 6.07 \times 10^{-5}$	0.36 ± 1.62 %	$5.40 \pm 24.3 \times 10^{-6}$
TEAOTF	Husk	$3.96 \pm 0.41 \times 10^{-4}$	10.57 ± 1.09 %	$1.58 \pm 0.16 \times 10^{-4}$
TEAOTF + Cellulase	Husk	$4.66 \pm 0.01 \times 10^{-4}$	12.43 ± 0.03 %	$1.86 \pm 0.003 \times 10^{-4}$

All sample calculations can be found in **Appendix C.1** and **C.2**. From the chromatograms, it was determined the biomass treatment of corn husks with TEA-OTF and cellulase enzyme yielded the highest concentration of ethanol, while the treatment method which utilized corn husks and TEA-BS yielded the least. The difference in yield for these IL's may be partially explained by the thermodynamics of the coordination of triethylammonium and bisulfate as previously described. Another factor, however, may be contributing to the lower yield. The bisulfate anion may be interfering with the enzymes present in the yeast [2,11,15,29]. This may explain why TEA-BS had such a low yield, even relative to paper. The control

treatment was able to extract almost three times as much fermentable sugars from corn husks as paper. One factor which would contribute to this may be the trace chemicals present in the paper. One of the steps in creating paper involves treating it with numerous dyes, bleaches, and other additives, which may still be present in trace amounts in the paper [31,55], and may inhibit or even deactivate the yeast. It was shown that the cellulase was able to assist in digesting the paper, as indicated by the increased ethanol content. In the table, it can also be shown that while the TEA-OTF alone was able to extract a significant amount of fermentable sugars from corn husks, the cellulase enzyme with the ionic liquid is able to increase the yield of ethanol by a small percentage. This furthermore shows that the cellulase enzyme is compatible with the IL to a certain extent. This could prove useful for future experiments regarding IL-assisted cellulose digestion, as it negates the need for an extra separation step, saving time and resources downstream.

5. CONCLUSIONS AND FUTURE WORK

5.1. Conclusions

A series of experiments were performed to compare the digestion of processed and unprocessed biomass. A synthesis of TEA-OTF was performed, and was successful, with minimal impurities and spectral evidence of synthesis.

The thermodynamic analyses of the mixing of the ions in the ionic liquid for TEA-BS and TEA-OTF were performed, and it was determined that triethylammonium was able to coordinate better with the 4-carbon hydroxy group on glucose than with the anion portions of the ionic liquids. The same site that was the most favorable with glucose is also one of the linkage sites for cellulose. It was also determined, however, that the coordination with triflate was significantly less favorable than the bisulfate, which may be justified, in part, by the electron-withdrawing ability of the fluorine groups on the neighboring carbons of the triflate anion, contributing to a reduced negative charge, and thus, a less stable bond and a greater hydrogen bonding distance. This also helps to explain the significant difference in ethanol yield for these IL's. The use of extended quantum mechanical simulations to assess the solvation and subsequent hydrolysis of cellulose, as approximated by cellobiose, in TEA-OTF was performed. Results showed that solvation is favored at all compositions and that the solvation is stable at 298.15 K. The hydrolysis was also shown to be favored.

A series of digestive treatments of processed and unprocessed lignocellulosic biomass using cellulase enzymes, ionic liquids, and microwave radiation, and subsequent fermentation was

performed. Fermentation of biomass was confirmed by the visual evidence of organisms in the presence of fermentation, which included mold and fruit flies.

A protocol towards the development of an HPLC calibration curve in order to quantify the content of fermentable sugars present and determine the makeup of these sugars was attempted. Glucose was visible from the HPLC curve; however, the curve did not show proper Gaussian behavior until higher concentrations were used, and furthermore, the mass spectra did not match literature spectral data for glucose. The results were inconclusive, and will likely be a point of focus in future work.

Finally, the fermented substrates were processed via GC and analyzed using established calibration curve data to determine the mass of ethanol present in each injection and the concentration of ethanol present in solution. Between processed and non-processed biomass, under the same conditions, the unprocessed corn stover had a greater yield than the processed paper. The fact remains, however, that paper can still be biologically processed to form biofuels. This was also evidenced by the increased yield from the treatment of paper with cellulase enzyme. Between the two protic ionic liquids used in these experiments, TEA-OTF gave a much higher yield than TEA-BS, which resulted in the lowest amount of ethanol yielded. The unusually low yield from TEA-BS could possibly be explained by the thermodynamic analysis and potential enzymatic interference in the yeast. Finally, it was shown that cellulase is compatible with the triflate anion to a certain extent, as evidenced by the increased yield of ethanol from the IL treatment alone.

5.2. Future Work

The synthesis of protic ionic liquids has been shown to be successful. However, they are also very specialized, depending on the components. Future experiments in IL synthesis may

involve using different cations, quaternary ammonium salts with different substituents, or different anion components. These could be used to build a library of ionic liquids which may have applications in other fields as well.

The thermodynamics of the mixing of ions in IL systems have the potential to be an excellent predictor of solvation potential. Therefore, it is important to develop an accurate quantum-mechanical basis from which one can obtain these thermodynamic parameters. Processing limitations can greatly affect the degree of accuracy of the system from which thermodynamic parameters are obtained. As technology improves and computers become more powerful more intensive quantum mechanical simulations can be performed. Future experiments may focus more on the coordination of the IL with oligomers of cellulose instead of the glucose monomer, or with systems that have multiple cellulose chains. Such as with the synthesis of new IL's with the intent to create a library of IL's, it is also possible to calculate thermodynamic parameters for these IL's, including the Flory-Huggins mixing parameters. Experiments may also involve the determination of true thermodynamic parameters, using analytical techniques such as calorimetry.

Another important focus for future work is the development of a calibration curve using HPLC and mass spectrometry. This is important because it would allow for improved quantification of the digestion of lignocellulosic biomass. By using mass spectrometry techniques, one can obtain the true chemical makeup of unknown compounds, including those present in post-digestion solution. If these compounds are separable by HPLC, then one can also quantify the amounts of materials present, using a calibration curve, much like the GC calibration curve used in this paper.

LIST OF REFERENCES

[1] Guo, M.; Song, W.; Buhain, J. *Renew. Sustain. Energy Rev.* **2015**, *42*, 712–725.

[2] Engel, P.; Mladenov, R.; Wulfhorst, H.; Jäger, G.; Spiess, A. C. *Green Chem.* **2010**, *12* (11), 1959.

[3] Sims, R. E. H.; Mabee, W.; Saddler, J. N.; Taylor, M. *Bioresour. Technol.* **2010**, *101* (6), 1570–1580.

[4] Naik, S. N.; Goud, V. V.; Rout, P. K.; Dalai, A. K. *Renew. Sustain. Energy Rev.* **2010**, *14* (2), 578–597.

[5] *From 1st- to 2nd-Generation Biofuel Technologies*; International Energy Agency Bioenergy, 2008; p 124.

[6] Clark, S. Ionic Liquids as Solvents for the Digestion of Biomass for Fuel Production, Rose-Hulman Institute of Technology, 2016.

[7] Aro, E.-M. *Ambio* **2016**, *45* (S1), 24–31.

[8] Albert, J.; Wasserscheid, P. *Green Chem* **2015**, *17* (12), 5164–5171.

[9] Kuhad, R. C.; Gupta, R.; Singh, A. *Enzyme Res.* **2011**, *2011*, 1–10.

[10] Havlík, P.; Schneider, U. A.; Schmid, E.; Böttcher, H.; Fritz, S.; Skalský, R.; Aoki, K.; De Cara, S.; Kindermann, G.; Kraxner, F.; Leduc, S.; McCallum, I.; Mosnier, A.; Sauer, T.; Obersteiner, M. *Energy Policy* **2011**, *39* (10), 5690–5702.

[11] Gladden, J. M.; Park, J. I.; Bergmann, J.; Reyes-Ortiz, V.; D'haeseleer, P.; Quirino, B. F.; Sale, K. L.; Simmons, B. A.; Singer, S. W. *Biotechnol. Biofuels* **2014**, *7* (1), 15.

[12] Ocreto, M. B. *USM RD J.* **2013**, *21* (1), 1–20.

[13] Martin, M. A. *New Biotechnol.* **2010**, *27* (5), 596–608.

[14] Marshall, L.; Sugg, Z. *Corn Stover for Ethanol Production: Potential and Pitfalls*; 4; World Resources Institute, 2009.

[15] Ungurean, M.; Csanádi, Z.; Gubicza, L.; Péter, F. *BioResources* **2014**, *9* (4), 6100–6116.

[16] Tyner, W. E. *BioScience* **2008**, *58* (7), 646.

[17] *Biofuels*; Tomes, D., Lakshmanan, P., Songstad, D., Eds.; Springer New York: New York, NY, 2011.

[18] *From the Sugar Platform to biofuels and biochemicals*; E4tech, 2015.

[19] Ethanol - Energy Explained, Your Guide To Understanding Energy - Energy Information Administration https://www.eia.gov/energyexplained/?page=biofuel_ethanol_home (accessed Jul 4, 2017).

[20] Biofuels - Second Generation Biofuels http://biofuel.org.uk/second-generation-biofuels.html (accessed Jan 5, 2018).

[21] ICM INC - Ethanol Timeline http://www.icminc.com/innovation/ethanol/ethanol-timeline.html (accessed Aug 12, 2017).

[22] Turning Grass into Gas for Less http://www.nersc.gov/news-publications/nersc-news/science-news/2011/turning-grass-into-gas-for-less/ (accessed Jan 5, 2018).

[23] Simpson-Holley, M.; Higson, A.; Evans, G. *TCE Chem. Eng.* **2007**, No. 795, 46–49.

[24] Kemp, L. *Cellulosic Ethanol from Corn Stover: Can We Get It Right?*; Stashwick, S., Series Ed.; R-15-08-A; Natural Resources Defense Council, 2015; p 26.

[25] Songstad, D.; Lakshmanan, P.; Chen, J.; Gibbons, W.; Hughes, S.; Nelson, R. In *Biofuels*; Tomes, D., Lakshmanan, P., Songstad, D., Eds.; Springer New York: New York, NY, 2011; pp 1–7.

[26] Fan, L.; Gharpuray, M. M.; Lee, Y.-H. *Cellulose Hydrolysis*; Aiba, S., Fan, L., Fiechter, A., Klein, J., Schügerl, K., Series Eds.; Biotechnology Monographs; Springer Berlin Heidelberg: Berlin, Heidelberg, 1987; Vol. 3.

[27] Binder, J. B.; Raines, R. T. *Proc. Natl. Acad. Sci.* **2010**, *107* (10), 4516–4521.

[28] Liebert, T. In *Cellulose Solvents: For Analysis, Shaping and Chemical Modification*; Liebert, T. F., Heinze, T. J., Edgar, K. J., Eds.; American Chemical Society, Series Ed.; American Chemical Society: Washington, DC, 2010; Vol. 1033, pp 3–54.

[29] Ilmberger, N.; Pottkämper, J.; Streit, W. *Catalysts* **2013**, *3* (2), 584–587.

[30] Reese, E. T. *Appl. Microbiol.* **1956**, *4* (1), 39–45.

[31] Tamburini, F.; Kelly, T.; Weerapana, E.; Byers, J. A. *J. Chem. Educ.* **2014**, *91* (10), 1574–1579.

[32] Cellulase - Worthington Enzyme Manual http://www.worthington-biochem.com/cel/default.html (accessed Jun 30, 2017).

[33] Kirk, T. K. In *Microbial degradation of organic compounds.*; Microbiology Series; Marcel Dekker, Inc.: New York, NY, 1984; Vol. 13.

[34] Win, D. *Assumpt. Univ. J Tech* **2005**, *8* (4), 185–190.

[35] *2016 Billion-Ton Report*; U.S. Department of Energy, 2016.

[36] Tenenbaum, D. J. *Environ. Health Perspect.* **2008**, *116* (6), A254–A257.

[37] History of Ethanol Production and Policy — Energy https://www.ag.ndsu.edu/energy/biofuels/energy-briefs/history-of-ethanol-production-and-policy (accessed Jul 3, 2017).

[38] Biofuels - First Generation Biofuels http://biofuel.org.uk/first-generation-biofuel.html (accessed Jan 5, 2018).

[39] Diverting Food to Fuel - NYTimes.com http://www.nytimes.com/imagepages/2011/04/07/world/20110407_cassava_graphic.html (accessed Jan 5, 2018).

[40] Chi, C.; Chang, H.; Li, Z.; Jameel, H.; Zhang, Z. *BioResources* **2012**, *8* (1), 172–181.

[41] Chambers, P. J.; Pretorius, I. S. *EMBO Rep.* **2010**, *11* (12), 914–920.

[42] Lenihan, P.; Orozco, A.; O'Neill, E.; Ahmad, M. N. M.; Rooney, D. W.; Walker, G. M. *Chem. Eng. J.* **2010**, *156* (2), 395–403.

[43] Morey, S. Gas or Vapour Engine. USX4378, April 1, 1826.

[44] History of Biofuels - BioFuel Information http://biofuel.org.uk/history-of-biofuels.html (accessed Jul 3, 2017).

[45] Yinghuai, Z.; Tang, K.; S., N. In *Ionic Liquids - New Aspects for the Future*; Kadokawa, J., Ed.; InTech, 2013.

[46] Zhang, Z.; Zhao, Z. K. *Bioresour. Technol.* **2010**, *101* (3), 1111–1114.

[47] Sasaki, M.; Kabyemela, B.; Malaluan, R.; Hirose, S.; Takeda, N.; Adschiri, T.; Arai, K. *J. Supercrit. Fluids* **1998**, *13* (1–3), 261–268.

[48] Fischer-Tropsch Synthesis https://www.netl.doe.gov/research/coal/energy-systems/gasification/gasifipedia/ftsynthesis (accessed Jun 25, 2017).

[49] *U.S. Billion-Ton Update: Crop Residues and Agricultural Wastes*; U.S. Department of Energy, 2011.

[50] *Spartan '16*; Wavefunction, Inc.: Irvine, CA.

[51] Flory, P. J. *J. Chem. Phys.* **1942**, *10* (1), 51–61.

[52] Shell, M. S. *Thermodynamics and statistical mechanics: an integrated approach*; Cambridge series in chemical engineering; Cambridge University Press: Cambridge, 2015.

[53] Fruit flies – fermented-fruit connoisseurs – are relentless party crashers. *UW News*.

[54] AIST:Spectral Database for Organic Compounds,SDBS http://sdbs.db.aist.go.jp/sdbs/cgi-bin/direct_frame_top.cgi (accessed Jan 6, 2018).

[55] Smith, V. How Paper is Made http://wipapercouncil.org/about-paper/how-paper-is-made/ (accessed Jan 6, 2018).

[56] Density http://macro.lsu.edu/HowTo/solvents/Density%20.htm (accessed Jan 5, 2017).

[57] Grubbs, F. E.; Beck, G. *Technometrics* **1972**, *14* (4), 847–854.

APPENDICES

APPENDIX A– THERMODYNAMIC DATA

Appendix A.1 – Ionic Liquid Interactions

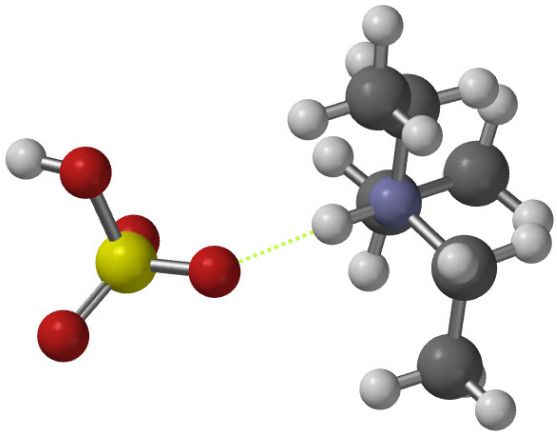

Figure A-1: TEA-BS in its most stable configuration as determined by Spartan. Green dotted line indicates hydrogen bonding.

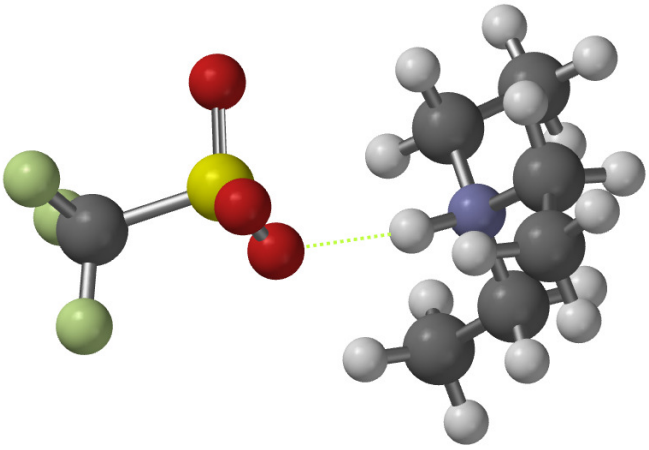

Figure A-2: TEA-OTF in its most stable configuration as determined by Spartan. Green dotted line indicates hydrogen bonding.

Appendix A.2– Solvent-Monomer Interactions

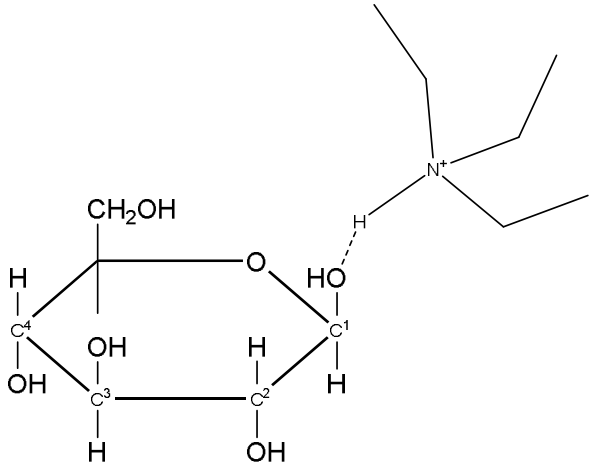

Figure A-3: Simplified drawing of the triethylammonium cation interaction with the hydroxy group associated with the anomeric carbon in β-D-glucose. Dotted line indicates hydrogen bonding.

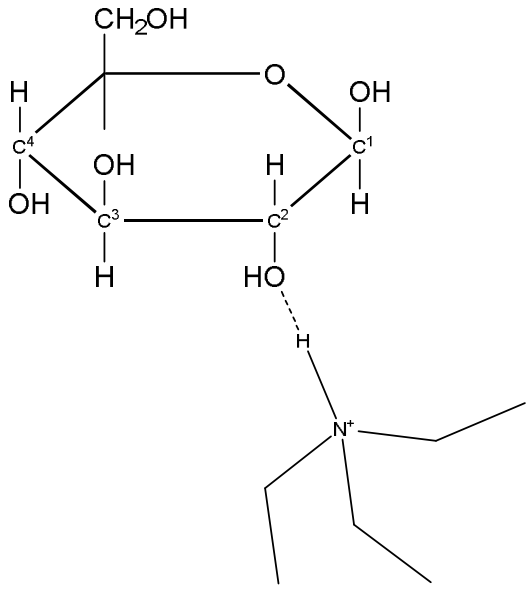

Figure A-4: Simplified drawing of the triethylammonium cation interaction with the hydroxy group associated with the second carbon in β-D-glucose. Dotted line indicates hydrogen bonding.

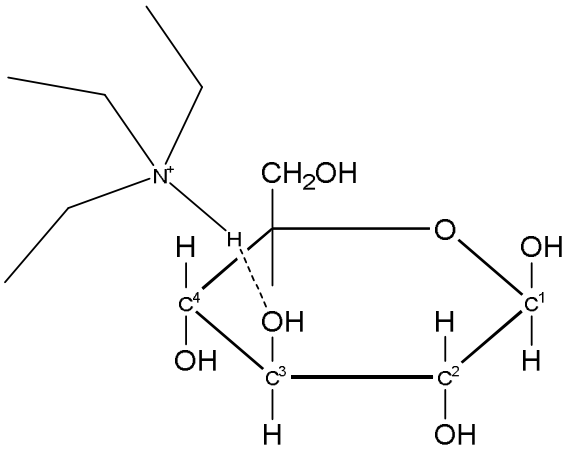

Figure A-5: Simplified drawing of the triethylammonium cation interaction with the hydroxy group associated with the third carbon in β-D-glucose. Dotted line indicates hydrogen bonding.

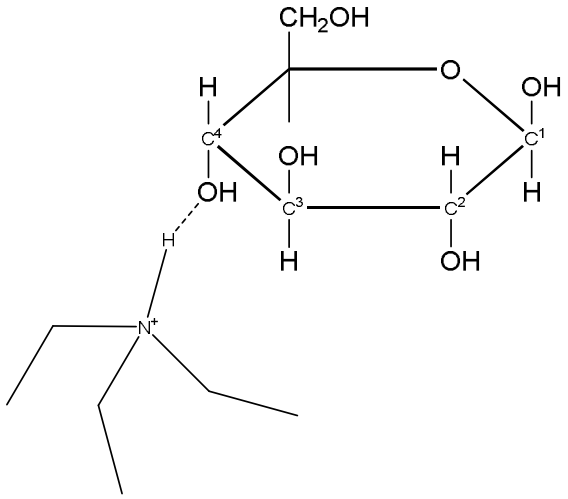

Figure A-6: Simplified drawing of the triethylammonium cation interaction with the hydroxy group associated with the fourth carbon in β-D-glucose. Dotted line indicates hydrogen bonding.

Appendix A.3 – Flory-Huggins Thermodynamic Data

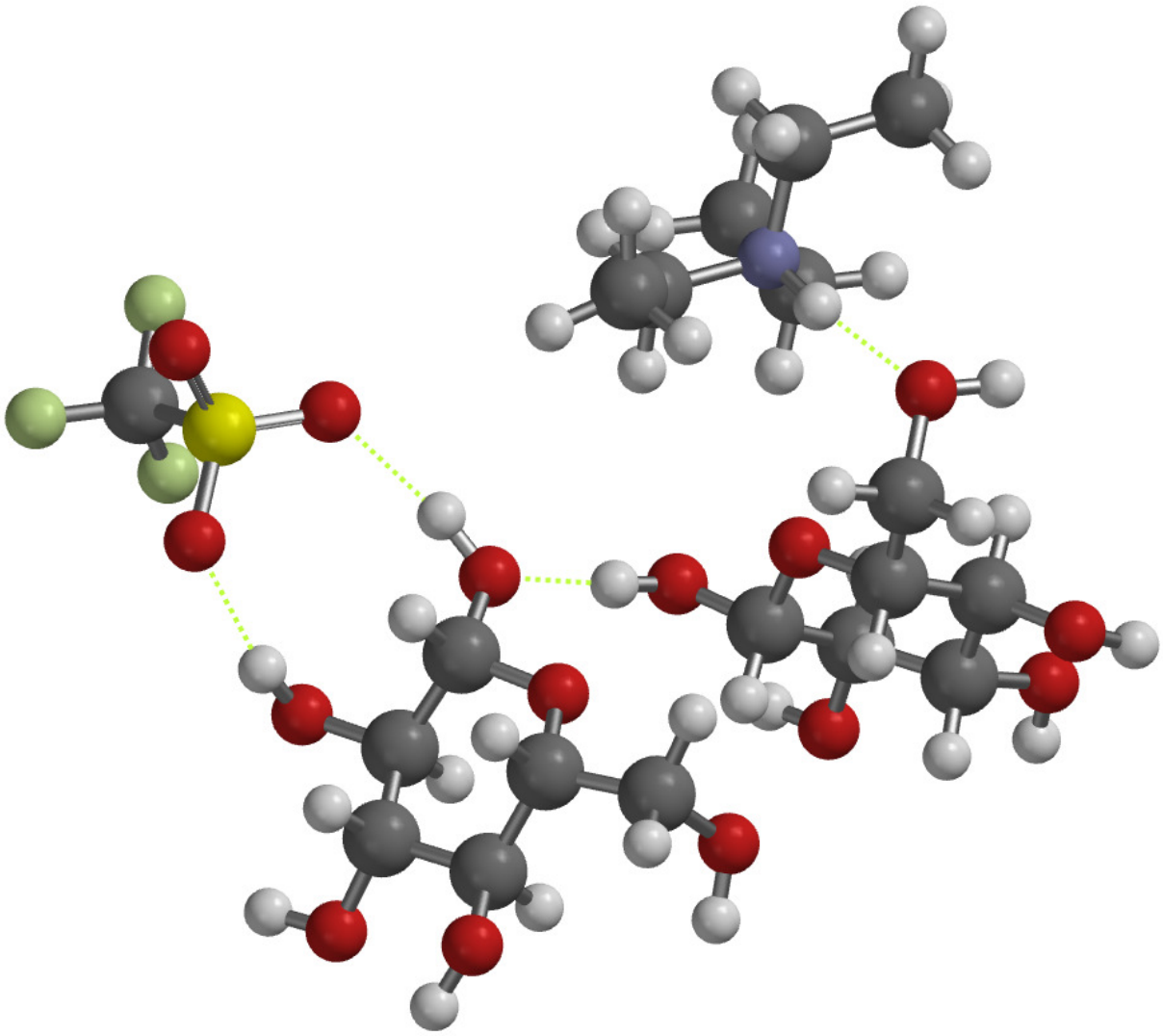

Figure A-7: TEA-OTF interacting with the hydrolyzed glucose in its most stable configuration as determined by Spartan. Green dotted lines indicate hydrogen bonds.

Table A-1: Changes in molar internal energy, entropy, and Gibbs free energy associated with the mixing of cellulose and TEA-OTF based on the quantum mechanical calculations.

X_P	X_S	$\Delta \underline{U}_{mix}$ (J/mol)	$\Delta \underline{S}_{mix}$ (J/mol K)	$\Delta \underline{G}_{mix}$ (J/mol)
0.00	1.00	0	0	0
0.05	0.95	-30572.9	1.650508	-31065
0.10	0.90	-57927.6	2.702826	-58733.4
0.15	0.85	-82064.1	3.514516	-83112
0.20	0.80	-102982	4.160479	-104223
0.25	0.75	-120683	4.675404	-122076
0.30	0.70	-135164	5.078888	-136679
0.35	0.65	-146428	5.383043	-148033
0.40	0.60	-154474	5.595598	-156142
0.45	0.55	-159301	5.721369	-161007
0.50	0.50	-160910	5.76301	-162628
0.55	0.45	-159301	5.721369	-161007
0.60	0.40	-154474	5.595598	-156142
0.65	0.35	-146428	5.383043	-148033
0.70	0.30	-135164	5.078888	-136679
0.75	0.25	-120683	4.675404	-122076
0.80	0.20	-102982	4.160479	-104223
0.85	0.15	-82064.1	3.514516	-83112
0.90	0.10	-57927.6	2.702826	-58733.4
0.95	0.05	-30572.9	1.650508	-31065
1.00	0.00	0	0	0

APPENDIX B– CHROMATOGRAPHY AND SPECTRAL DATA

Appendix B.1 – NMR Spectra

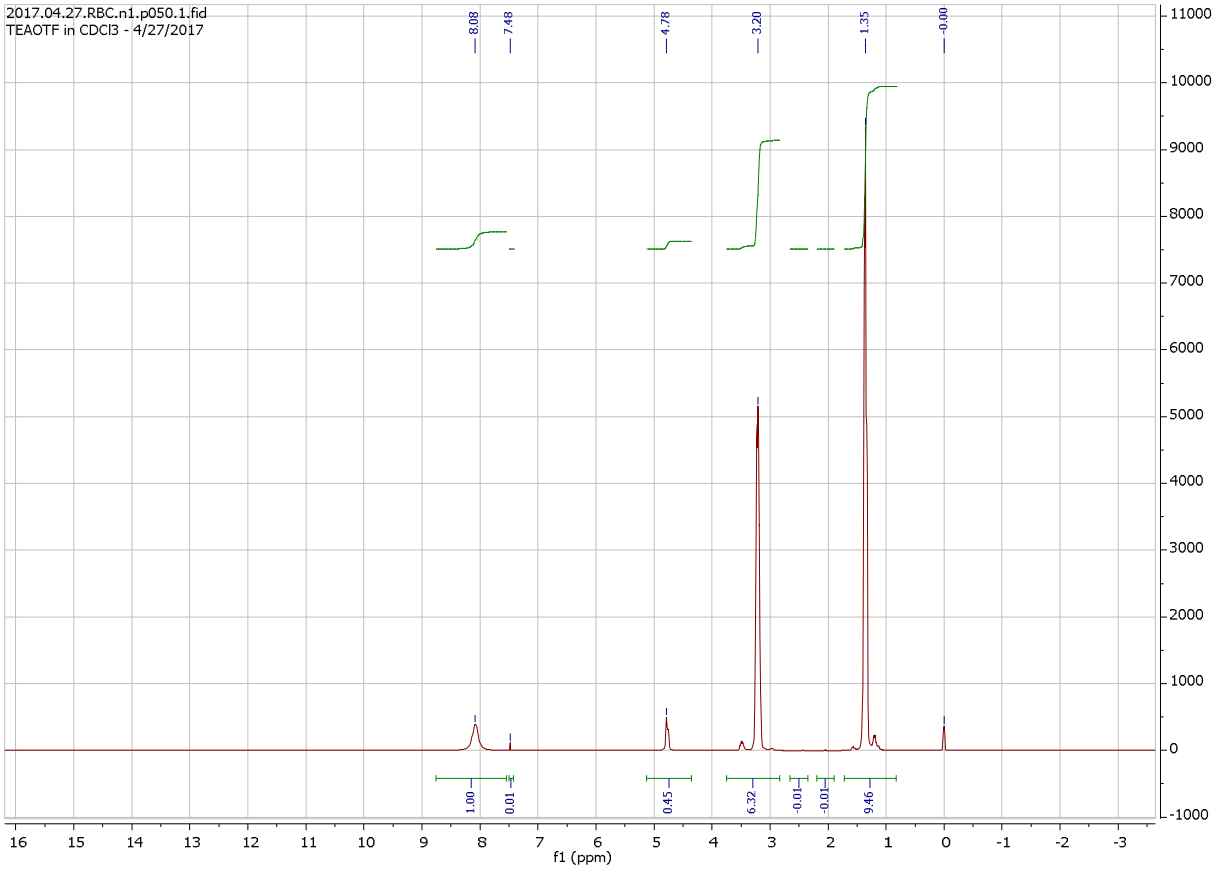

Figure B-1: ^{1}H NMR spectrum for TEA-OTF

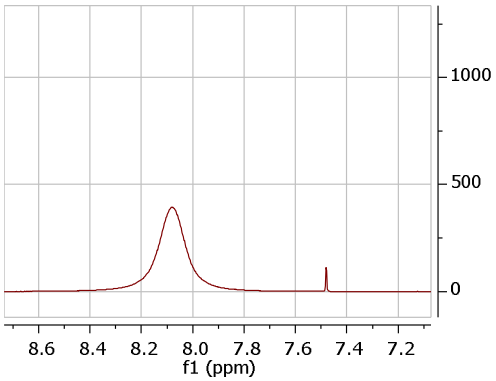

Figure B-2: Expansion of the ^{1}H NMR spectrum showing chemical shifts at 7.5 ppm and 8.1 ppm

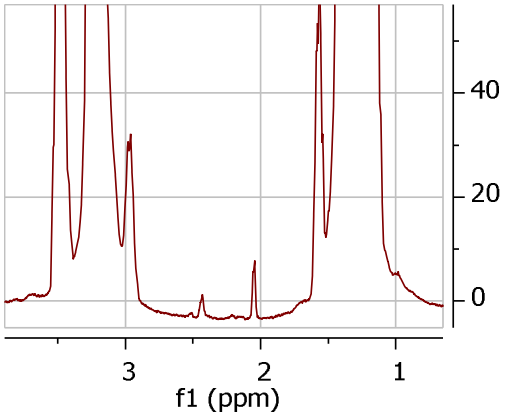

Figure B-3: Expansion of the ^{1}H NMR spectrum showing chemical shifts at 1.3 ppm, 2 ppm, 2.5 ppm, and 3.25 ppm

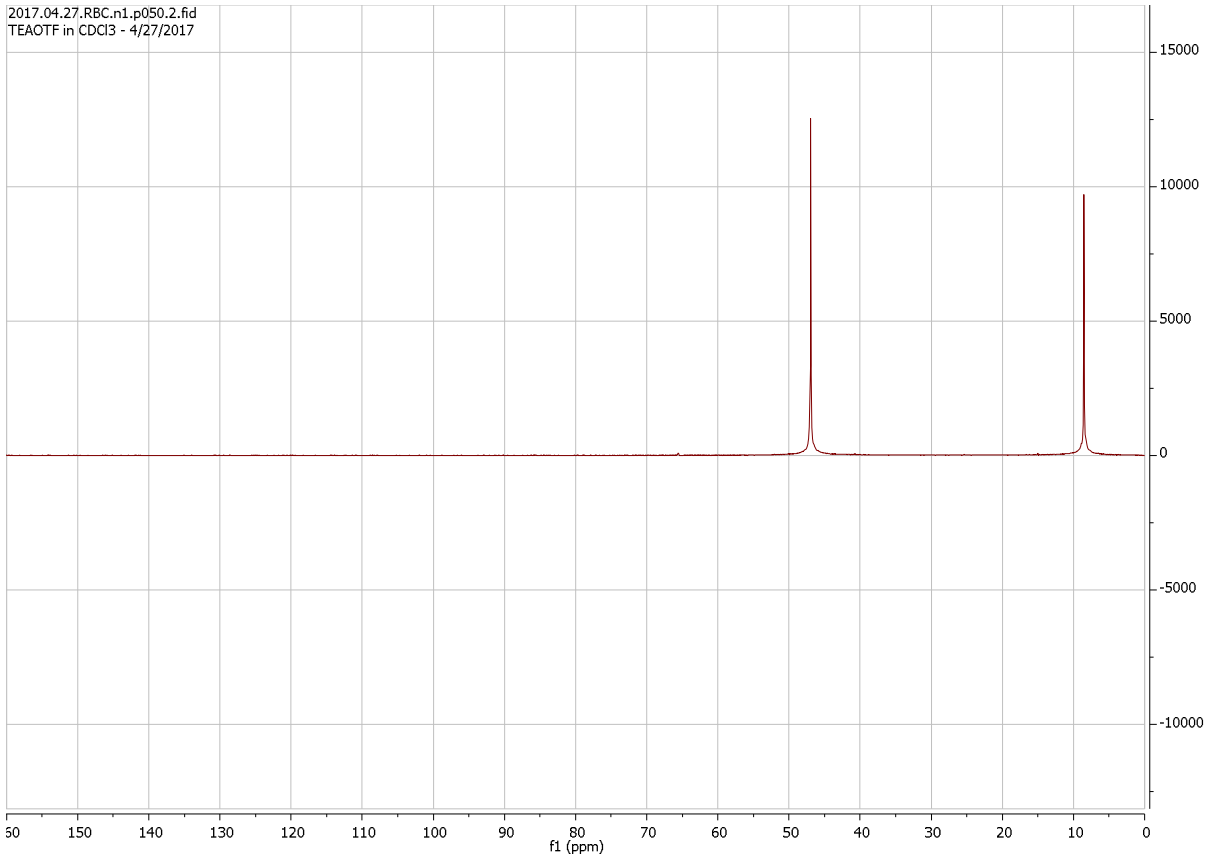

Figure B-4: ^{13}C NMR for TEA-OTF

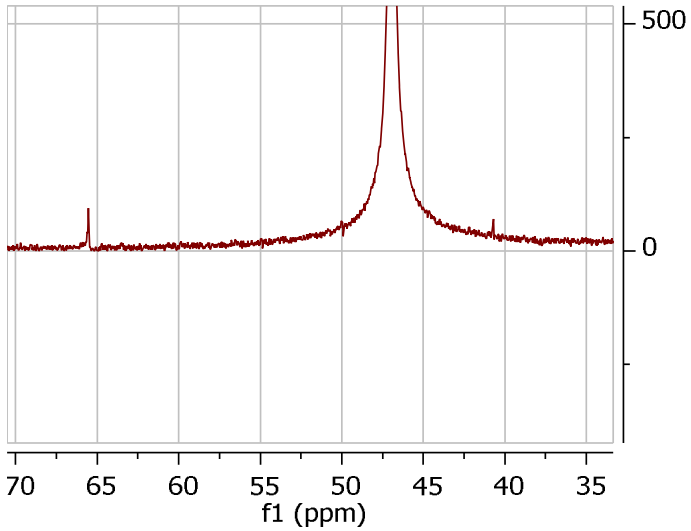

Figure B-5: Expansion of the ^{13}C NMR spectrum showing chemical shifts at 41 ppm, 46 ppm, and 65 ppm

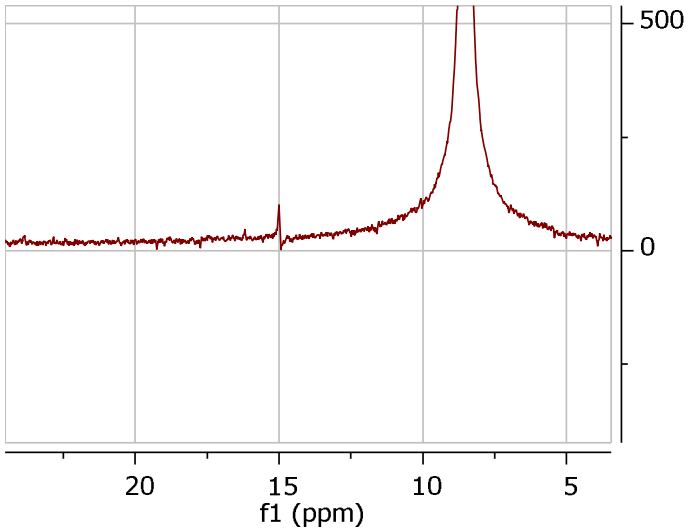

Figure B-6: Expansion of the ^{13}C NMR spectrum showing chemical shifts at 8 ppm and 15 ppm

Appendix B.2 – Calibration Curve Data

Table B-1: Concentrations of ethanol in 10 % n-propanol solution associated with the calibration curve, along with their respective curve areas, masses of ethanol injected, and area ratios.

Concentration EtOH (v/v)	**Area n-PrOH**	**Area EtOH**	**Mass injected (g)**	**PrOH/EtOH Area Ratio**
0.5 %	3147983818	4827645	1.87×10^{-5}	133.5722506
0.5 %	2895102155	4137783	1.87×10^{-5}	133.6413679
0.5 %	2907230135	4893303	1.87×10^{-5}	133.6414782
1 %	3016139760	7851882	3.75×10^{-5}	208.8004096
1 %	2869988136	6972211	3.75×10^{-5}	183.4519195
1 %	3091529152	5596756	3.75×10^{-5}	177.3870905
1 %	2380494884	4367727	3.75×10^{-5}	165.9771482
3 %	3068333668	9095538	1.12×10^{-4}	337.3449342
3 %	3032184543	10384924	1.12×10^{-4}	207.9791478
3 %	3065107278	9623357	1.12×10^{-4}	229.8534824
5 %	3030079807	14511848	1.87×10^{-4}	384.1295323
5 %	2866702629	13783606	1.87×10^{-4}	291.979464
5 %	2912630006	12671681	1.87×10^{-4}	318.5070738
7 %	2801267699	15269765	2.62×10^{-4}	411.6324271
7 %	2780423972	15674331	2.62×10^{-4}	552.3787623
7 %	2742376518	16522615	2.62×10^{-4}	545.0191562
10 %	2847238382	21316092	3.75×10^{-4}	652.074421
10 %	2821896285	21115440	3.75×10^{-4}	699.6747183
10 %	2773284790	20751677	3.75×10^{-4}	594.1242827

Table B-2: Area ratio average data for the calibration curve, along with standard deviation of area ratio, and injected masses of ethanol

Concentration EtOH (v/v)	EtOH injected (g)	PrOH/EtOH Area Ratio	Standard Deviation
0.5 %	1.8744E-05	133.61836	0.03993
1 %	3.7487E-05	183.90414	43.39306
3 %	11.246E-05	258.39252	38.23717
5 %	18.744E-05	331.53869	16.66395
7 %	26.241E-05	503.01011	8.87258
10 %	37.487E-05	648.62447	95.81546

Table B-3: Linear regression data for the calibration curve

Slope	1427537.435
Intercept	106.8274614
R^2 value	0.984738532

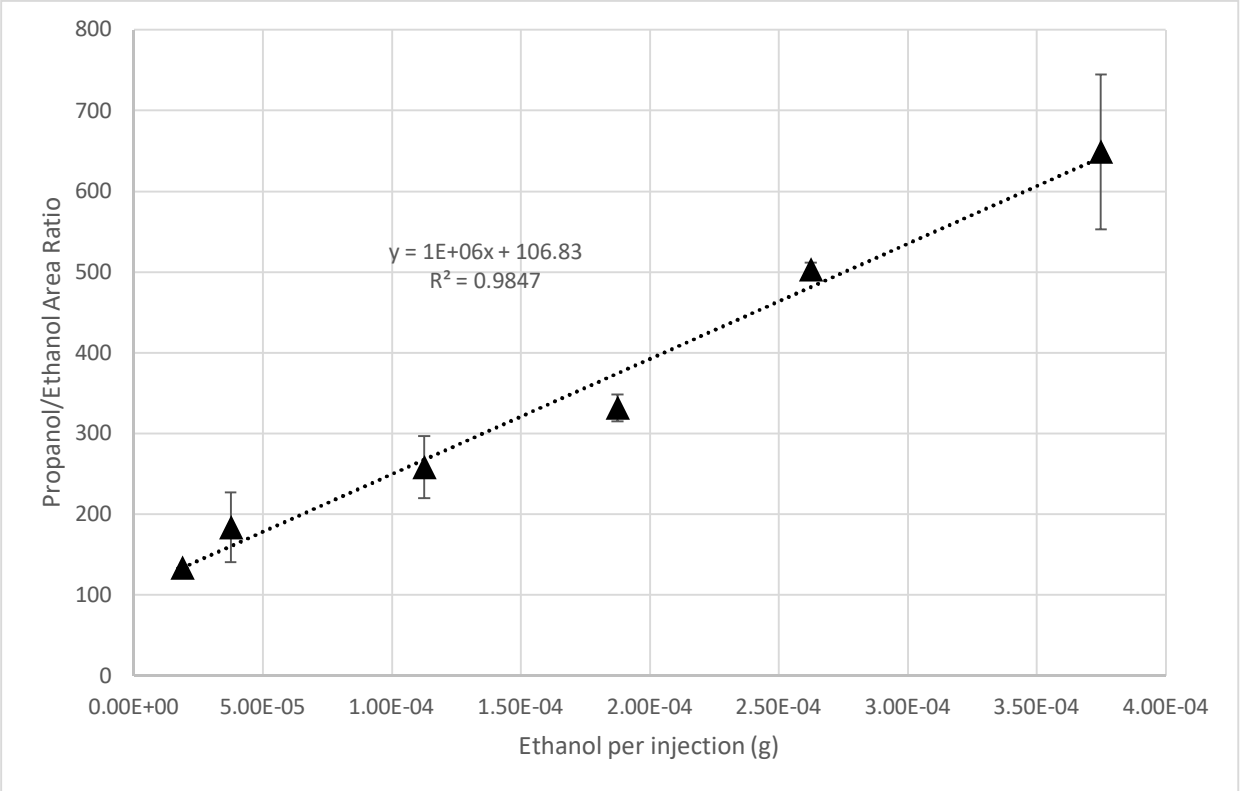

Figure B-7: Calibration curve with the points corresponding to their respective concentrations and calculated masses.

Appendix B.3 – Fermentation Chromatograms

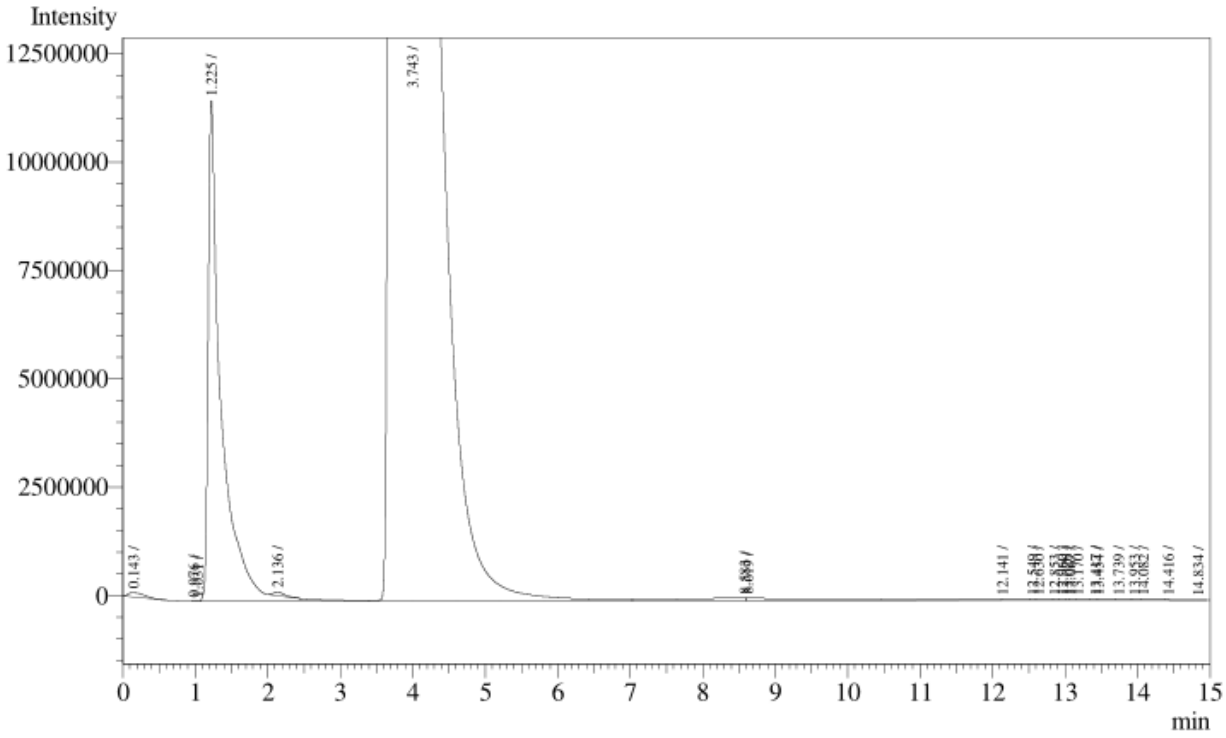

Peak#	Ret.Time	Area	Height	Conc.	Unit	Mark	ID#	Cmpd Name
1	0.143	1701317	104672	0.000				
2	0.976	2270	1209	0.000				
3	1.031	11894	4564	0.000		V		
4	1.225	146385451	11540278	0.000		SV		
5	2.136	900954	86162	0.000		T		
6	3.743	2169564328	81308867	0.000		V		
7	8.583	3848435	52627	0.000		V		
8	8.619	6909796	52566	0.000		V		
9	12.141	364660	16219	0.000		V		
10	12.549	57427	13755	0.000		V		
11	12.630	183173	13487	0.000		V		
12	12.853	62936	11997	0.000		V		
13	12.960	57723	11526	0.000		V		
14	13.026	34452	11245	0.000		V		
15	13.067	54661	11059	0.000		V		
16	13.170	119673	10525	0.000		V		
17	13.417	61949	9625	0.000		V		
18	13.454	139546	9561	0.000		V		
19	13.739	95461	8094	0.000		V		
20	13.953	53629	6817	0.000		V		
21	14.082	98606	6183	0.000		V		
22	14.416	63716	3781	0.000		V		
23	14.834	3990	768	0.000		V		
Total		2330776047	93295587					

Figure B-8: Trial 1 for the microwave control treatment of paper

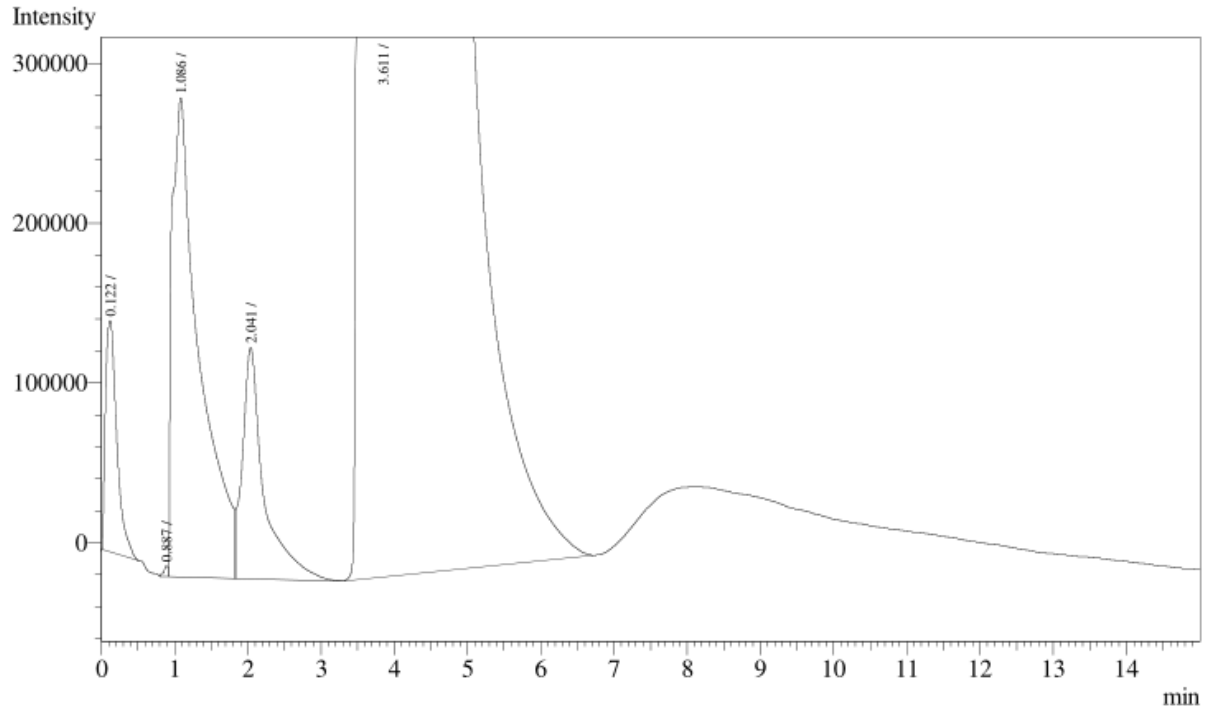

Peak#	Ret.Time	Area	Height	Conc.	Unit	Mark	ID#	Cmpd Name
1	0.122	1560443	144783	0.000				
2	0.887	25041	6491	0.000				
3	1.086	7776584	299989	0.000		V		
4	2.041	2984114	144696	0.000		V		
5	3.611	2196323963	86862107	0.000				
Total		2208670145	87458066					

Figure B-9: Trial 2 for the microwave control treatment of paper

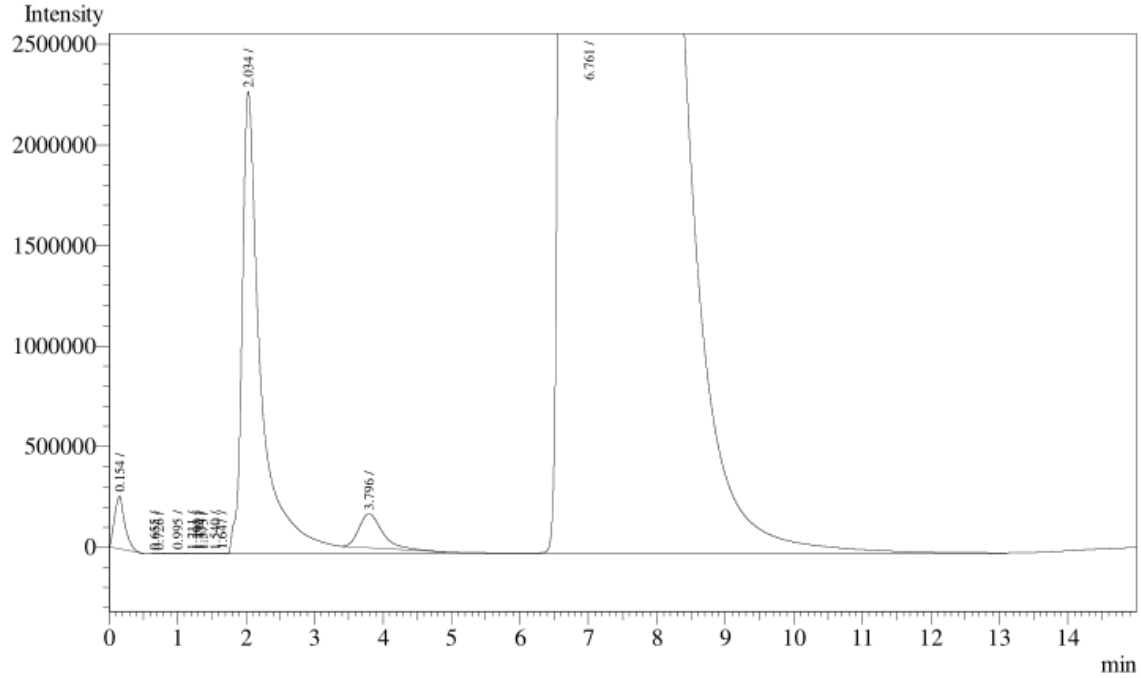

Peak#	Ret.Time	Area	Height	Conc.	Unit	Mark	ID#	Cmpd Name
1	0.154	2706897	263167	0.000				
2	0.655	1763	690	0.000				
3	0.726	3652	1026	0.000		V		
4	0.995	51237	3160	0.000		V		
5	1.211	4794	945	0.000		V		
6	1.290	1922	802	0.000		V		
7	1.334	1954	831	0.000		V		
8	1.373	4698	800	0.000		V		
9	1.540	4721	1190	0.000				
10	1.647	16015	3185	0.000		V		
11	2.034	46756745	2298323	0.000		SV		
12	3.796	4008641	168095	0.000		T		
13	6.761	2124223511	41373344	0.000		SV		
Total		2177786550	44115558					

Figure B-10: Trial 3 for the microwave control treatment of paper

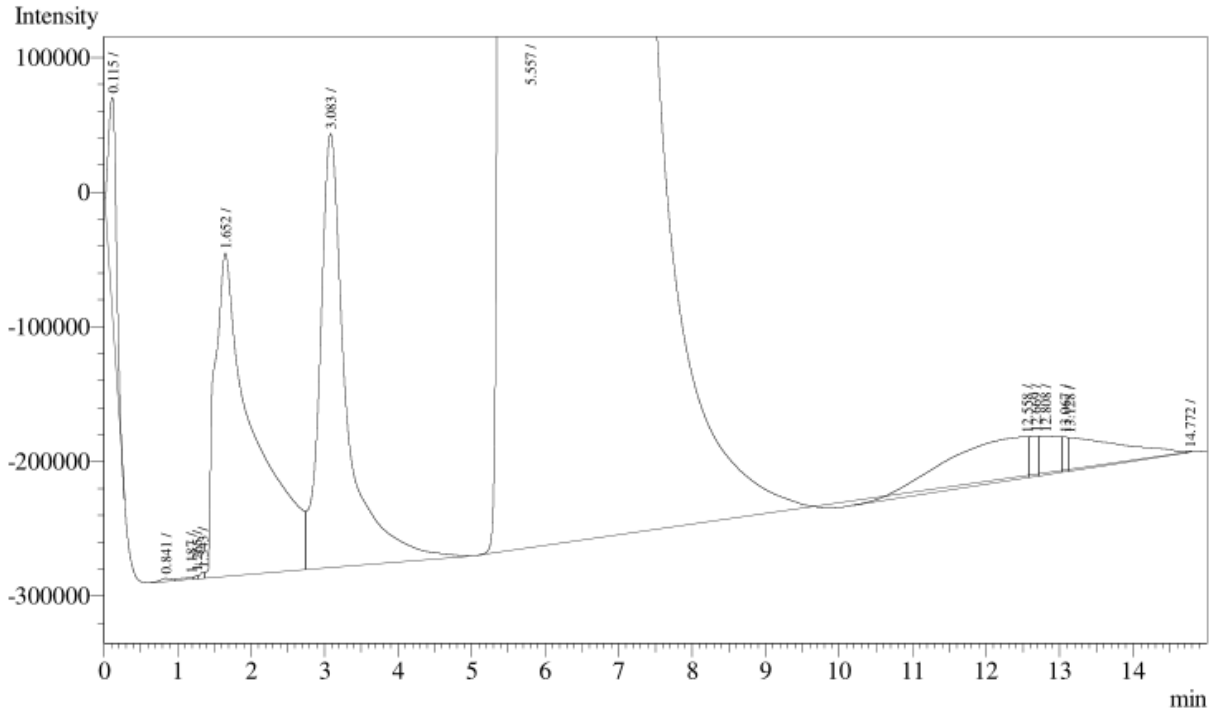

Peak#	Ret.Time	Area	Height	Conc.	Unit	Mark	ID#	Cmpd Name
1	0.115	1205043	162469	0.000				
2	0.841	23943	2354	0.000				
3	1.187	19646	1341	0.000		V		
4	1.265	7020	2346	0.000		V		
5	1.343	20139	4764	0.000		V		
6	1.652	8802318	240054	0.000		V		
7	3.083	8207377	322491	0.000		SV		
8	5.557	2025682351	48949465	0.000		S		
9	12.558	2589305	30510	0.000		T		
10	12.669	250293	29690	0.000		TV		
11	12.808	513822	28591	0.000		TV		
12	13.067	122355	25767	0.000		TV		
13	13.128	1223872	25122	0.000		TV		
14	14.772	1404	218	0.000		TV		
Total		2048668888	49825182					

Figure B-11: Trial 1 for the microwave control treatment of corn husks

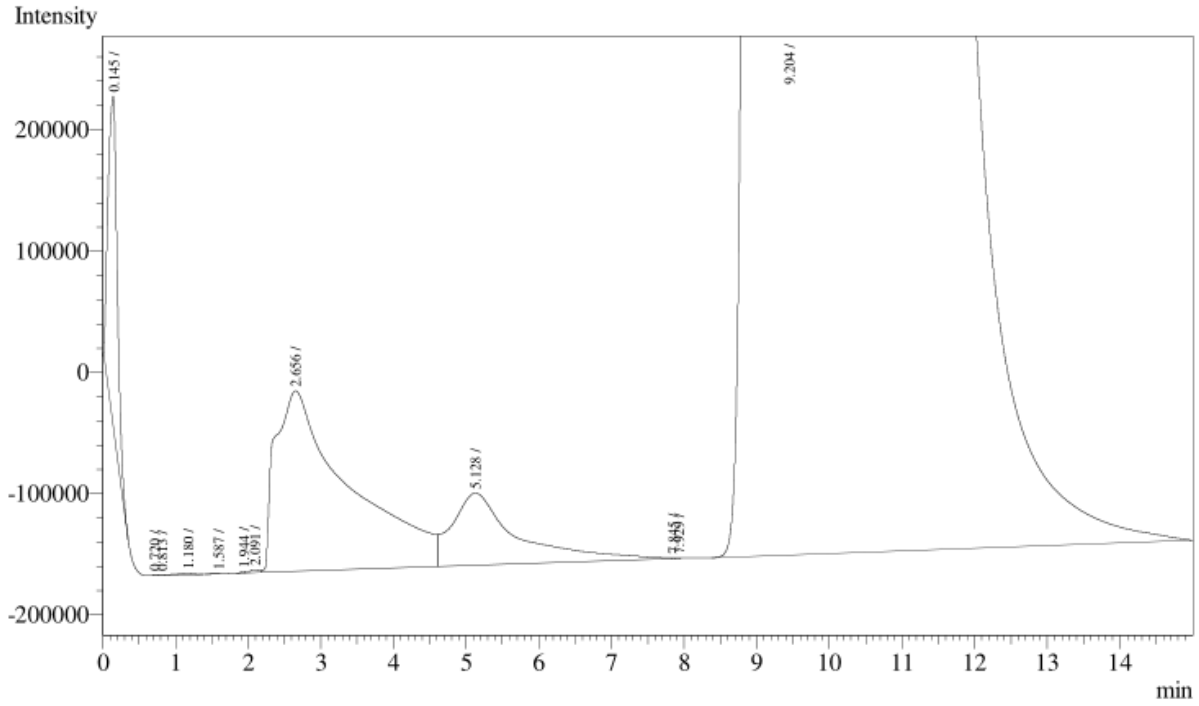

Peak#	Ret.Time	Area	Height	Conc.	Unit	Mark	ID#	Cmpd Name
1	0.145	2343951	272668	0.000				
2	0.720	1398	458	0.000				
3	0.813	1505	340	0.000		V		
4	1.180	22826	1425	0.000		V		
5	1.587	1757	212	0.000				
6	1.944	4842	1090	0.000		V		
7	2.091	23297	2688	0.000		V		
8	2.656	10453463	149025	0.000		V		
9	5.128	3748724	59555	0.000		V		
10	7.845	2120	690	0.000		V		
11	7.929	1953	466	0.000		V		
12	9.204	2050745869	27721992	0.000				
Total		2067351705	28210609					

Figure B-12: Trial 2 for the microwave control treatment of corn husks

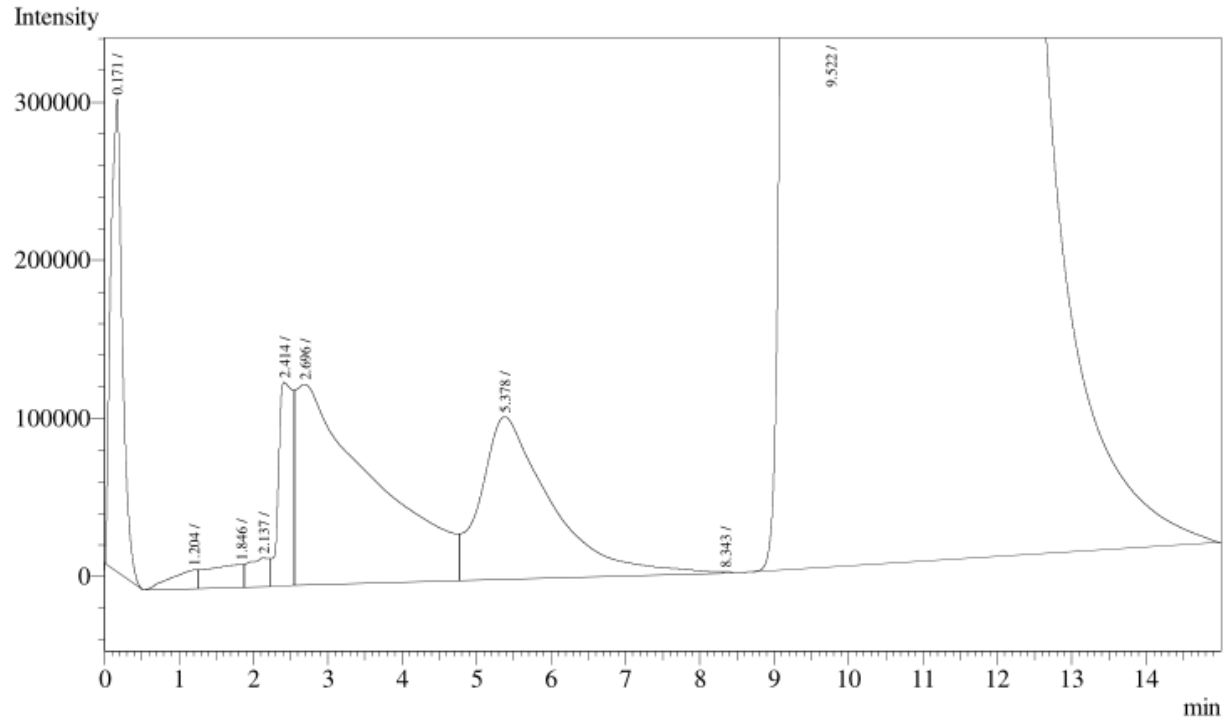

Peak#	Ret.Time	Area	Height	Conc.	Unit	Mark	ID#	Cmpd Name
1	0.171	3239727	299069	0.000				
2	1.204	289330	11682	0.000				
3	1.846	486220	14448	0.000		V		
4	2.137	336152	18112	0.000		V		
5	2.414	1751606	128688	0.000		V		
6	2.696	9225908	126994	0.000		V		
7	5.378	6760905	102789	0.000		V		
8	8.343	3103	518	0.000		V		
9	9.522	2602175245	31680173	0.000				
Total		2624268196	32382473					

Figure B-13: Trial 3 for the microwave control treatment of corn husks

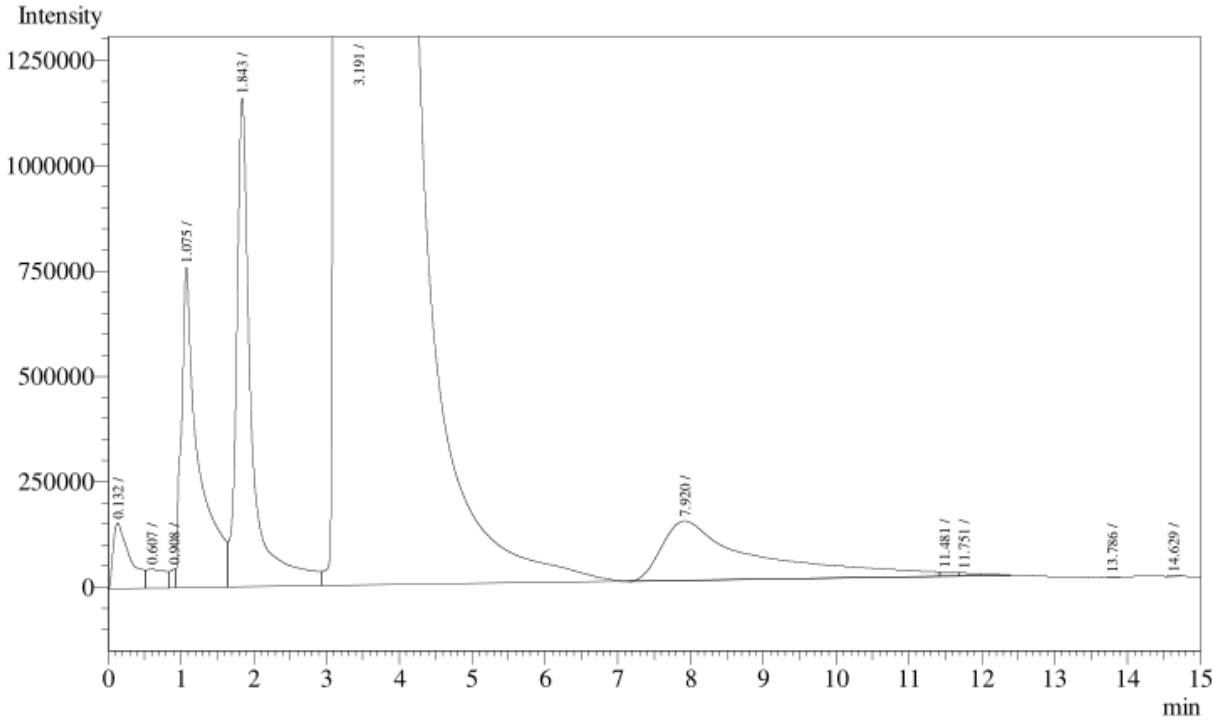

Peak#	Ret.Time	Area	Height	Conc.	Unit	Mark	ID#	Cmpd Name
1	0.132	2458319	155983	0.000				
2	0.607	826364	45584	0.000		V		
3	0.908	247580	45262	0.000		V		
4	1.075	12459552	759297	0.000		V		
5	1.843	16465930	1159022	0.000		V		
6	3.191	2404982666	106134168	0.000		SV		
7	7.920	12699783	141231	0.000		T		
8	11.481	146256	10222	0.000		TV		
9	11.751	165708	7066	0.000		TV		
10	13.786	1077	238	0.000				
11	14.629	4979	748	0.000				
Total		2450458214	108458821					

Figure B-14: Trial 1 for the enzymatic treatment of paper with cellulase from *T. reesei*

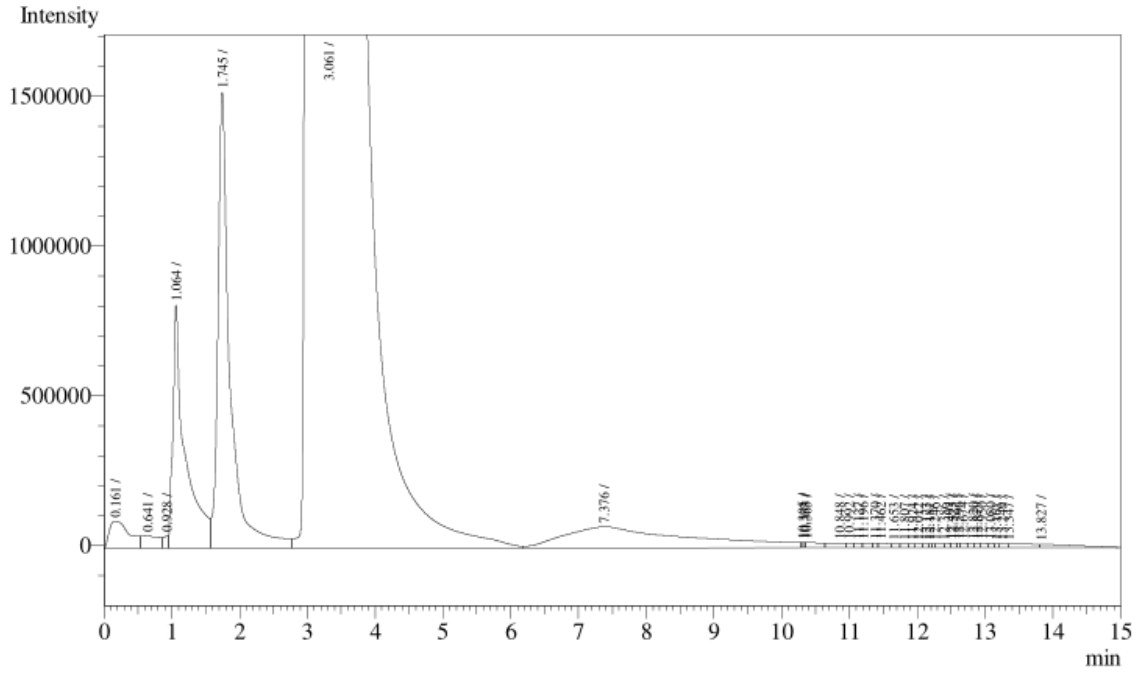

Peak#	Ret.Time	Area	Height	Conc.	Unit	Mark	ID#	Cmpd Name
1	0.161	1867965	90174	0.000				
2	0.641	737126	41705	0.000		V		
3	0.928	215066	41350	0.000		V		
4	1.064	10153011	812346	0.000		V		
5	1.745	19025344	1521973	0.000		V		
6	3.061	1770042429	84115617	0.000		V		
7	7.376	8983145	70506	0.000		V		
8	10.305	32704	16701	0.000		V		
9	10.333	32635	16675	0.000		V		
10	10.365	275068	16669	0.000		V		
11	10.848	292796	15864	0.000		V		
12	10.992	103385	15473	0.000		V		
13	11.127	115603	15376	0.000		V		
14	11.196	131901	15237	0.000		V		
15	11.370	76724	14473	0.000		V		
16	11.462	160428	14378	0.000		V		
17	11.653	101033	13514	0.000		V		
18	11.807	92668	13322	0.000		V		
19	11.924	78647	13494	0.000		V		
20	12.012	101631	13657	0.000		V		
21	12.123	66356	13193	0.000		V		
22	12.181	40338	13142	0.000		V		
23	12.246	36720	13154	0.000		V		
24	12.386	112035	13566	0.000		V		
25	12.493	80418	13787	0.000		V		
26	12.525	65512	13803	0.000		V		
27	12.596	42241	13736	0.000		V		
28	12.674	88352	13766	0.000		V		
29	12.820	81254	13977	0.000		V		
30	12.879	66577	14028	0.000		V		
31	12.950	100473	13981	0.000		V		
32	13.080	83818	13702	0.000		V		
33	13.161	49126	13539	0.000		V		
34	13.249	105296	13481	0.000		V		
35	13.347	342105	13342	0.000		V		
36	13.827	407887	10596	0.000		V		
Total		1814387817	87103297					

Figure B-15: Trial 2 for the enzymatic treatment of paper with cellulase from *T. reesei*

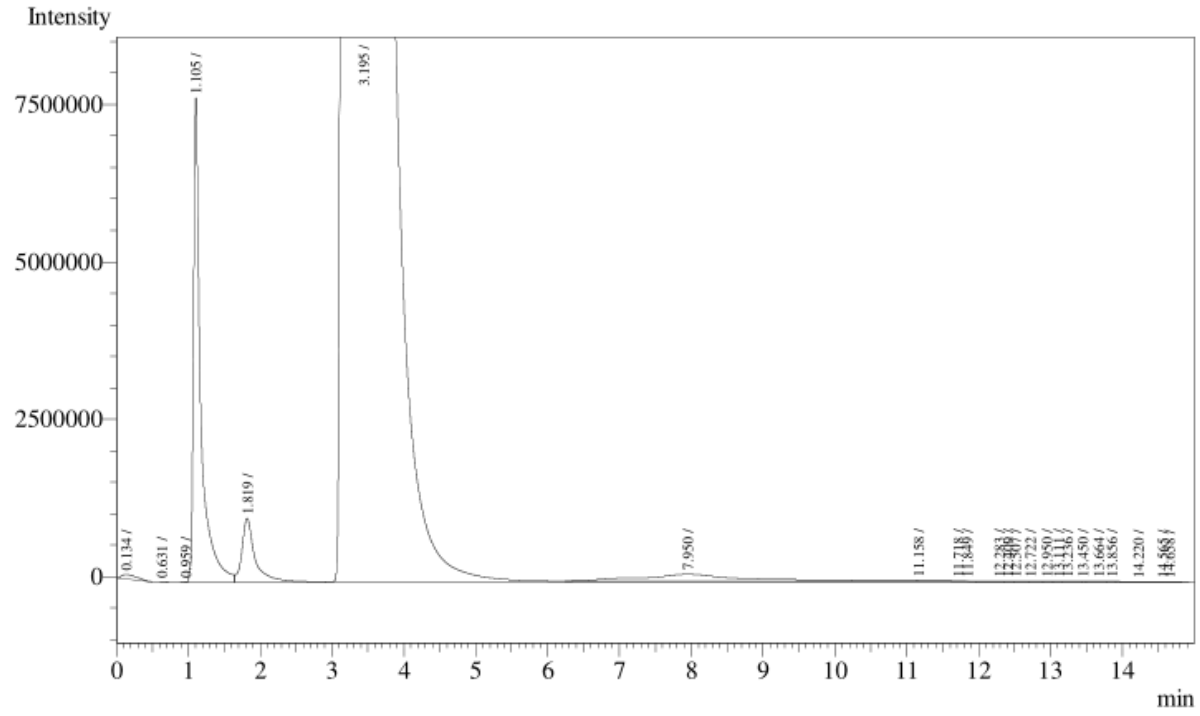

Peak#	Ret.Time	Area	Height	Conc.	Unit	Mark	ID#	Cmpd Name
1	0.134	1023103	71153	0.000				
2	0.631	5523	956	0.000				
3	0.959	20416	6060	0.000				
4	1.105	55145639	7690399	0.000		V		
5	1.819	13444973	1024531	0.000		V		
6	3.195	2215024294	95696830	0.000		SV		
7	7.950	11794548	111299	0.000		T		
8	11.158	373240	12447	0.000		TV		
9	11.718	67456	9816	0.000		TV		
10	11.849	80479	9534	0.000		TV		
11	12.283	181013	7153	0.000		TV		
12	12.409	59325	7100	0.000		TV		
13	12.507	88777	7186	0.000		TV		
14	12.722	73309	6515	0.000		TV		
15	12.950	44939	5643	0.000		TV		
16	13.111	37591	5465	0.000		TV		
17	13.236	96581	5929	0.000		TV		
18	13.450	19963	5563	0.000		TV		
19	13.664	84436	4843	0.000		TV		
20	13.856	28201	4101	0.000		TV		
21	14.220	54712	2100	0.000		TV		
22	14.565	30489	993	0.000		TV		
23	14.658	9417	971	0.000		TV		
Total		2297788424	104696587					

Figure B-16: Trial 3 for the enzymatic treatment of paper with cellulase from *T. reesei*

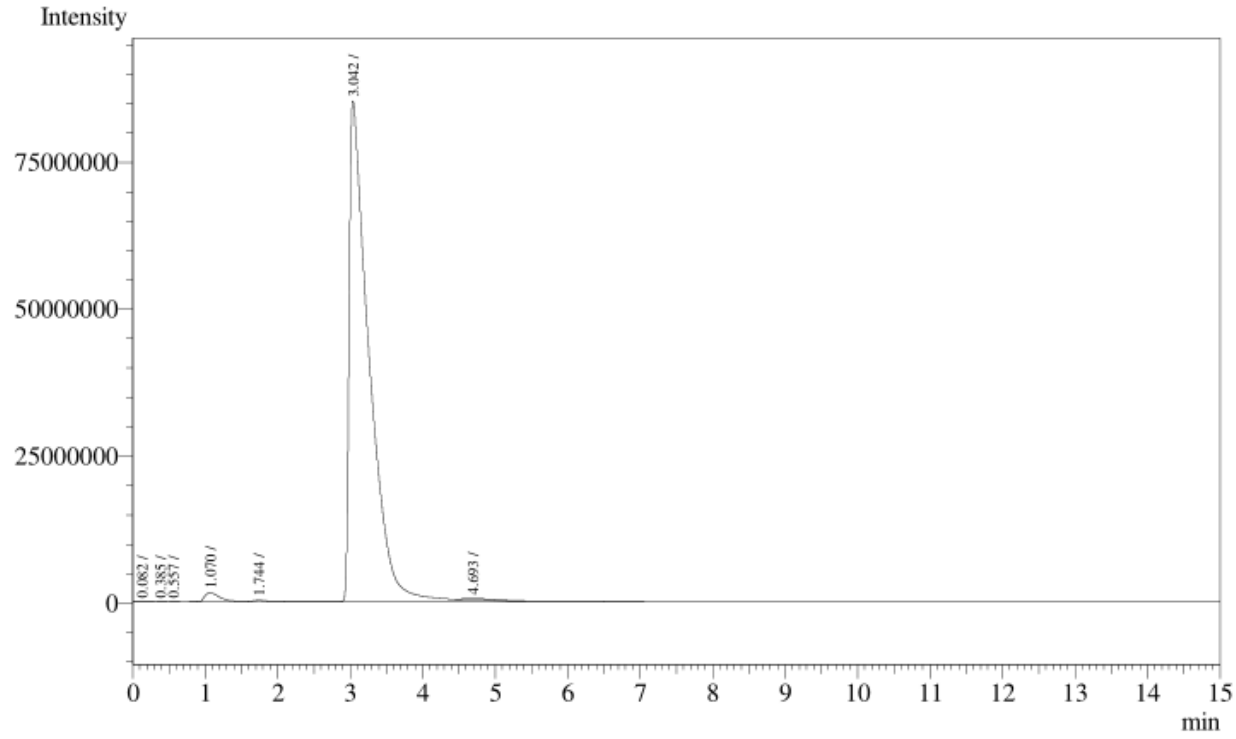

Peak#	Ret.Time	Area	Height	Conc.	Unit	Mark	ID#	Cmpd Name
1	0.082	159051	18517	0.000				
2	0.385	2009	444	0.000				
3	0.557	3077	693	0.000				
4	1.070	24715925	1591245	0.000				
5	1.744	5637139	307484	0.000		V		
6	3.042	1635273969	85264673	0.000		SV		
7	4.693	5197948	189586	0.000		T		
Total		1670989118	87372642					

Figure B-17: Trial 1 for the ionic liquid treatment of corn husks with TEABS

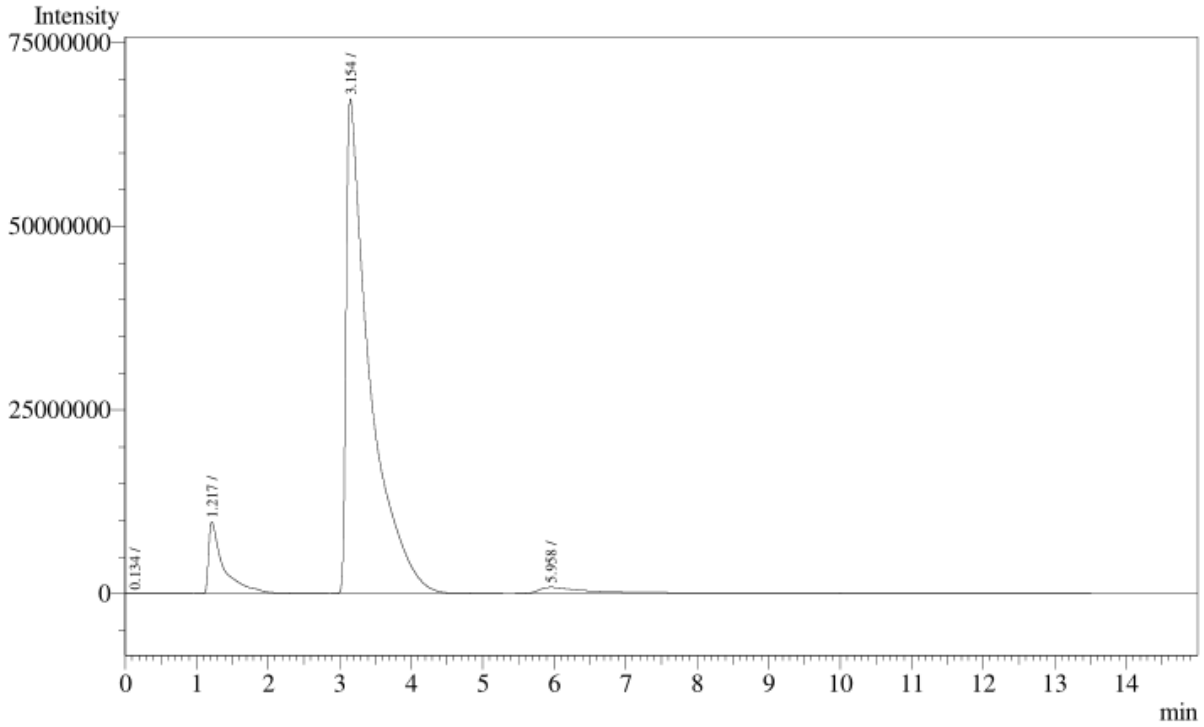

Peak#	Ret.Time	Area	Height	Conc.	Unit	Mark	ID#	Cmpd Name
1	0.134	166003	7206	0.000				
2	1.217	143652771	9772550	0.000				
3	3.154	1532449718	67323573	0.000				
4	5.958	50346315	849627	0.000				
Total		1726614807	77952956					

Figure B-18: Trial 2 for the ionic liquid treatment of corn husks with TEABS

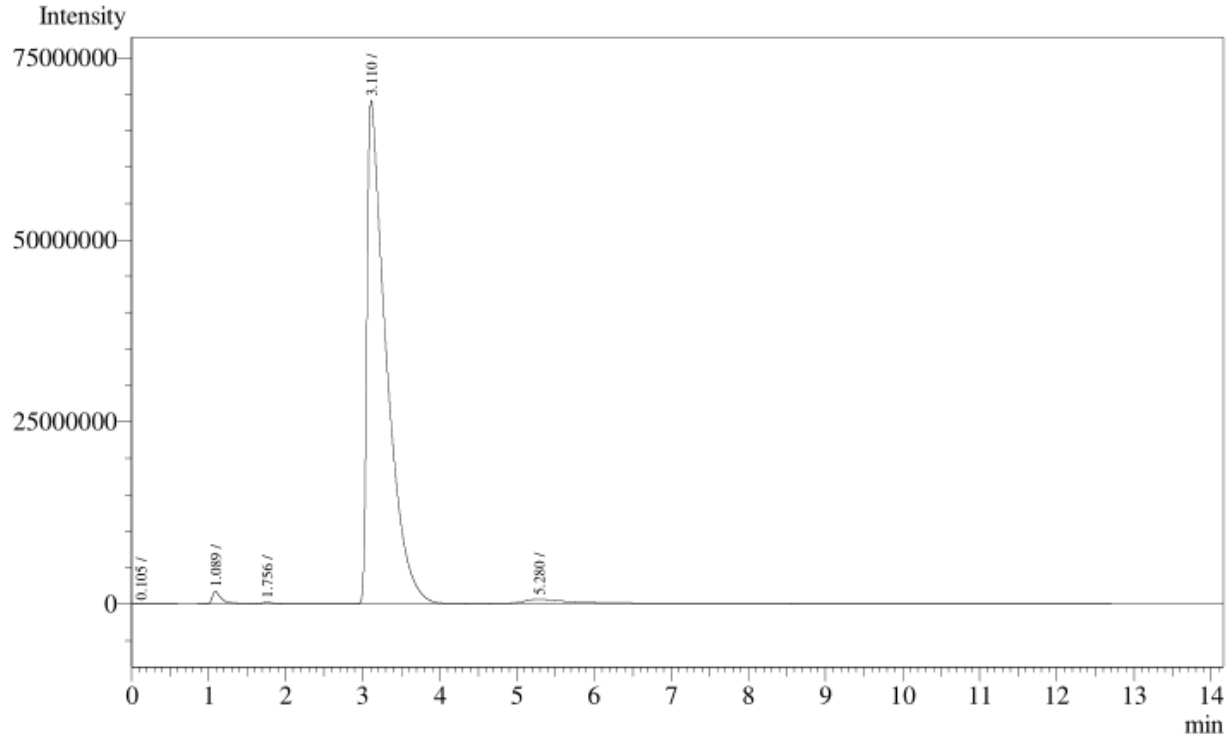

Peak#	Ret.Time	Area	Height	Conc.	Unit	Mark	ID#	Cmpd Name
1	0.105	218369	16630	0.000				
2	1.089	16173340	1772995	0.000				
3	1.756	3511319	274448	0.000		V		
4	3.110	1203392572	69128907	0.000		V		
5	5.280	45903287	659035	0.000		V		
Total		1269198887	71852015					

Figure B-19: Trial 3 for the ionic liquid treatment of corn husks with TEABS

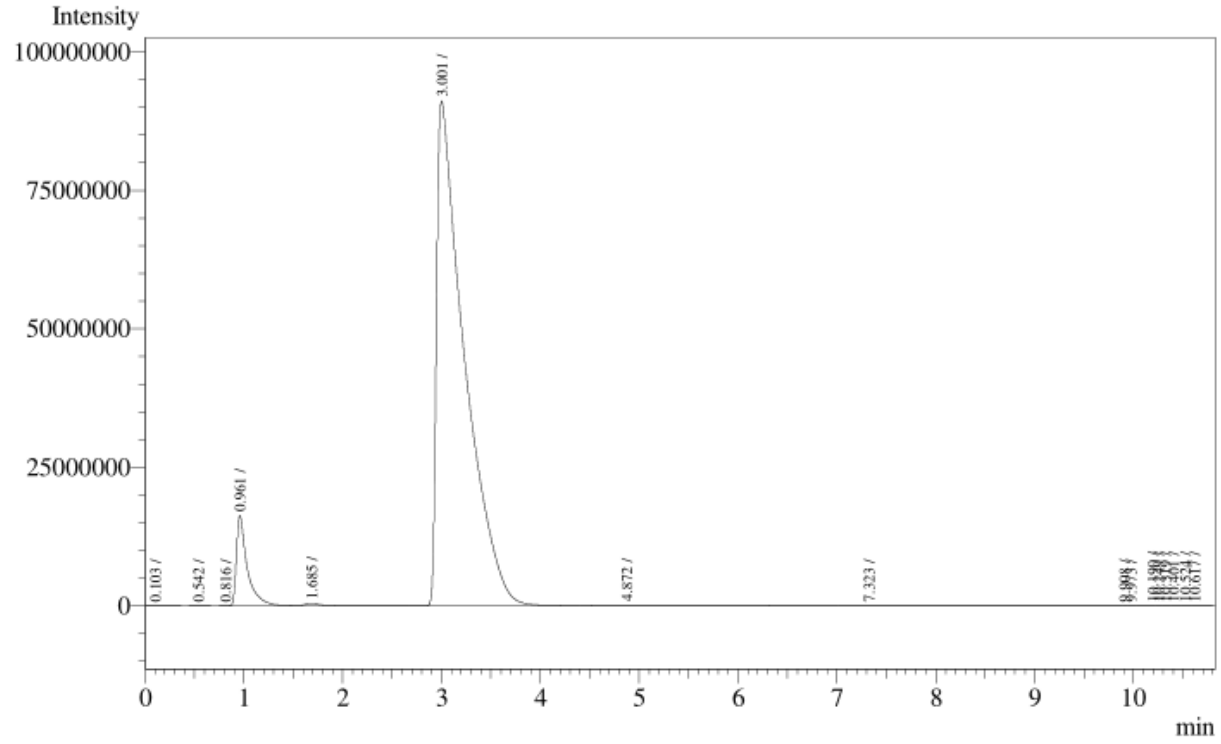

Peak#	Ret.Time	Area	Height	Conc.	Unit	Mark	ID#	Cmpd Name
1	0.103	304896	28275	0.000				
2	0.542	6178	1175	0.000				
3	0.816	9784	3416	0.000				
4	0.961	125366101	16314554	0.000		V		
5	1.685	6897587	533633	0.000		V		
6	3.001	1773914758	91112197	0.000		V		
7	4.872	13014443	170042	0.000		V		
8	7.323	2623368	32819	0.000		V		
9	9.908	9783	2948	0.000		V		
10	9.973	13407	2723	0.000		V		
11	10.190	28338	2318	0.000		V		
12	10.249	7665	2147	0.000		V		
13	10.319	10714	1965	0.000		V		
14	10.401	10852	1754	0.000		V		
15	10.524	7146	1256	0.000		V		
16	10.617	6292	885	0.000		V		
Total		1922231312	108212107					

Figure B-20: Trial 1 for the ionic liquid treatment of corn husks with TEAOTF

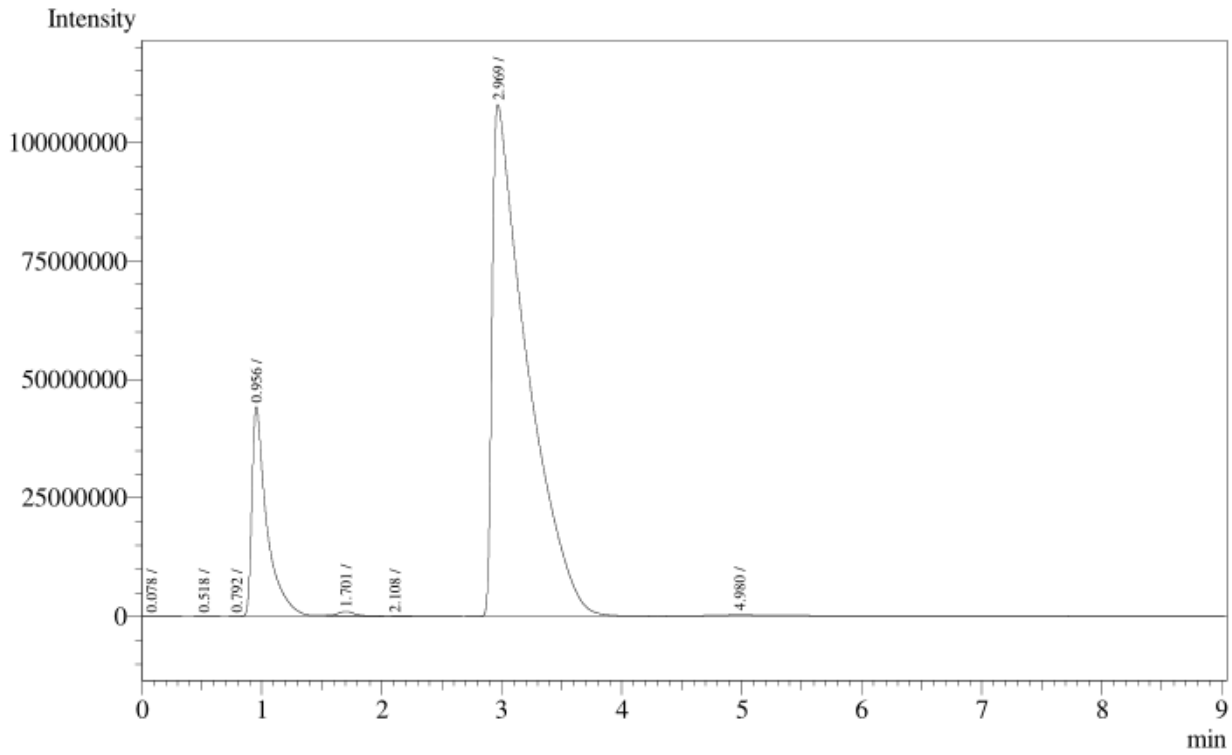

Peak#	Ret.Time	Area	Height	Conc.	Unit	Mark	ID#	Cmpd Name
1	0.078	248597	27470	0.000				
2	0.518	5612	1167	0.000				
3	0.792	8558	3067	0.000				
4	0.956	394049060	44288712	0.000		SV		
5	1.701	8570052	906401	0.000		T		
6	2.108	29290	3440	0.000		T		
7	2.969	2176536768	107923479	0.000				
8	4.980	29728999	361316	0.000		V		
Total		2609176936	153515052					

Figure B-21: Trial 2 for the ionic liquid treatment of corn husks with TEAOTF

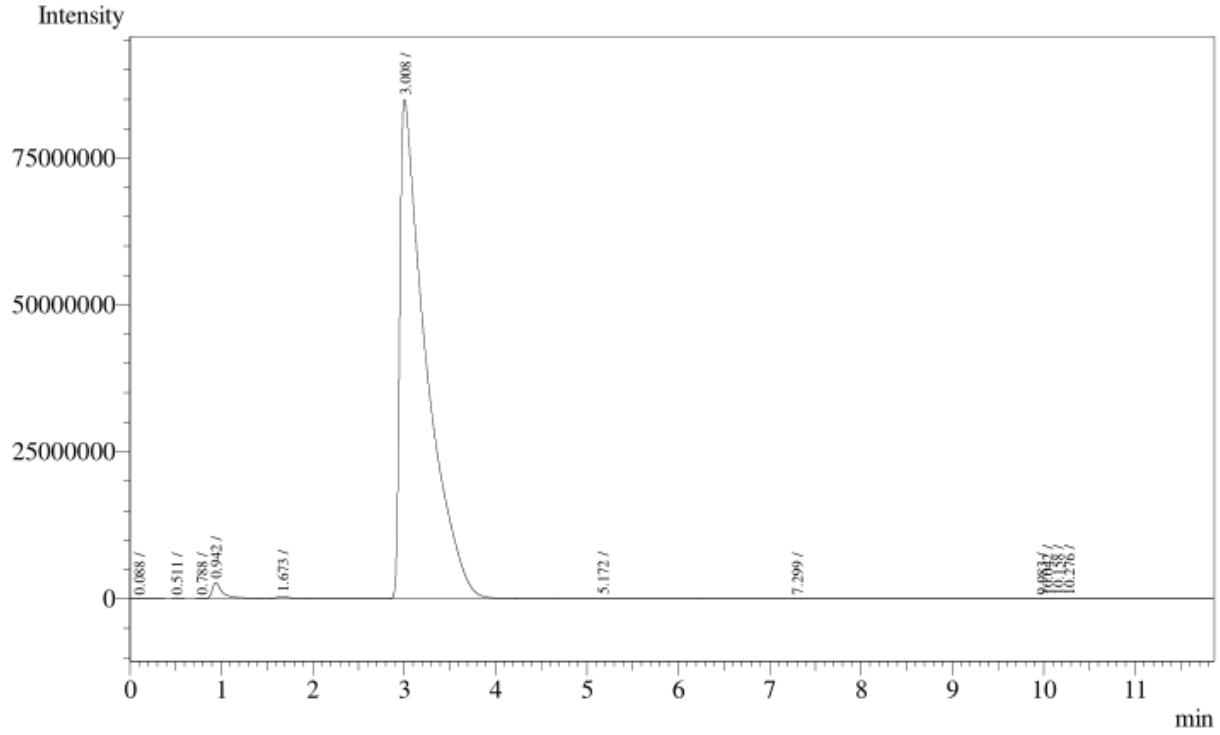

Peak#	Ret.Time	Area	Height	Conc.	Unit	Mark	ID#	Cmpd Name
1	0.088	333784	33461	0.000				
2	0.511	3969	989	0.000				
3	0.788	8935	3431	0.000				
4	0.942	23880061	2773006	0.000		V		
5	1.673	5682381	436561	0.000		V		
6	3.008	1682122643	84983679	0.000		V		
7	5.172	11318350	112198	0.000		V		
8	7.299	3430011	39462	0.000		V		
9	9.983	28598	7320	0.000		V		
10	10.042	45145	7342	0.000		V		
11	10.158	43405	7411	0.000		V		
12	10.276	394366	7466	0.000		V		
Total		1727291648	88412326					

Figure B-22: Trial 3 for the ionic liquid treatment of corn husks with TEAOTF

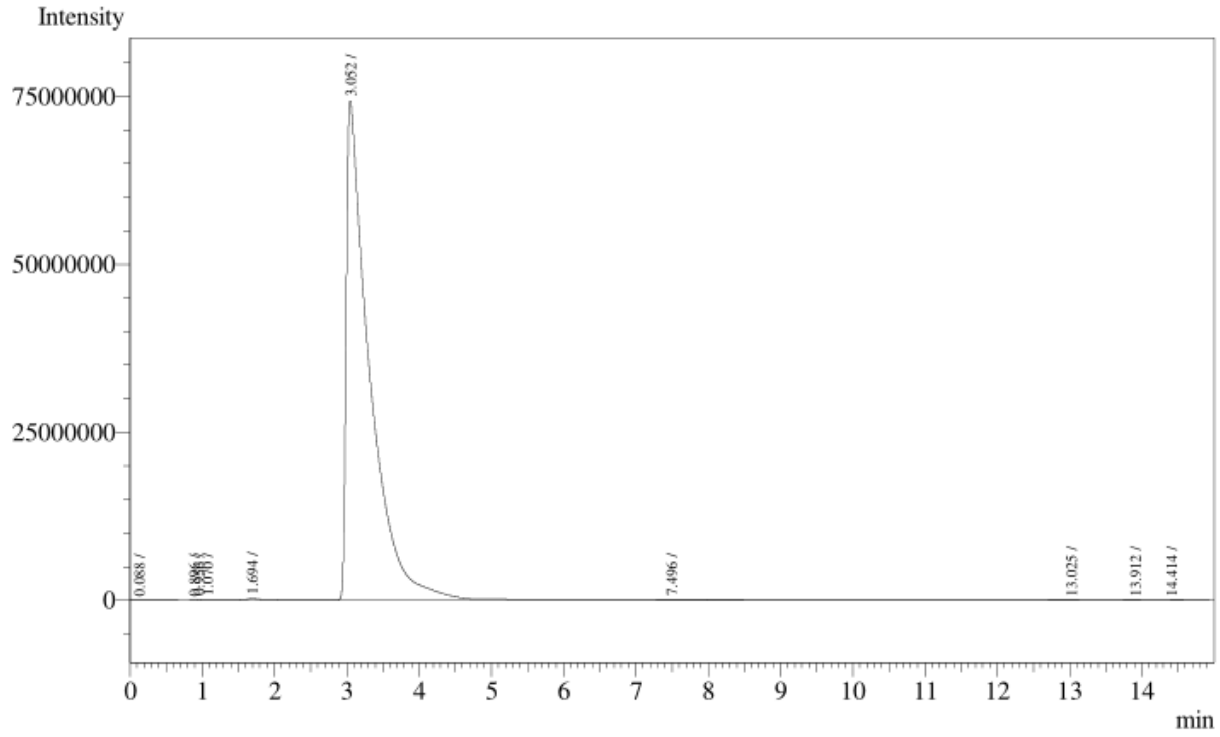

Peak#	Ret.Time	Area	Height	Conc.	Unit	Mark	ID#	Cmpd Name
1	0.088	229371	13639	0.000				
2	0.896	4698	1502	0.000				
3	0.956	155190	60707	0.000		V		
4	1.070	2158896	80309	0.000		V		
5	1.694	5446906	304434	0.000		V		
6	3.052	1680504628	74362165	0.000		SV		
7	7.496	157840	3977	0.000		T		
8	13.025	1436	78	0.000		TV		
9	13.912	1551	142	0.000		TV		
10	14.414	1221	96	0.000		TV		
Total		1688661737	74827049					

Figure B-23: Trial 1 for the combined ionic liquid and enzymatic treatment of corn husks with TEAOTF and cellulase from *T. reesei*

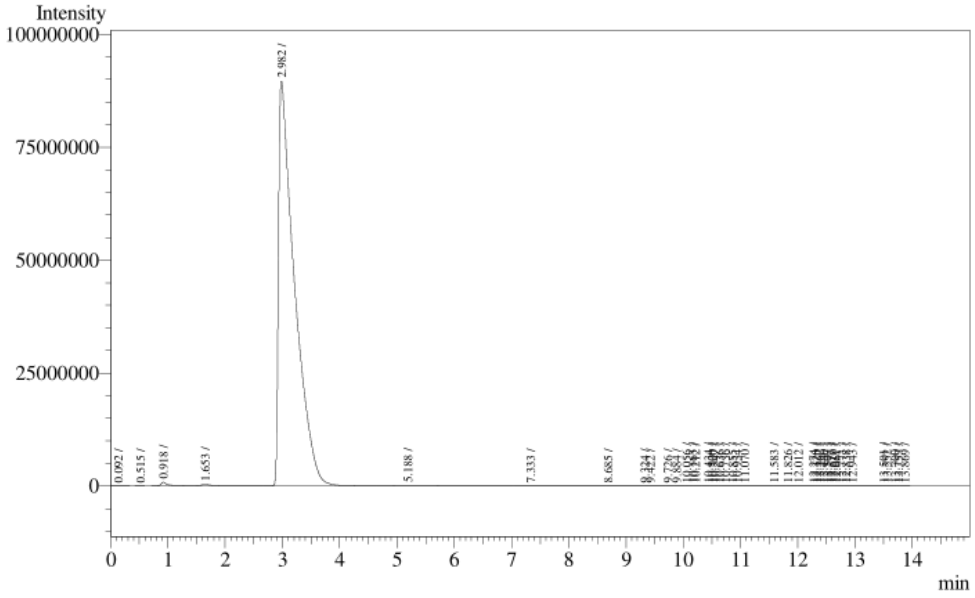

Peak#	Ret.Time	Area	Height	Conc.	Unit	Mark	ID#	Cmpd Name
1	0.092	349329	33140	0.000				
2	0.515	5921	1335	0.000				
3	0.918	8239574	855622	0.000				
4	1.653	5624456	407087	0.000		V		
5	2.982	1739148462	89676589	0.000		V		
6	5.188	6609482	66240	0.000		V		
7	7.333	2292632	29638	0.000		V		
8	8.685	630616	17354	0.000		V		
9	9.324	80075	14448	0.000		V		
10	9.422	232102	14124	0.000		V		
11	9.726	118829	13043	0.000		V		
12	9.884	134377	12533	0.000		V		
13	10.056	50194	11996	0.000		V		
14	10.163	59569	11806	0.000		V		
15	10.212	93986	11725	0.000		V		
16	10.434	104168	11287	0.000		V		
17	10.500	37313	11131	0.000		V		
18	10.547	51909	10995	0.000		V		
19	10.636	30089	10754	0.000		V		
20	10.736	107111	10690	0.000		V		
21	10.855	57654	10371	0.000		V		
22	10.934	80634	10141	0.000		V		
23	11.070	266672	9626	0.000		V		
24	11.583	89965	7244	0.000		V		
25	11.826	69576	6359	0.000		V		
26	12.012	79676	5664	0.000		V		
27	12.274	16148	4815	0.000		V		
28	12.320	13207	4734	0.000		V		
29	12.362	14159	4623	0.000		V		
30	12.440	25181	4527	0.000		V		
31	12.507	18089	4362	0.000		V		
32	12.577	9356	4204	0.000		V		
33	12.610	12541	4119	0.000		V		
34	12.661	23745	3990	0.000		V		
35	12.773	12179	3662	0.000		V		
36	12.838	18299	3506	0.000		V		
37	12.943	83180	3292	0.000		V		
38	13.501	3334	1221	0.000		V		
39	13.552	8134	1091	0.000		V		
40	13.700	1759	607	0.000		V		
41	13.753	1299	479	0.000		V		
42	13.869	2729	288	0.000		V		
Total		1764907710	91330462					

Figure B-24: Trial 2 for the combined ionic liquid and enzymatic treatment of corn husks with TEAOTF and cellulase from *T. reesei*

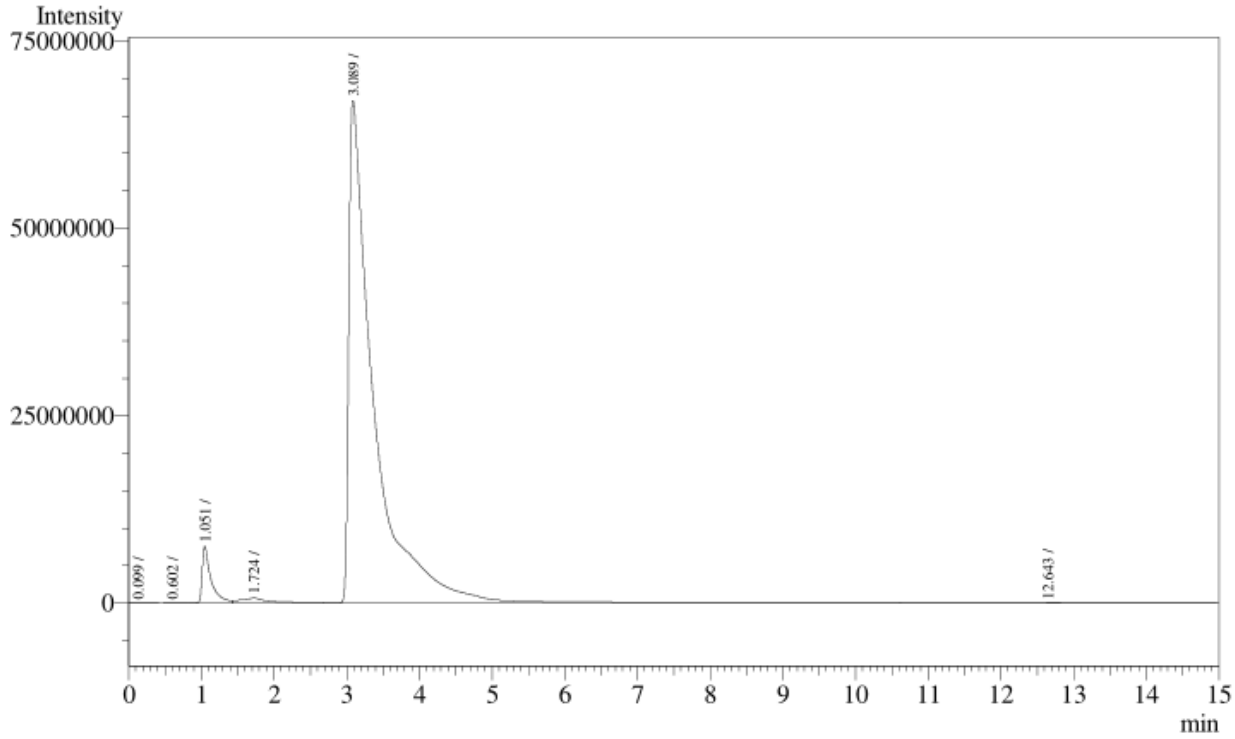

Peak#	Ret.Time	Area	Height	Conc.	Unit	Mark	ID#	Cmpd Name
1	0.099	263186	19579	0.000				
2	0.602	10954	1210	0.000				
3	1.051	64768830	7585956	0.000				
4	1.724	21152988	710288	0.000		V		
5	3.089	1620629977	67070079	0.000		SV		
6	12.643	1610	86	0.000		T		
Total		1706827545	75387198					

Figure B-25: Trial 3 for the combined ionic liquid and enzymatic treatment of corn husks with TEAOTF and cellulase from *T. reesei*

Appendix B.4 – Fermentation Data

Table B-4: Gas chromatography areas and area ratios associated with the lignocellulosic substrates and their treatment methods

Treatment Method(s)	Substrate	PrOH Area	EtOH Area	PrOH/EtOH Area Ratio (measured)	PrOH/EtOH Area Ratio (scaled up)
Control	Paper	2169564328	146385451	14.82090135	37.05225337
Control	Paper	2196323963	7776584	282.4278582	706.0696454
Control	Paper	2124223511	46756745	45.43138131	113.5784533
Control	Husk	2025682351	8802318	230.1305578	575.3263944
Control	Husk	2050745869	10453463	196.1786127	490.4465317
Control	Husk	2602175245	9225905	282.0509473	705.1273683
Cellulase	Paper	2404982666	16465930	146.0581131	365.1452827
Cellulase	Paper	1770042429	19025344	93.03602757	232.5900689
Cellulase	Paper	2215024294	13444973	164.7473962	411.8684906
TEA-BS	Husk	1635273969	24715925	66.16276627	165.4069157
TEA-BS	Husk	1532449718	143652771	10.66773517	26.66933793
TEA-BS	Husk	1203392572	16173340	74.40594039	186.014851
TEA-OTF	Husk	1773914758	6897587	257.1790335	642.9475837
TEA-OTF	Husk	2176536768	8570052	253.9700772	634.925193
TEA-OTF	Husk	1682122643	5682381	296.0242622	740.0606555
TEA-OTF + Cellulase	Husk	1680504628	5446906	308.5246244	771.3115611
TEA-OTF + Cellulase	Husk	1739148462	5624456	309.211853	773.0296326
TEA-OTF + Cellulase	Husk	1620629977	21152988	76.61470696	191.5367674

Table B-5: Masses of ethanol obtained from the calibration curve, and their adjusted values based on volume injected into the chromatograph

Treatment Method(s)	**Substrate**	**Mass EtOH (g) (Calibration curve)**	**Mass EtOH (g) (Scaled down)**
Control	Paper	-4.8878×10^{-5}	-2.57805×10^{-5}
Control	Paper	4.19773×10^{-4}	4.92037×10^{-5}
Control	Paper	4.72912×10^{-6}	-1.72034×10^{-5}
Control	Husk	3.28187×10^{-4}	3.45499×10^{-5}
Control	Husk	2.68728×10^{-4}	2.50364×10^{-5}
Control	Husk	4.19113×10^{-4}	4.90981×10^{-5}
Cellulase	Paper	1.80953×10^{-4}	1.09925×10^{-5}
Cellulase	Paper	8.80976×10^{-5}	-3.8644×10^{-6}
Cellulase	Paper	2.13683×10^{-4}	1.62293×10^{-5}
TEA-BS	Husk	4.10353×10^{-5}	-1.13944×10^{-5}
TEA-BS	Husk	-5.61513×10^{-5}	-2.69442×10^{-5}
TEA-BS	Husk	5.54713×10^{-5}	-9.0846×10^{-6}
TEA-OTF	Husk	3.75556×10^{-4}	4.21289×10^{-5}
TEA-OTF	Husk	3.69936×10^{-4}	4.12298×10^{-5}
TEA-OTF	Husk	4.43584×10^{-4}	5.30135×10^{-5}
TEA-OTF + Cellulase	Husk	4.65476×10^{-4}	5.65161×10^{-5}
TEA-OTF + Cellulase	Husk	4.66679×10^{-4}	5.67087×10^{-5}
TEA-OTF + Cellulase	Husk	5.93395×10^{-5}	-8.4657×10^{-6}

Table B-6: Average values for the mass of ethanol based on the calibration curve, along with standard deviations, and concentrations

Treatment Method(s)	**Substrate**	**Mass EtOH (g) (Calibration curve)**	**Standard Deviation (g)**	**Concentration of EtOH**
Control	Husk	3.39×10^{-4}	7.57394×10^{-5}	9.03%
Control	Paper	1.25×10^{-4}	2.56505×10^{-4}	3.34%
Cellulase	Paper	1.61×10^{-4}	6.51476×10^{-5}	4.29%
TEABS	Husk	1.35×10^{-5}	6.07087×10^{-5}	0.36%
TEAOTF	Husk	3.96×10^{-4}	4.09949×10^{-5}	10.57%
TEAOTF + Cellulase	Husk	3.30×10^{-4}	2.34831×10^{-4}	8.82%

Table B-7: Rejected data from the Grubbs test (bolded and crossed out)

Treatment Method(s)	**Substrate**	**PrOH Area**	**EtOH Area**	**PrOH/EtOH Area Ratio (scaled up)**	**Mass EtOH (g) (Calibration curve)**
Control	Paper	2169564328	146385451	37.05225337	-4.8878×10^{-5}
Control	Paper	2196323963	7776584	706.0696454	4.19773×10^{-4}
Control	Paper	2124223511	46756745	113.5784533	4.72912×10^{-6}
Control	Husk	2025682351	8802318	575.3263944	3.28187×10^{-4}
Control	Husk	2050745869	10453463	490.4465317	2.68728×10^{-4}
Control	Husk	2602175245	9225905	705.1273683	4.19113×10^{-4}
Cellulase	Paper	2404982666	16465930	365.1452827	1.80953×10^{-4}
Cellulase	Paper	1770042429	19025344	232.5900689	8.80976×10^{-5}
Cellulase	Paper	2215024294	13444973	411.8684906	2.13683×10^{-4}
TEA-BS	Husk	1635273969	24715925	165.4069157	4.10353×10^{-5}
TEA-BS	Husk	1532449718	143652771	26.66933793	-5.61513×10^{-5}
TEA-BS	Husk	1203392572	16173340	186.014851	5.54713×10^{-5}
TEA-OTF	Husk	1773914758	6897587	642.9475837	3.75556×10^{-4}
TEA-OTF	Husk	2176536768	8570052	634.925193	3.69936×10^{-4}
TEA-OTF	Husk	1682122643	5682381	740.0606555	4.43584×10^{-4}
TEA-OTF + Cellulase	Husk	1680504628	5446906	771.3115611	4.65476×10^{-4}
TEA-OTF + Cellulase	Husk	1739148462	5624456	773.0296326	4.66679×10^{-4}
~~**TEA-OTF + Cellulase**~~	~~**Husk**~~	~~**1620629977**~~	~~**21152988**~~	~~**191.5367674**~~	~~**5.93395×10^{-5}**~~

Table B-8: Average masses and concentrations of ethanol after rejecting outliers

Treatment Method(s)	**Substrate**	**Mass EtOH (g) (Calibration curve)**	**Concentration of EtOH**
Control	Husk	3.39×10^{-4}	9.03%
Control	Paper	1.25×10^{-4}	3.34%
Cellulase	Paper	1.61×10^{-4}	4.29%
TEABS	Husk	1.35×10^{-5}	0.36%
TEAOTF	Husk	3.96×10^{-4}	10.57%
TEAOTF + Cellulase	Husk	4.66×10^{-4}	12.43%

Appendix B.5 – HPLC Chromatograms and Mass Spectra

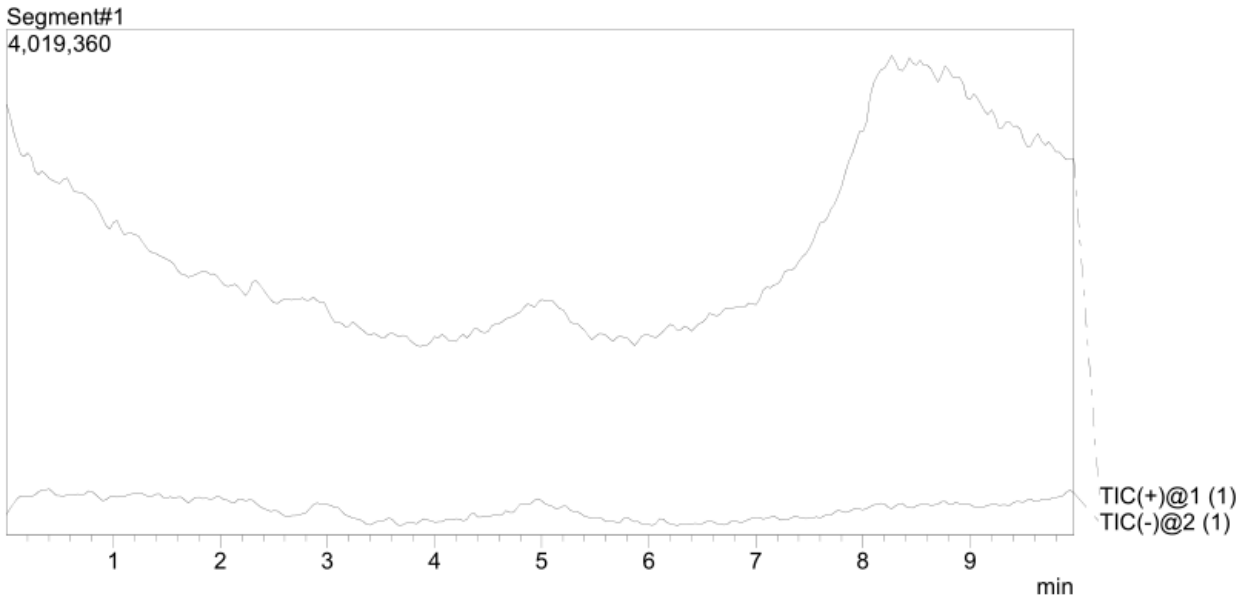

Figure B-26: High-pressure liquid chromatogram for the solution containing pure water

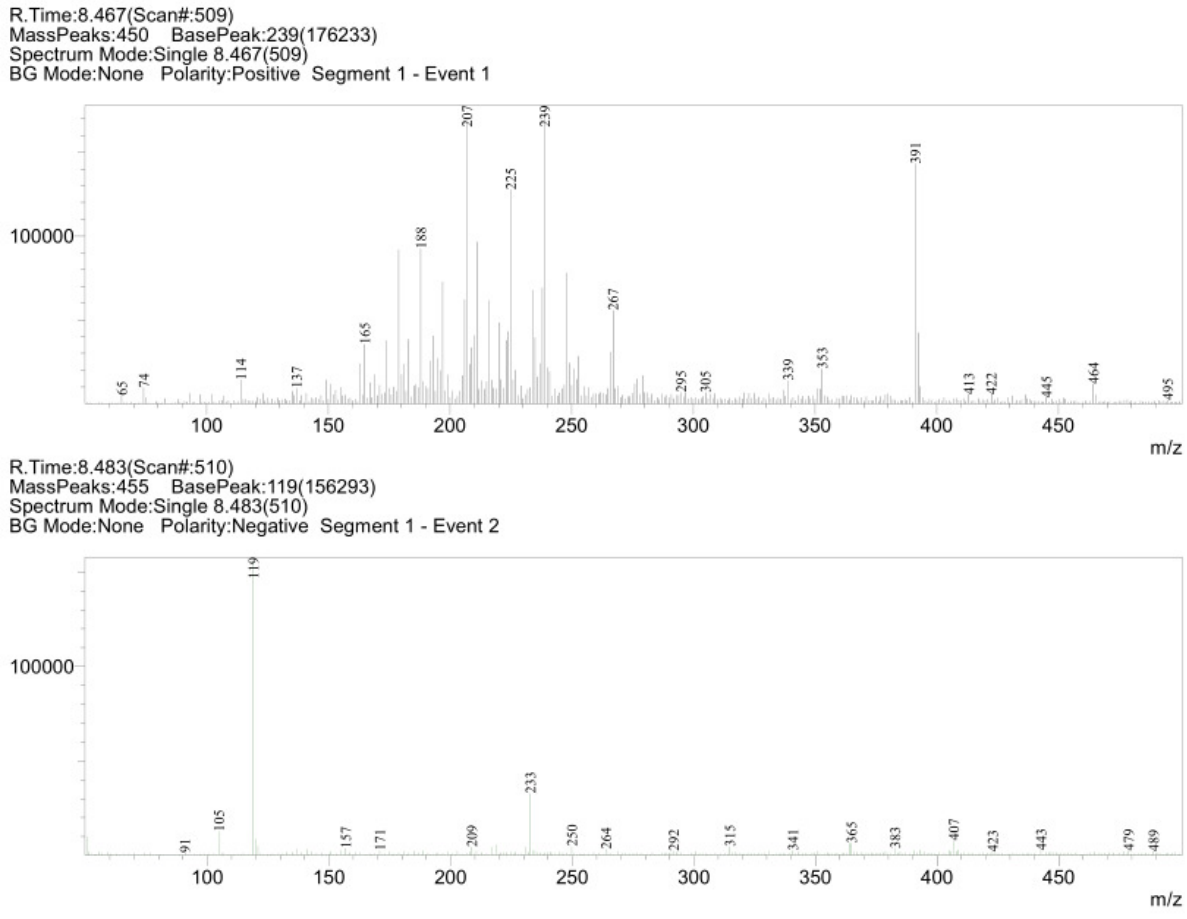

Figure B-27: Positive and negative ion mass spectra for the solution containing pure water

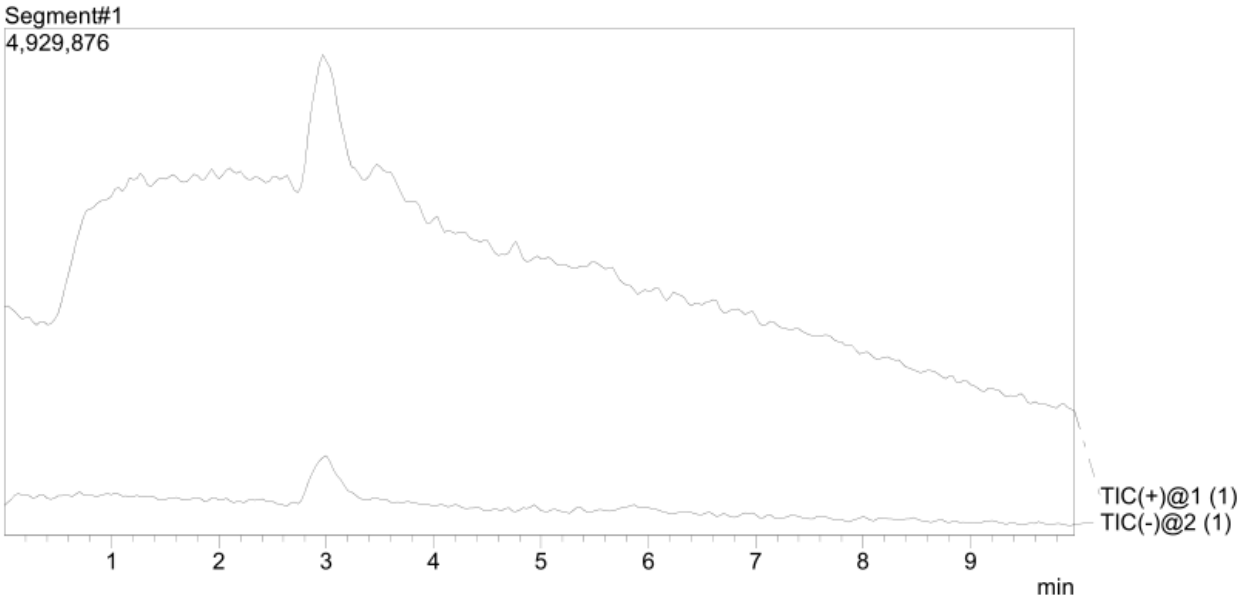

Figure B-28: High-pressure liquid chromatogram for the solution containing 15 mg glucose in 100 mL water

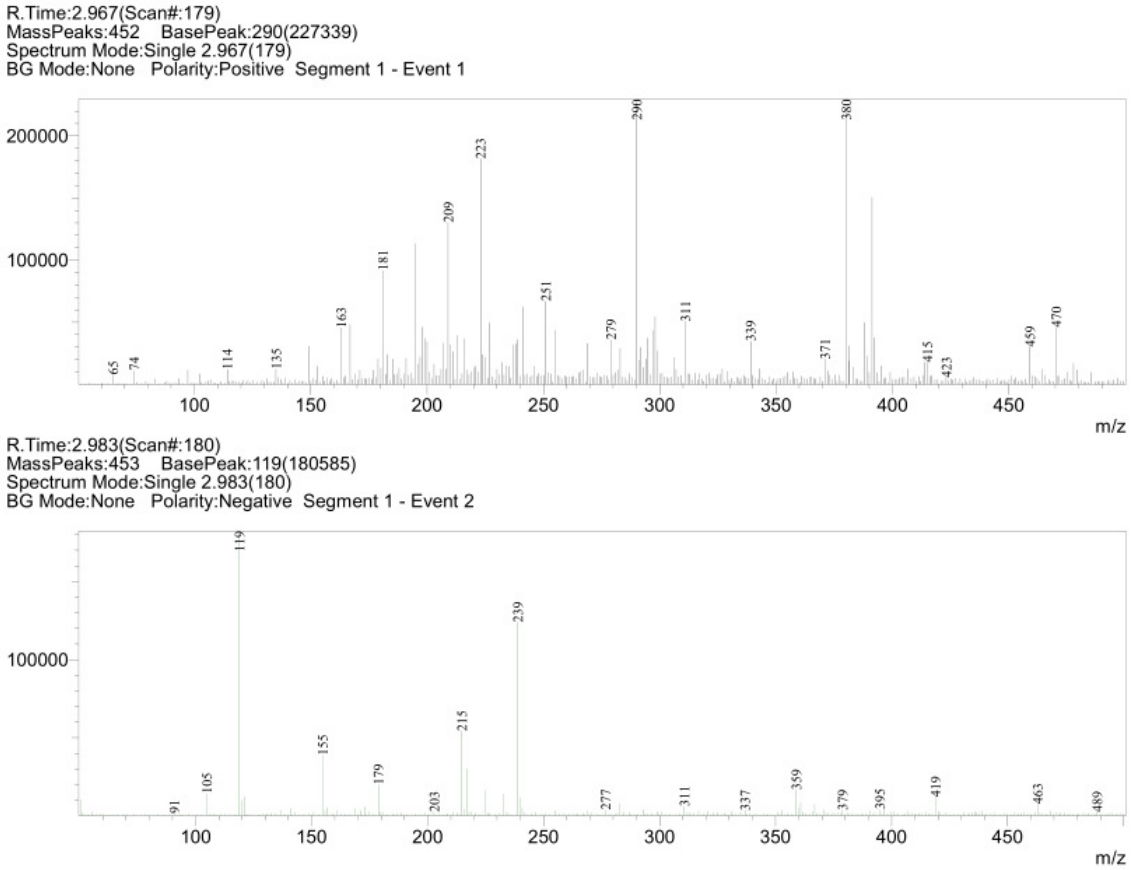

Figure B-29: Positive and negative ion mass spectra for the solution containing 15 mg glucose in 100 mL water

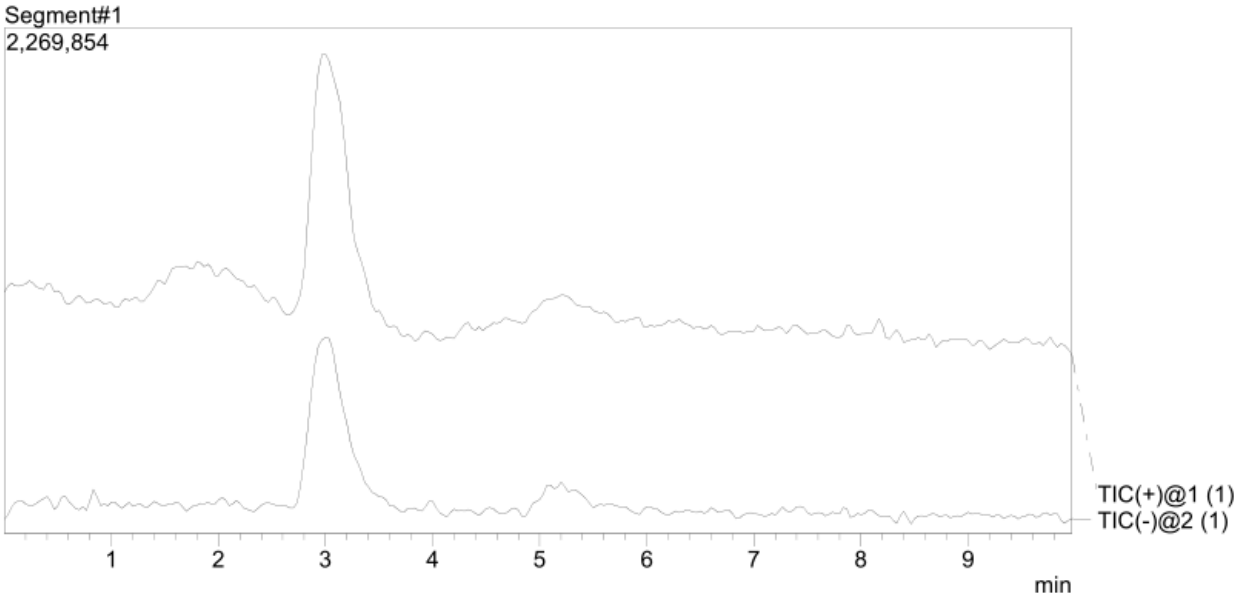

Figure B-30: High-pressure liquid chromatogram for the solution containing 40 mg glucose in 100 mL water

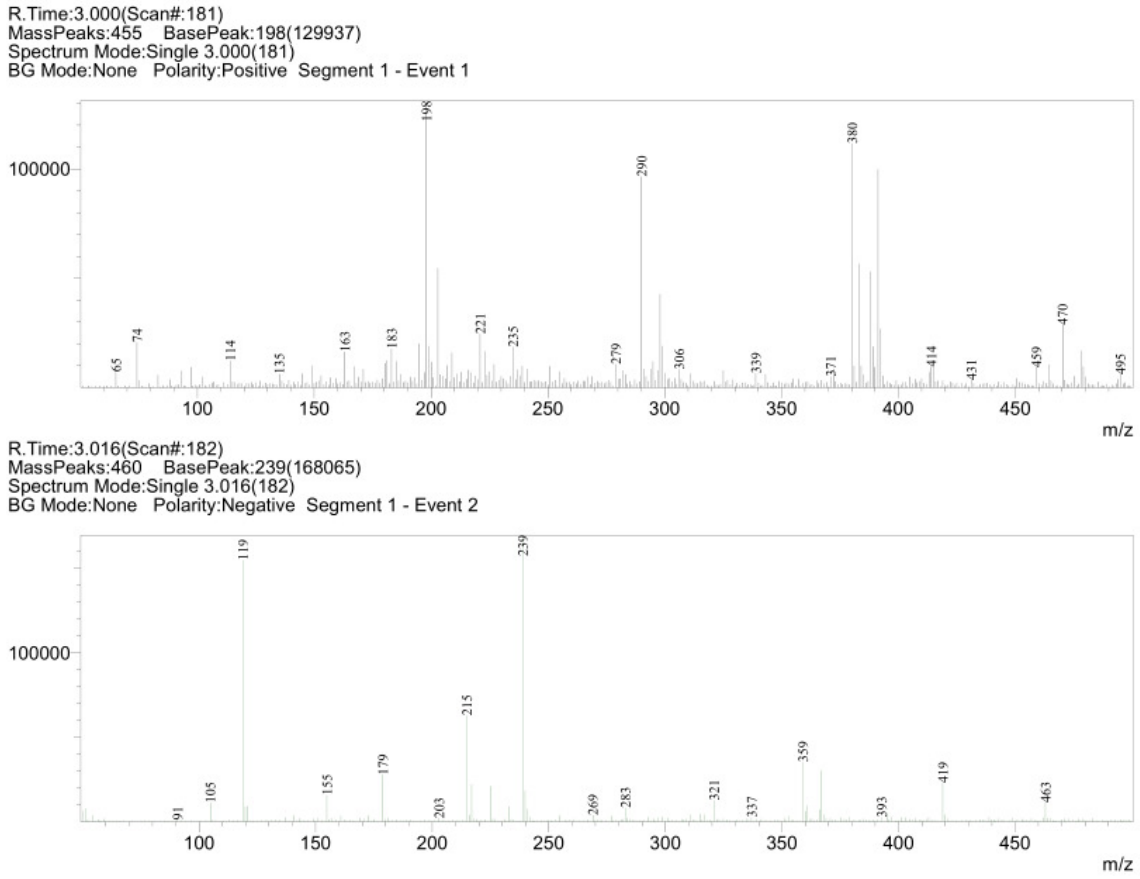

Figure B-31: Positive and negative ion mass spectra for the solution containing 40 mg glucose in 100 mL water

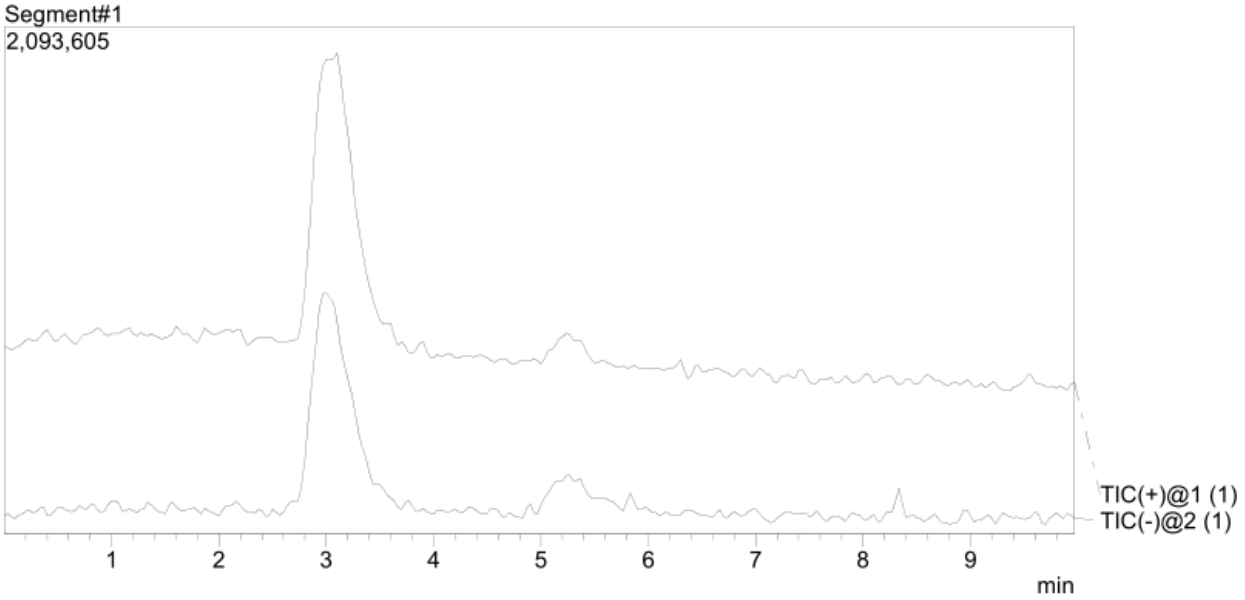

Figure B-32: High-pressure liquid chromatogram for the solution containing 58 mg glucose in 100 mL water

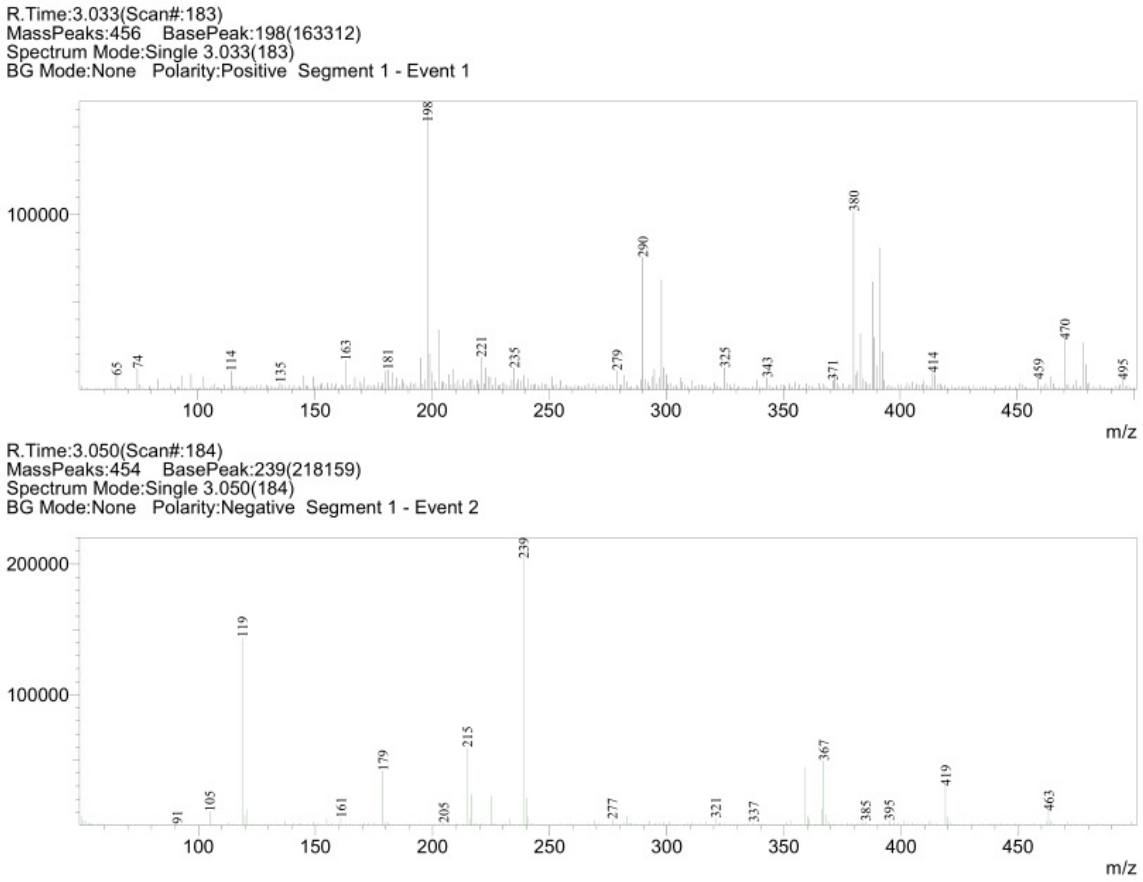

Figure B-33: Positive and negative ion mass spectra for the solution containing 58 mg glucose in 100 mL water

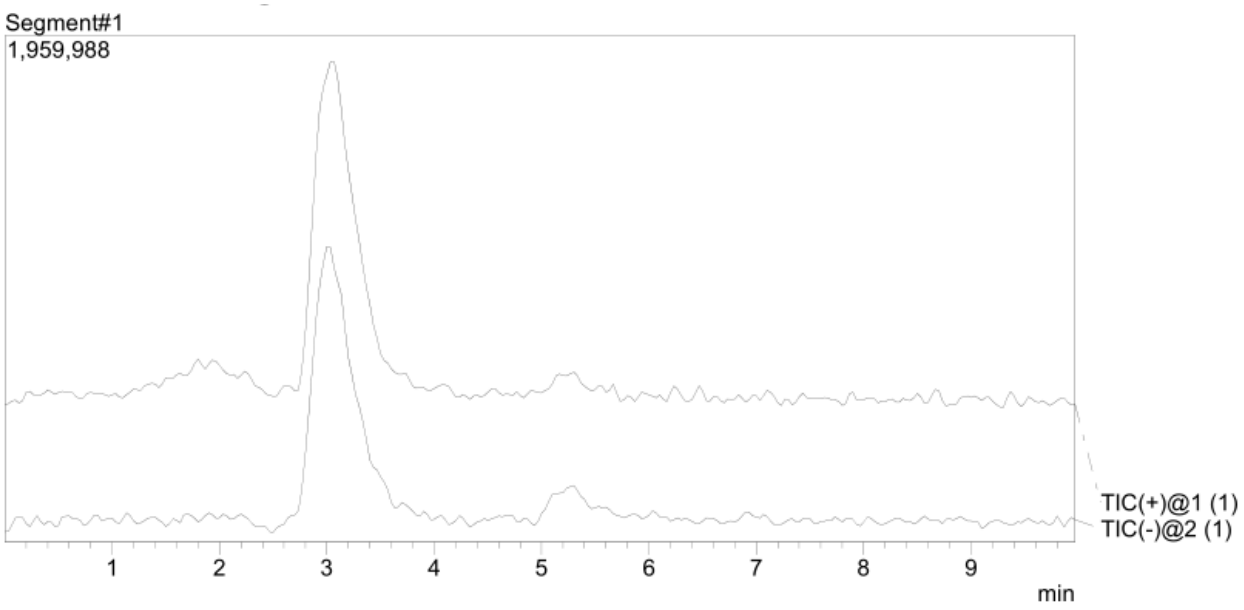

Figure B-34: High-pressure liquid chromatogram for the solution containing 78 mg glucose in 100 mL water

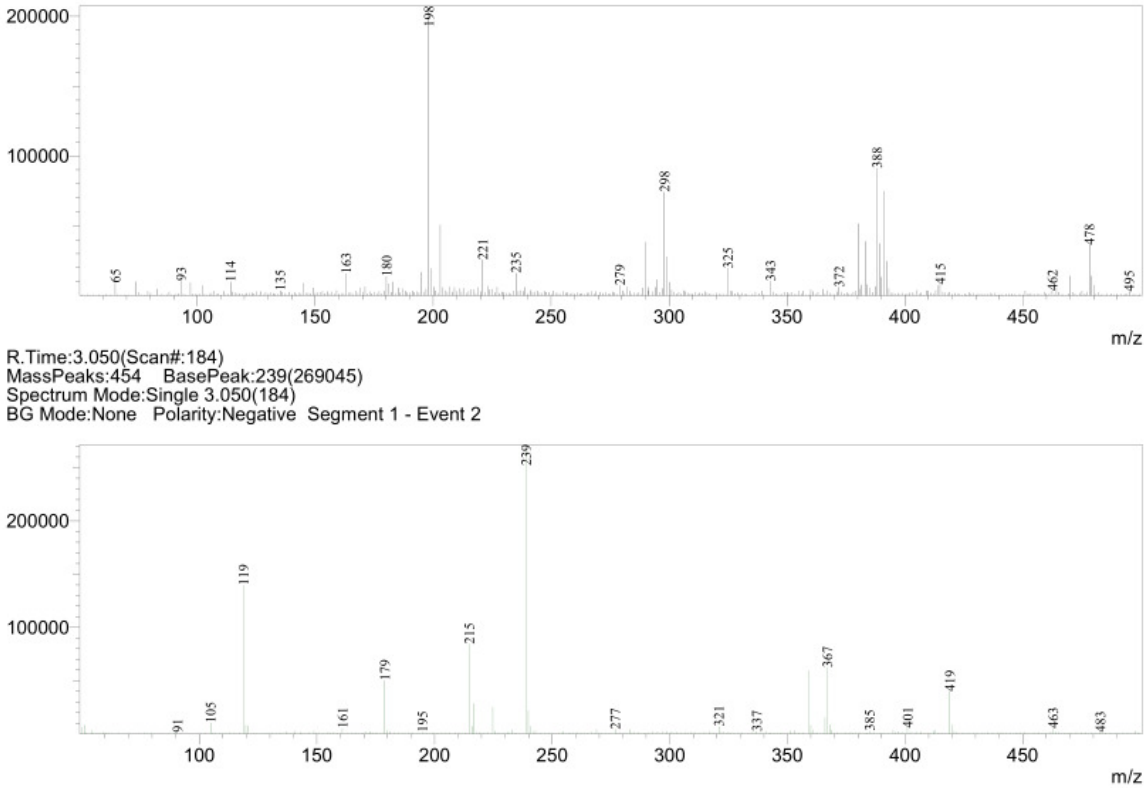

Figure B-35: Positive and negative ion mass spectra for the solution containing 78 mg glucose in 100 mL water

APPENDIX C– SAMPLE CALCULATIONS

Appendix C.1 – Thermodynamic Calculations

**Change in internal energy associated with the mixing of cellulose and TEA-OTF and subsequent hydrolysis. The values were obtained from the quantum mechanical calculations in Spartan. (See Section 4.2 in Results)

Equation 3: Total change in internal energy (for a dilute equimolar solution of TEA-OTF and cellulose in water)

$$\Delta \underline{U} = \Delta \underline{U_{mix}} + \Delta \underline{U_{rxn}}$$

$$\Delta \underline{U} = \left(-160.91 \frac{\text{kJ}}{\text{mol}}\right) + \left(-51.3 \frac{\text{kJ}}{\text{mol}}\right)$$

$$\Delta \underline{U} = -212.21 \frac{\text{kJ}}{\text{mol}}$$

Determination of the Flory-Huggins chi parameter (for a dilute equimolar solution of TEA-OTF and cellulose in water at 25°C)

$$\Delta U_{mix} = N\, x_P\, x_S\, k_B\, T\, \chi_{PS}$$

$$\Delta \underline{U_{mix}} = x_P\, x_S\, k_B\, T\, \chi_{PS}$$

$$\chi_{PS} = \frac{\Delta \underline{U_{mix}}}{x_P\, x_S\, k_B\, T}$$

$$\chi_{PS} = \frac{\left(-160.91 \frac{\text{kJ}}{\text{mol}}\right) \cdot \left(1000 \frac{\text{J}}{\text{kJ}}\right)}{(0.5) \cdot (0.5) \cdot \left(1.38064852 \cdot 10^{-23} \frac{\text{J}}{\text{K} \cdot \text{molecule}}\right) \cdot \left(6.022 \cdot 10^{23} \frac{\text{molecule}}{\text{mol}}\right) \cdot (298.15\ \text{K})}$$

$$\chi_{PS} = -259.647610151938$$

Determination of the entropy of mixing (for $x_P = 0.25$ and $x_S = 0.75$)

For a non-ideal system:

$$\Delta \underline{S}_{mix} = -k_B \ (x_P ln\, x_P + x_S ln\, x_S) + \underline{S}^{Excess}$$

Assuming ideal mixing:

$$\underline{S}^{Excess} = 0$$

$$\Delta \underline{S}_{mix} = -k_B \ (x_P ln\, x_P + x_S ln\, x_S)$$

$$\Delta \underline{S}_{mix} = -\left(6.0222 \cdot 10^{23} \frac{\text{molecule}}{\text{mol}}\right)\left(1.38064852 \cdot 10^{-23} \frac{\text{J}}{\text{K} \cdot \text{molecule}}\right) \left((0.25)\ ln(0.25) + (0.75)\ ln(0.75)\right)$$

$$\Delta \underline{S}_{mix} = \left(4.675404 \frac{\text{J}}{\text{mol K}}\right)$$

Determination of the free energy of mixing (for $x_P = 0.25$ and $x_S = 0.75$)

Equation 4: Fundamental equation of internal energy for a closed system

$$\mathrm{d}U = T\mathrm{d}S - P\mathrm{d}V$$

Equation 5: Fundamental equation of enthalpy for a closed system

$$\mathrm{d}H = T\mathrm{d}S + V\mathrm{d}P$$

Equation 6: Fundamental equation of Gibbs free energy for a closed system

$$\mathrm{d}G = -S\mathrm{d}T + V\mathrm{d}P$$

Equation 7: Integrated form of enthalpy equation in terms of internal energy, pressure, and volume

$$\mathrm{H} = \mathrm{U} + \mathrm{PV}$$

$$\Delta H = \Delta U + \Delta(PV) = \Delta U + P\Delta V + V\Delta P$$

Equation 8: Integrated form of Gibbs free energy equation in terms of enthalpy, temperature, and entropy

$$\mathrm{G} = \mathrm{H} - \mathrm{TS}$$

$$\Delta G = \Delta H + \Delta(TS) = \Delta H + S\Delta T + T\Delta S$$

Assuming volume is additive (ideal mixing), and that temperature and pressure are constant:

$$\Delta V = 0$$

$$\Delta H = \Delta U$$

$$\Delta G = \Delta U - T\Delta S$$

$$\Delta \underline{G} = \Delta \underline{U} - T\Delta \underline{S}$$

$$\Delta \underline{G_{mix}} = \Delta \underline{U_{mix}} - T\Delta \underline{S_{mix}}$$

$$\Delta \underline{G_{mix}} = x_P\, x_S\, k_B\, T\, \chi_{PS} - k_B\, T\, (x_P ln\, x_P + x_S ln\, x_S)$$

$$\Delta \underline{G_{mix}} = \Big(6.0222 \cdot 10^{23}\, \frac{\text{molecule}}{\text{mol}}\Big)\Big((0.25)\,(0.75)\,\Big(1.38064852 \cdot 10^{-23}\, \frac{\text{J}}{\text{K} \cdot \text{molecule}}\Big)\,(298.15\ \text{K})\,(-259.647610151938) - \Big(1.38064852 \cdot 10^{-23}\, \frac{\text{J}}{\text{K} \cdot \text{molecule}}\Big)\,(298.15\ \text{K})\,\big((0.25)\, ln(0.25) + (0.75)\, ln(0.75)\big)\Big)$$

$$\Delta \underline{G_{mix}} = -122.0764716\, \frac{\text{kJ}}{\text{mol}}$$

Appendix C.2 – Calibration Curve Calculations

All calculations in **Appendix C.2 utilized the first trial of the 3% ethanol solution, and its other trials when applicable. All data for these calculations are found in **Table B-1**.

Calculation for ratio of GC curves of propanol and ethanol

Equation 9: Propanol/ethanol area ratio (unitless)

$$R_{area} = \frac{A_{PrOH}}{A_{EtOH}}$$

$$R_{area} = \frac{3068333668}{9095538}$$

$$R_{area} = 337.3449342$$

Determination of volume of ethanol in solution

Equation 10: Volume of ethanol based on volume concentration

$$V_{EtOH} = C_{EtOH,solution}\, C_{EtOH,CC}\, V_{total}$$

$$V_{EtOH} = (0.03)\ (0.95)\ (5 \cdot 10^{-6}\ \text{L})$$

$$V_{EtOH} = 1.425 \cdot 10^{-7}\ \text{L}$$

Determination of mass based on density [56]

Equation 11: Mass of ethanol from density and volume

$$m_{EtOH} = \rho_{EtOH}\, V_{EtOH}$$

$$m_{EtOH} = \left(0.7892\,\frac{\text{g}}{\text{mL}}\right) \cdot \left(1000\,\frac{\text{mL}}{\text{L}}\right) \cdot (1.425 \cdot 10^{-7}\ \text{L})$$

$$m_{EtOH} = (1.125 \cdot 10^{-4}\ \text{g})$$

Determination of averages and standard deviations of area ratios

Equation 12: Average of the set of numbers

$$\bar{x} = \frac{(\sum_{i=1}^{n} x_i)}{n}$$

$$\bar{x} = \frac{\big((337.3449342) + (207.9791478) + (229.8534824)\big)}{(3)}$$

$\bar{x} = 258.39252$

Equation 13: Sample standard deviation

$$s_x = \sqrt{\frac{\left(\sum_i^n (x_i - \bar{x})^2\right)}{n-1}}$$

$$s_x = \sqrt{\frac{\big((337.3449342) - (258.39252)\big)^2 + \big((207.9791478) - (258.39252)\big)^2 + \big((229.8534824) - (258.39252)\big)^2}{(3) - 1}}$$

$s_x = 38.23717$

Linear regression

Equation 14: Slope-intercept equation for the calibration curve

$$y = m_0\, x + b_0$$

Substitute the area ratio and mass of ethanol for y and x, respectively,

$$R_{area} = m_0\, m_{EtOH} + b_0$$

Values for m_0, b_0, and R^2 determined by linear regression:

$m_0 = 1427537.435\ \mathrm{g}^{-1}$
$b_0 = 106.8274614$
$R^2 = 0.984738532$

Appendix C.3 – Gas Chromatography Back-Calculations

All calculations in **Appendix C.3 utilized the third trial of the combined treatment of TEA-OTF and cellulase enzyme, and its other trials when applicable. All data for these calculations are found in **Table B-4**.

Calculation for ratio of GC curves of propanol and ethanol (unitless)

$$R_{area} = \frac{A_{PrOH}}{A_{EtOH}}$$

$$R_{area} = \frac{1620629977}{21152988}$$

$$R_{area} = 76.61470696$$

Scaling up to 5 µL to use the calibration curve

$$R_{area,adjusted} = (176.61470696)\left(\frac{5\ \mu L}{2\ \mu L}\right)$$

$$R_{area,adjusted} = 191.5367674$$

Determination of mass injected from the calibration curve

$$R_{area,adjusted} = m_0\, m_{EtOH} + b_0$$

$$m_{EtOH} = \frac{R_{area,adjusted} - b_0}{m_0}$$

$$m_{EtOH} = \frac{(191.5367674) - (106.8274614)}{(1427537.435\ g^{-1})}$$

$$m_{EtOH} = 5.93395 \cdot 10^{-5}\ g$$

Determining the concentration of ethanol in solution based on mass from calibration curve

$$C_{EtOH} = \frac{m_{EtOH}}{C_{EtOH,CC}\ \rho_{EtOH}\ V_{injected,cal.curve}}$$

$$C_{EtOH} = \frac{(5.93395 \cdot 10^{-5}\ \text{g})}{(0.95) \cdot \left(0.7892\ \frac{\text{g}}{\text{mL}}\right) \cdot (5\ \mu\text{L}) \cdot \left(\frac{1\ \text{mL}}{1000\ \mu\text{L}}\right)}$$

$$C_{EtOH} = 8.82\%$$

Scaling mass down to the true amount

$$m_{EtOH,true} = (5.93395 \cdot 10^{-5}\ \text{g}) \cdot \left(\frac{2\ \mu\text{L}}{5\ \mu\text{L}}\right)$$

$$m_{EtOH,true} = 2.37358 \cdot 10^{-5}\ \text{g}$$

Determination of average and standard deviation

$$\bar{x} = \frac{(\sum_{i=1}^{n} x_i)}{n}$$

$$s_x = \sqrt{\frac{\left(\sum_{i}^{n}(x_i - \bar{x})^2\right)}{n-1}}$$

$$\bar{x} = \frac{\left((0.000465476\ \text{g}) + (0.000466679\ \text{g}) + (0.0000593395\ \text{g})\right)}{(3)}$$

$$\bar{x} = 0.000330\ \text{g}$$

$$s_x = \sqrt{\frac{\left((0.000465476) - (0.000330\ \text{g})\right)^2 + \left((0.000466679) - (0.000330\ \text{g})\right)^2 + \left((0.0000593395) - (0.000330\ \text{g})\right)^2}{(3) - 1}}$$

$$s_x = 0.000234831\ \text{g}$$

Grubbs' test calculations to eliminate potential outliers

Equation 15: Grubbs' equation to determine the Gr-value of the farthest point from the average

$$Gr = \frac{\max|x_i - \bar{x}|}{s_x}$$

$$Gr = \frac{\max\left|\left((0.000465476\ \text{g}), (0.000466679\ \text{g}), (0.0000593395\ \text{g})\right) - (0.000330\ \text{g})\right|}{s_x}$$

$$Gr = \frac{\max|(0.000135476\ \text{g}), (0.000136679\ \text{g}), (-0.0002706605\ \text{g})|}{s_x}$$

$$Gr = \frac{\max\big((0.000135476\ \text{g}), (0.000136679\ \text{g}), (0.0002706605\ \text{g})\big)}{s_x}$$

$$Gr = \frac{(0.0002706605\ \text{g})}{(0.000234831\ \text{g})}$$

$$Gr = 1.155$$

In order for a data point to be rejected [57]:

$$Gr > Gr_{critical}$$

Rejection criterion for a one-sided t-test with α=0.05, using tabulated data [57]:

$$Gr_{criitical} = 1.153$$

$$(1.155) > (1.153), \therefore \text{ data point can be rejected}$$